San Joaquin Valley Drainage Authority

San Joaquin River
Up-Stream DO TMDL Project
ERP-02D-P63

Task 8

Linking the San Joaquin River to the Stockton Deep Water Ship Channel

May, 2008

Gary M. Litton
Mark Brunell
Jordan C. Monroe

Civil Engineering Department
Department of Biology
University of the Pacific
Stockton, CA

Nigel W.T. Quinn

Lawrence-Berkeley National Laboratory
Berkeley, CA

Table of Contents

Abstract

A three-year effort to characterize the presence, transport and fate of algae in the San Joaquin River (SJR) was performed during the summers of 2005 to 2007 as part of a larger study investigating low dissolved oxygen in the Stockton Deep Water Ship Channel (DWSC). Previous investigations show that algae dominate the oxygen demands entering the DWSC during summer months (Lehman et al. 2004). In the present study, the mechanisms controlling algal fate in the San Joaquin River were investigated by measuring changes in algal pigmentsl and other water quality parameters and by determining the diversity and abundance of the zooplankton grazing community. Lagrangian monitoring was used to track a parcel of water over a 31 mile non-tidal to tidal reach upstream of the DWSC. A plug-flow reactor model was developed to describe and estimate the relative contribution of potential mechanisms responsible for the decline of algal populations upon entry into the tidal regime of the SJR and subsequent transport to the DWSC. The two dominant mechanisms for the decay of chlorophyll *a* below Mossdale appear to be zooplankton grazing and the reduction of available light associated with increased river depth. Settling during slack tide periods and dispersion associated with tidal flows may also contribute, but are much less important.

Objectives

The goal of the project is to quantitatively determine the cause for the decrease in chlorophyll and associated oxygen demands between Vernalis and the DWSC. The following objectives are proposed to meet this goal:

- Quantify oxygen demands entering the DWSC.
- Characterize the growth and decay of algae from Vernalis to the DWSC and the dominant mechanisms responsible for there growth and decay.
- Estimate biochemical oxygen demand (BOD) decay.
- Provide a comprehensive data set for model development and calibration from Vernalis to the DWSC.

While this work seeks to develop a mechanistic understanding of algal processes between Vernalis and the DWSC, utilization of a water quality model may prove necessary to fully explain the generated data. As such, development of a comprehensive data set for model algorithm development and calibration is included as one of the objectives.

Task 9 augments Task 8 by assessing algae grazing and changes in algal populations between Vernalis and the DWSC. A separate interim report has been prepared by Dr. Mark Brunell for Task 9.

Background

The growth and decay dynamics of algae in the San Joaquin River (SJR) reach between Vernalis and the DWSC is poorly characterized despite 2 years of intensive study performed during 2000 and 2001. Contradictory data exist for algal growth and decay between Vernalis and the DWSC (Jones & Stokes 1998; Lehman 2001; Foe, Gowdy, and McCarthy 2002). However, the data do strongly indicate a significant loss of algal biomass downstream of Vernalis and Mossdale (Jones & Stokes 2002; Lehman 2001). Extant DWSC models rely on input data generated at Mossdale, but this model over predicts the chlorophyll entering the DWSC by approximately 3 times and under predicts the dissolved oxygen (DO) by 2 mg L^{-1} for 2001 (Jones & Stokes 2002).

The work conducted in 2001 and 2001 did not explain the apparent losses of algal biomass between Mossdale and the DWSC. Estimates were made in 2001 of inflows and diversions to this SJR reach (Quinn and Tullock 2002). However, this work was based on scanty historic information and a boat survey and was not sufficient to characterize the algal dynamics or other mechanisms responsible for the algal decline. The SJR reach between Vernalis and the DWSC is important since it dictates the loading of live or decaying algae that directly affect oxygen removal from the water column in the DWSC. Tidal effects complicate the dynamics of this reach and slow the transport of biological material to the DWSC and its passage through the DWSC.

This study identifies important mechanisms that control the transport and fate of algae entering the DWSC. These elements are important for developing an accurate water quality model of the SJR and DWSC.

Approach and Methods

Location of Project

This component of the 2003 SJR low DO project is located in the San Joaquin River downstream of Vernalis and upstream of Channel Point at the DWSC as shown in Figure 1.

Approach Overview

The loss of algae as indicated by the decline in chlorophyll *a* concentrations above the DWSC may be associated with diminished exposure to light as the San Joaquin River deepens in the tidal prism of the Delta, dilution (dispersion) of the San Joaquin River during flood tides with water from the DWSC that exhibits much lower chlorophyll *a* concentrations, or settling out of the water column. Dye measurements may provide evidence of mass balance and losses and would indicate diversions from the San Joaquin River, when used in combination with current and planned flow and water quality modeling in this reach. Additional self-contained, continuous, monitoring stations captured additional data including chlorophyll *a,* DO, pH, and water temperature. Light-dark bottle field tests are proposed to quantify algal DO productivity. Long-term BOD bottle tests will quantify DO decay and nitrification rates. In addition, as part of an adaptive management approach zooplankton grazing and algal decay microcosm experiments and additional nutrient monitoring was added in 2007.

The investigation was conducted during 2005, 2006, and 2007. Flexibility was built into the approach to permit adaptive monitoring within the SJR between Vernalis and the DWSC. During 2005, four Lagrangian monitoring event were conducted during each month from July to October. Two of the Lagrangian trials were performed in 2006. These monitoring events were consistent with the original proposed schedule, except that the work was started in July instead of June due to extremely high flows. For 2007, only one Lagrangian trial was scheduled and the purpose of this run was to resolve issues or answer questions arising from the first two years of the investigation. Unfortunately, 2005 and 2006 were anomalous wet precipitation years and the severe dissolved oxygen deficits that usually develop in the DWSC during the summer and fall did not occur due to the high net flows passing through Stockton, CA. When 2007 developed into a dry year, as part of the adaptive research approach, additional monitoring was undertaken to collect as much information as possible, even though the original work plan scheduled only one Lagrangian monitoring event.

The additional research that was conducted in 2007 included six investigations in July, August, and September in which longitudinal water quality profiling was performed during multiple tidal stages and at different times over a 24-hr day. The deployment and maintenance of water quality sondes from Vernalis to the DWSC was extended to virtually the entire summer and fall instead of deployment only during the week of the Lagrangian trial. Additional microcosm work was also performed to assess zooplankton grazing and long-term algal decay when exposed to prolonged darkness. Lastly, dissolved silica, orthophosphate, and total phosphorus were added to the nutrient analyses for 2007. Quantification of nitrifying bacteria concentrations was the only research

element that was reduced from the original scope of work due to the relatively low ammonia concentrations observed in the San Joaquin River over the three years of work. Historically, the dominant source of ammonia in the study reach came from the City of Stockton wastewater treatment plant outfall. In years prior to this study, high ammonia concentrations exerted a significant oxygen demand in the DWSC. However, the ammonia discharge was significantly diluted by the high flows of 2005 and 2006, and by June, 2007, the treated municipal wastewater discharged by the City of Stockton was nitrified. Limited quantification of nitrifying bacteria was performed, but other research activities were determined to be of a higher priority with the absence of high ammonia concentrations during the summer and fall.

The monitoring runs were designed to address extant questions about the SJR, but as discussed above the emphasis on certain study elements was modified to better address the objectives of the study or resolve new questions.

Each monitoring run involved four specific tasks:

Task 8.1: Deployment of four continuous monitoring sondes at selected locations for approximately 4-5 days while Task 8.2 tasks are performed. The sondes measured water temperature, dissolved oxygen, electrical conductivity, pH, turbidity, chlorophyll *a*, and instrument depth. This subtask provided a data set for modeling and assisted with interpreting the results of Task 8.2. The positioning of the monitoring sondes in the SJR provided uniform coverage of the study reach.

Task 8.2: Perform Lagrangian monitoring to assess losses of algae and oxygen demanding substances in route to the DWSC below Vernalis. Rhodamine WT tracer was released at Vernalis or in special cases at the HOR, and then followed as this parcel of water flows to the DWSC. In situ measurements of water temperature, dissolved oxygen, electrical conductivity, pH, turbidity, chlorophyll *a,* and rhodamine WT, instrument depth, water depth were collected at intervals varying from 2 to 60 seconds and stamped with time and coordinate location. Water samples are collected periodically and analyzed for nitrogen species (NH_3, NO_2^-, NO_3^-, TKN) , chlorophyll *a*, pheophytin *a,* total suspended solids (TSS), volatile suspended solids (VSS), and long-term biochemical oxygen demand (BOD), carbonaceous BOD, and nitrogenous BOD. Dissolved silica, orthophosphate, and total phosphorus were added to the suite of nutrients in 2007 as part of the adaptive monitoring approach. Lagrangian monitoring performed in 2005 and 2006 showed that light limitation and zooplankton were important mechanisms controlling the decline of algae below Mossdale. As such, microcosm experiments were added to the scope of work in 2007 to assess zooplankton grazing and long-term algal decay as part of the adaptive monitoring approach.

Task 8.3: Augment fieldwork with the laboratory assessment of BOD decay and nitrification kinetics. Long-term BOD laboratory trials were performed in a dark, temperature controlled environment.

Task 8.4: Field light/dark bottle experiments. Light and dark bottles are suspended at regular depths in the water column to measure chlorophyll *a* and dissolved oxygen production as a function of light. Light intensity is measured as a function of depth during the deployment of the bottles.

Water Quality Measurements

Continuous Water Quality Measurements

Tasks 8.1 and 8.2 were performed with multiparameter sondes manufactured by Hach, Inc. (Hydrolab 5XDS, Hach Environmental, Loveland, CO) or YSI, Inc. (YSI 6600 EDS Yellow Springs, OH). Calibration was performed per standard methods (APHA 1998, APHA 2005) or manufacturer's specifications and checked periodically in the field or at the end of deployment. The data acquisition frequency was set to 15 minutes. Continuous measurements performed from the monitoring boat utilized a YSI 600 XL sonde with separate SCUFA fluorometers (Turner Instruments, Sunnyvale, CA) for chlorophyll *a* and rhodamine WT. During the 2006 and 2007 trials, a second YSI 6600 EDS or Hydrolab 5XDS sonde with temperature, EC, pH, DO, chlorophyll fluorescence, and turbidity sensors was also deployed on the boat to serve as a backup. The longitudinal profiles measured from the DWSC to Mossdale were performed with either a Hydrolab 5XDS or YSI 6600 EDS.

Discrete Water Sample Collection and Analysis

All the tasks required the collection of water samples for constituent quantification. Sampling was performed by manual grab methods or peristaltic pumps. Analysis was conducted in accordance with standard methods (AHPA 1998, AHPA 2005). TSS and VSS was performed by SMs 2540 D and E, respectively, using filters required for chlorophyll *a* (SM 10200H) instead of filters required by SMs 2540 D and E to obtain better correlations among VSS, chlorophyll *a,* and BOD. Filter pore sizes for TSS and VSS can be significantly larger than pores sizes of filters specified for chlorophyll *a* analysis. Chlorophyll *a* and pheophytin *a* was extracted using an acetone/water solution and UV absorption in accord with SM 10200H. Biochemical oxygen tests wereof a long-term nature (SM 5210 C) to facilitate determination of decay rate constants. Ammonia, nitrite, and nitrate quantification was performed with an ion specific electrode using standard methods and the manufacture's instructions and ionic strength or pH adjusting solutions (SM 4500-NH_3 D, SM 4500-NO_3^- D).

Task Descriptions

Task 8.1: Deployment of Continuous Recording Sensors

Four additional monitoring sites on the San Joaquin River were instrumented between Vernalis and the DWSC. These sondes were deployed at Vernalis(VNS), Midway (MID), Mossdale (MSD), Brandt Bridge (BDT), Stockton Brick Co. (SBC), and the Outfall Pier (OP) as shown on Figure 1. Some of these stations were also monitored as part of Task 10. Continuous water quality sondes (Hydrolab 5SDX or YSI 6600 EDS), measuring chlorophyll *a,* turbidity, EC, pH, DO, and water temperature were deployed at these locations for approximately 1 week during the Lagrangian dye tracking measurements of Task 8.1. These sondes capture the diurnal patterns of algal growth and respiration and provide data sets for model calibration.

Task 8.2: Lagrangian Monitoring

Lagranian monitoring was also performed during the three years by spreading rhodamine WT dye across the SJR and following it downstream in a boat instrumented with water quality sensors. Monthly injections of dye and deployment of light-dark bottle experiments were conducted in July, August, September, and October of 2005, July and August of 2006, and June and July of 2007. Most of the Lagrangian experiments were started at Vernalis, with the exception of the trial performed in August, 2006 in which dye was release at the Head of Old River in an effort to focus on spatial variations in zooplankton concentrations (see Task 9). In situ measurements of dye concentration, chlorophyll *a,* pH, DO, turbidity, water temperature, water depth, and instrument depth were captured electronically with the time and their global positioning system (GPS) coordinate location. Figure 2 presents a photograph of the monitoring boat and a schematic diagram of the equipment required for this task. This system allows for the simultaneous collection of all data from five different instruments every second. Actual data collection frequency was set at 2 s during 2005, and later extended to 10 or 60 s in 2006 and 2007 to facilitate faster post-processing of the data. These data were collected in real-time and displayed graphically using MATLAB (MathWorks, Natick, MA). This algorithm also calculates the San Joaquin River mile location based on USGS 7.5 quadrangle topographic maps and the measured GPS coordinates (e.g., Navy Bridge just above the DWSC and Vernalis are located at rm40 and rm72, respectively). To augment the continuous monitoring, discrete water quality samples were also collected for quantification of chlorophyll *a,* pheophytin *a,* VSS, TSS, BOD, CBOD, and nitrogen species. Water samples collected during these trials was then transported to the laboratory and processed or preserved as appropriate.

As part of the adaptive monitoring approach, longitudinal profiling from Mossdale to the DWSC replaced the Lagrangian monitoring method when the net flow to the DWSC ceased in July, 2007 The longitudinal monitoring was continued through September, 2007. In addition, zooplankton grazing experiments and algal decay experiments were added in 2007 to estimate the rate at which zooplankton consume algae from the water column and assess the rate of conversion of chlorophyll *a* to pheophytin *a* and the subsequent decay of pheophytin *a*. Water samples collected from MSD, BDT, SBC, and OP were used for the chlorophyll *a* decay evaluation. Chlorophyll *a* and pheophytin *a* were measured by extraction methods (AHPA, 2005) and fluorescence over a 13-day period. Lastly, orthophosphate, total phosphorus and dissolved silica were also added to the constituent list in 2007.

Task 8.3: BOD Decay and Nitrification Rates

The BOD and CBOD tests were performed over 20 days to determine kinetic decay rate constants of BOD, CBOD, and NBOD. The low concentrations of ammonia (generally non-detectable) in the river precluded the monitoring of ammonia decay. These tests were performed with water samples collected during the Lagrangian monitoring events and the longitudinal profiles added to the study in 2007.

Task 8.4: Light-Dark Bottle Experiments

As part of the Lagrangian studies, light-dark bottle experiments were also performed to assess whether the apparent decay of algal biomass from Mossdale to the DWSC may be associated with reduced exposure to light as the river channel depth increases within the tidal prism and provide data on algal productivity in the study reach. To assess algal productivity and respiration, light-dark bottles were suspended from a buoy at various depths while following the dye slug or assessed independently during the longitudinal monitoring conducted in 2007. Light intensity was also measured at each depth periodically. The pH, DO, chlorophyll *a,* and pheophytin *a* concentrations were quantified before and after suspension in the water column. These tests provided data necessary to evaluate the effect of light limitation on chlorophyll *a* decay between Mossdale and the DWSC. These data also yield algal productivity and DO response curves as a function of light intensity, data important for modeling the study reach.

Results and Discussion

Completed Work

The following elements of Task 8 have been completed.

- Lagrangian and fixed-location sonde water quality monitoring was performed in July, August, September, and October of 2005, July and August, 2006, June and July, 2007. Near zero low net flows to the DWSC after June, 2007 required that longitudinal measurements be performed every 2 to 4 miles from the DWSC to Mossdale instead of the Lagrangian monitoring. The longitudinal profiling was added to the investigation scope of work as part of the adaptive monitoring plan. A bathymetric survey along the approximate river thalweg from Vernalis to the DWSC as also been compiled.

- Light-dark bottle experiments were deployed during the three study years. Zooplankton grazing microcosm evaluations were added to the investigation plan in 2007 as part of the adaptive monitoring approach.

- Long-term BOD tests were conducted with all the Lagrangian and longitudinal monitoring performed from 2005 to 2007. A limited number of ammonia oxidizing bacteria concentrations measurements were performed because ammonia concentrations in the river during the study periods were often low, yielding low oxygen demands and low bacteria concentrations. Laboratory algal decay investigations were added to the study as part of the adaptive monitoring approach.

- Provisional data sets have been submitted. Final data sets will be available at the end of the contract period.

- Development of a numerical model to interpret the results of the Lagrangian water quality trackings has been developed and used to quantify light limitation effects and zooplankton grazing on algae in the study reach. The development of this algae model was added to the investigation in 2006 as part of the adaptive management of the task.

Overview of the river flows in 2005, 2006, and 2007

The Task 8 field investigation was scheduled to start in June, 2005. However, extremely high flows in the San Joaquin River postponed the work until July as high flows yield short travel times and data sets that are not representative of the river during periods of critical DO levels in the DWSC. Monitoring was again postponed to July in 2006, due to extremely high flows. Only two trials were performed in 2006 due to the persistent high flows. The flow conditions of 2007 proved to be more representative of typical Vernalis flows than 2005 and 2006. As shown in Figure 3, the 2004 and 2007 Vernalis flow are similar. Net flows fell to zero for most of July and August, 2007. A comparison of the 2004, 2005, 2006, and 2007 flows measured at Vernalis are presented in Figure 3 and show that May and June flows were in excess of 10,000 cfs for both 2005 and 2006. The historic flow during these time periods has often between 1000 and 2000 cfs. Figures 4, 5, and 6 provide a comparison of San Joaquin River flow at Vernalis and at Garwood Bridge for 2005, 2006, and 2007, respectively. The base river flow entering the DWSC was approximately 1000 cfs in 2005, but exceeded 1500 cfs during most of the summer of 2006. In June, 2007 the net flow entering the DWSC was approximately 800 cfs, but after July 15 the net flow fluctuated around zero until September. Previous studies have shown that dissolved oxygen concentrations remain above water quality objectives when net flows entering the DWSC exceed 1500 cfs (Foe *et al.*, 2002). During this study the dissolved oxygen deficits in the DWSC were not as severe as observed in past years. For 2005 and 2006, this was due to the relatively high flows passing through the DWSC. In 2007, dissolved oxygen levels in the DWSC were also relatively high for most of the summer (i.e., greater than 5 mg L^{-1}). This observation appears to be caused in part by the zero net flow and the subsequent exertion of the oxygen demand associated with the algae in the San Joaquin River above the DWSC. The City of Stockton also brought on-line new nitrification unit wastewater treatment processes that significantly reduced their nitrogenous and carbonaceous oxygen demands discharged to the San Joaquin River in June, 2007.

Water quality measurements from Vernalis to the DWSC.

Task 8.1 Deployment of Continuous Recording Sensors

Four water quality sondes were deployed at the Vernalis, Midway, Mossdale, Brandt Bridge, Stockton Brick Company, and Outfall pier stations shown previously in Figure 1. Examples of the dissolved oxygen, pH, and chlorophyll *a* results are shown in Figures 7 and 8 for the Midway and Brandt Bridge stations, respectively. Algal productivity is clearly shown in the diel variations of chlorophyll *a*. During daylight hours chlorophyll *a* levels increase until approximately 4:00 PM and then decrease during the night. The dissolved oxygen and pH also respond to this algal production and respiration. Shown in

the chemical representation below, the production of algae will yield higher DO and pH levels in the water (Stumm and Morgan, 1996).

$$106\ CO_2 + 16\ NO_3^- + HPO_4^{2-} + 122\ H_2O + 18\ H^+ \rightarrow \underset{\text{(algae)}}{C_{106}H_{263}O_{110}N_{16}P} + 138\ O_2$$

The pH increases from the consumption of 18 hydronium ions for each algal cell produced. This stoichiometry was also applied to the light-dark bottle experimental data to compare algal productivity measured by changes in chlorophyll *a*, dissolved oxygen production, and increases in pH. The data from the fixed sondes augments the results of the Lagrangian monitoring completed as Task 8.2 and are available for future model development and calibration.

Task 8.2 Lagrangian monitoring

Five trials were performed to track a water parcel from Vernalis to the DWSC in 2005 and 2006. A sixth trial started at the Head of Old River instead of Vernalis in August, 2006 due to the abnormally high flows. This trial focused on assessing spatial temporal variations in zooplankton populations. Details of the results of the plankton measurements are contained in the Task 9 annual report. The flows of 2007 were much lower than those observed in the previous two years. One Lagrangian tracking was conducted from Vernalis to the DWSC in June, 2007. The last Lagrangian event was performed in July, 2007, starting at Vernalis and ending at Mossdale. The near zero net flow below the Head of Old River prevented additional Lagrangian trials for the remainder of the summer as the travel time exceeded 10 days. Instead, longitudinal monitoring was performed in July, August, and September during slack tide periods from the DWSC to the Head of Old River.

The Lagrangian monitoring was initiated by dispersing Rhodamine WT dye into the San Joaquin River and tracking it to the DWSC with a fluorometer. In July 2005, the travel time to the DWSC was approximately 32 hours at a Vernalis flow rate of approximately 4500 cfs. The San Joaquin River flow splits at the Head of Old River, with approximately 1800 cfs continuing to the DWSC as measured at the Garwood Bridge USGS station (station code SJG at cdec.water.ca.gov). These flows are much higher than flows observed during drier water years and yield relatively fast travel times. The low net flows observed during 2007 prevented implementation of the Lagrangian monitoring in July, August, and September, as it would theoretically require an infinite amount of time to travel from the HOR to the DWSC if dispersion is neglected. During these months, longitudinal monitoring was performed every 2 miles from the HOR to the DWSC to assess water quality changes. The 2007 schedule of monitoring events is presented in Table 2.

Dispersion attenuates the peak tracer concentration as the dyed water moves downstream. In addition, approximately 50 to 60 percent of the water dyed at Vernalis flowed down

Old River and never reached the DWSC. As such, for each Lagrangian trial starting at Vernalis, the tracer plume was replenished below the Head of Old River.

2005 Lagrangian results

The response of chlorophyll *a* in the dyed parcel of water that flowed to the DWSC is shown in Figure 9 for the July, 2005 trial. Similar to the chlorophyll a data measured by the fixed sondes, these data also exhibit a diel pattern where chlorophyll a increases during the day and decreases by night. Figure 9 also contains chlorophyll *a* data measured in the laboratory from discrete water samples. The pH and DO data are also consistent with the chlorophyll results behavior. The pH and DO levels responded to diel cycles and increase or decrease with algae production or evening respiration.

Figure 10 shows the extracted pigment concentrations of chlorophyll *a* and pheophytin *a* during the July, 2005 Lagrangian monitoring. Also presented is the fraction of chlorophyll *a* relative to the sum of these two pigments (pigment fraction). Chlorophyll *a* is converted to pheophytin *a* when algae decays. Therefore, a pigment fraction of 1 is indicative of an algal community in perfect health. As shown in Figure 10, the chlorophyll *a* fraction remains high throughout the transport to the deep water ship channel, indicating that the algal community is in excellent physiological condition. As also shown in Figures 9 and 10, chlorophyll *a* concentrations remained relatively constant and above 50 $\mu g\ L^{-1}$ during the July, 2005 monitoring. However, this was not the case for the months of August, September and October, 2005 as shown in Figures 11-16. Each of these dye tracking trials measured a decay of chlorophyll *a* below Mossdale. In August, 2005 a decrease from 35 to 20 $\mu g\ L^{-1}$ was observed between Vernalis and the DWSC (Figures 12 and 13). September and October, 2005 trials yielded similar results with a decline from about 15 to 5 $\mu g\ L^{-1}$ as shown in Figures 13 to 16. Dissolved oxygen and pH exhibited similar trends.

The pigment fraction during August, September, and October of 2005 was also observed to decrease in route to the DWSC. From Vernalis to Mossdale both chlorophyll *a* and the pigment fraction were relatively stable, indicating little loss of algal biomass or physiological health of the community. However, below Mossdale both chlorophyll *a* and the pigment fraction decrease about 50 percent when compared to values measured at the DWSC. As shown later in this report, this decline appears to be associated with both light limiting effects associated with increased river depth and zooplankton grazing. It appears that the higher net flow of 1800 cfs to the DWSC during July, 2005 did not provide the residence time required for light limitation and zooplankton grazing to exert an observable effect on the algae.

2006 Lagrangian results

Similar data sets have been generated during the monitoring performed in July and August, 2006 are shown in Figures 17-20. As presented in Figures 17 and 19, chlorophyll a values exhibited the typical increase during the day and decline during night. Dissolved oxygen and pH also appear to be well-correlated with this diel pattern. Also shown in Figures 17 and 19, algal concentrations measured with fluorescence exhibited a similar decline between the Head of Old River and the DWSC. Extracted chlorophyll a concentrations for the two Lagrangian runs also exhibited a 20 to 25 $\mu g\ L^{-1}$ decrease between the HOR and DWSC. In 2006, the pigment ratios did not exhibit the 50 percent decrease observed in August, September, and October of 2005. For July, 2006, the chlorophyll *a* to total pigment ratio decreased from about 0.8 above Mossdale to 0.6 at the DWSC indicating some decline in the physiological state of the algae. This deterioration was similar to the August, 2006 data for the Lagrangian trial started at the Head of Old River. The pigment ratio was fairly uniform at 0.8 from the Head of Old River (rm54) to rm45, but then slowly decreased to 0.67 at the DWSC (rm40). These data sets will be further analyzed with the algae-zooplankton model presented later in this report.

2007 Lagrangian results

The June, 2007 Lagrangian monitoring results for chlorophyll and dissolved oxygen are presented in Figure 21. The travel time to the DWSC from Vernalis was over 65 hours for this monitoring event. Diel effects were strongest in the upper river, but evident throughout the 31 mile reach. For example, chlorophyll a concentrations increased from approximately 40 to 80 ug L^{-1} from 8:30 a.m. to sunset on June 12. Also shown in Figure 21 was the effect on dissolved oxygen associated with algal productivity during the day and respiration at night. The increase in chlorophyll *a* on June 12 also generated a rise in dissolved oxygen from 10 to 15 mg L^{-1}. As shown throughout the June, 2007 tracking, the rise and fall of chlorophyll and dissolved oxygen are well correlated with diel cycles. Figure 22 is presented to illustrate the effect of increased water depth to measured chlorophyll *a* and pheophytin *a* concentrations. Above Mossdale the average water depth is often about 5 ft. The depth of the photic zone, defined as the depth at which 1 percent of the incident light penetrates the water column, is also approximately 5 ft for the San Joaquin River. Below Mossdale, the average river depth increases from about 10 ft to 15 ft over 14 miles. The river then transitions from depths of 15 ft to 40 ft in the DWSC. With the deepening of the well-mixed San Joaquin River above the DWSC, the algae spend less time in the photic zone, an observation that appears to influence the reduced production of chlorophyll a and oxygen during the daylight periods. In Figure 22, the chlorophyll *a* decay product, pheophytin *a*, is also observed to increase, suggesting that light limitation in deeper waters is adversely effecting the physiological health of the algal community. However, as discussed later this rise in pheophytin *a* can also arise from zooplankton grazing.

This effect is better shown in Figure 23 where the chlorophyll a to total pigment ratio is plotted for the June, 2007 tracking from Vernalis to the DWSC. In this plot the decline in

the pigment ratio approximately parallels the average water depth of the San Joaquin River. While light limitation associated with increased river depth appears to influence the algal community, the decline in the pigment ratio may also be associated with the rise in the zooplankton population as presented in Figure 24. The exponential growth of the zooplankton concentration appears to be correlated to the decline in the chlorophyll *a* and the increase in the pheophytin *a* concentration. Zooplankton microcosm experiments presented later will show that algal losses due to grazing yields increases in pheophytin. These June, 2007 observations provide some of the best evidence that light limitation and zooplankton grazing are dominate mechanisms controlling the algal community while carried by the flow from Mossdale to the DWSC.

2007 longitudinal profiles

As discussed earlier, longitudinal monitoring of the San Joaquin River at discrete locations between Mossdale and the DWSC were performed in July, August, and September of 2007 when the net flow fluctuated around 0 cfs. For these flow conditions, the advective transport of algae and other oxygen demanding substances is effectively zero and dispersive transport mechanisms dominate. The dissolved oxygen, ultimate BOD, extracted chlorophyll a, and pigment ratios are presented in Figures 25 and 26 for the longitudinal monitoring performed during slack tide periods. These results exhibit a linear change in concentration from the HOR to the DWSC that is characteristic in dispersion dominated waters. For example, the dissolved oxygen decreased from about 11 mg L^{-1} at the HOR to 5 mg L^{-1} at the DWSC. The variation in the concentration at a fixed location is influenced by tidal flows and the time of day. Note that higher concentrations of DO were measured in early evening and the lowest concentrations were observed in early morning. The changes in BOD shown in this figure will be discussed later with Task 8.3 results.

As shown in Figure 26, the chlorophyll *a* concentration declines dramatically below the SBC site, located approximately 5 miles above the DWSC. These data suggest that the extent of tidal excursion up the San Joaquin River from the DWSC is about 5 miles. Ebb flows push the high chlorophyll a levels to rm44 while the flow reversal occurring with flood tide provide low chlorophyll *a* water coming from the DWSC up to rm 46. The effect on the physiological health of the algae community, as measured by the pigment ratio, also exhibits a decline between the HOR and the DWSC. Pigment ratios decrease from 0.8 to 0.4 over this 14-mile reach of the San Joaquin River. While not shown here, this drop in chlorophyll *a* and the pigment ratio has been shown to be correlated to peak concentrations in the zooplankton population.

The longitudinal monitoring was also performed in August and September and the results are displayed in Figures 27 to 30. The observed behavior of dissolved oxygen, chlorophyll a, and pigment ratio during these months was similar to that observed and discussed for the July, 2008 longitudinal monitoring.

2007 zooplankton and chlorophyll a comparisons

The identification of zooplankton species and quantification of mass concentrations were performed as part of the Task 9 monitoring. Details of the sampling and analysis protocols are described in the Task 9 report. Figures 31 through 36 provide examples of the longitudinal profiles of total zooplankton and chlorophyll *a* concentrations in the San Joaquin River between Mossdale and the DWSC during July, August and September, 2007. The net flow of the San Joaquin River during this period was approximately zero in July and August, and then it increased slowly to about 250 cfs by September 21. These net flows yield long travel times from HOR to the DWSC for the algal and zooplankton communities transported by the flow. For example, rhodamine WT dye released at HOR on September 20 was measured near the DWSC five days later.

Figure 31 presents the chlorophyll *a* and zooplankton concentrations measured on July 17 at the end of an ebb tide in the San Joaquin River from the HOR to the DWSC. At this time the net flow to the San Joaquin River was approximately zero, therefore, tidal flows and dispersion were the dominant transport mechanism for aquatic species moving from the upper San Joaquin River to the DWSC. Over this river reach, chlorophyll *a* concentrations decreased from approximately 160 $\mu g\ L^{-1}$ at the HOR to 20 $\mu g\ L^{-1}$ at the DWSC. The zooplankton concentration profile for this reach increased from approximately 50 $\mu g\ L^{-1}$ to a maximum of 120 $\mu g\ L^{-1}$ at rm46 before decreasing to 20 $\mu g\ L^{-1}$ at the DWSC. This maximum in the zooplankton concentration profiles between the HOR and the DWSC was consistently observed in July, August, and September of 2007 during this period of low net flow as also exhibited in Figures 31 through 36. These measurements suggest that the longer residence time associated with the low net flow to the DWSC provided sufficient time for zooplankton communities to flourish and effectively graze on the algae community traveling to the DWSC.

The location of the observed peak in the zooplankton concentration was also found to be relatively stable, generally ranging from rm46 during the end of an ebb tide to rm52 for strong flood tide reversals. This region of observed maximum zooplankton concentration appears to be consistent with the ebb tide excursion from the HOR during low net flows as measured with dye studies. For example, rhodamine dye released at HOR (rm 54) on September 20 at the end of a flood tide was observed 7 hours later at BDT (rm 48) at the end of the ebb tide. Since the net flow in the San Joaquin River was only 250 cfs and tidal flows exceed 2000 cfs, this pulse of dye was observed to pass the BDT station for several tidal cycles and eventually it entered the DWSC approximately 5 days later. The dye movement driven by tidal flows indicates that algae flowing to the DWSC can reach rm48 within a few hours, but then several days are required for the algae to reach the DWSC. During this time, the zooplankton population has sufficient time to develop to concentrations that can effectively reduce algal populations. Thus, when the net flow to the DWSC is less than approximately 250 cfs, the maximum zooplankton concentrations are observed 6 to 12 miles above the DWSC, a location where fresh algae can be readily transported below the HOR by ebb tide flows.

Zooplankton microcosm studies, discussed later in this report, provide estimates of grazing rates that range from 0.8 to 1.4 $m^3 \cdot gC^{-1} \cdot d^{-1}$. At the chlorophyll *a* and zooplankton

concentrations observed below the HOR, and at these microcosm grazing rates, zooplankton grazing can reduce chlorophyll *a* concentrations by approximately 15 to 30 $\mu g \cdot L^{-1} \cdot d^{-1}$. For the low net flows observed in the San Joaquin River during July, August, and September, the travel time below the HOR exceeds 5 days. For September 21, the travel time to the DWSC was approximately 5 days and measurements of the maximum zooplankton and chlorophyll *a* concentrations were approximately 180 and 80 $\mu g \cdot L^{-1}$, respectively. Using microcosm grazing rates, approximately 35 to 60 $\mu g \cdot L^{-1}$ was estimated to be lost to grazing based on the September 21 longitudinal monitoring. Other mechanisms, such as light attenuation associated with the deepening of the San Joaquin River below the HOR are probably responsible for the additional loss of chlorophyll *a* entering the DWSC. Inspection of Figures 31 to 36 suggests that zooplankton grazing is a significant mechanism for the loss of chlorophyll *a* above the DWSC under conditions of low net flows because residence time is long and zooplankton populations are sufficient to dramatically reduce chlorophyll *a* concentrations.

Zooplankton microcosm studies

To further quantify the effect of zooplankton grazing on the algae community, two zooplankton microcosm experiments were performed in late September and early October. The results shown in Figure 37 indicate that concentrated zooplankton populations can dramatically reduce the chlorophyll a concentration and raise pheophytin *a* levels. These microcosms were maintained in the photic zone (2 ft depth) for 4.5 hours prior to performing final measurements. The control microcosm received no additional zooplankton above background. After 4.5 hours in the water column the chlorophyll *a* concentration in the control microcosm had doubled from 65 to 130 ug L^{-1}. However, the microcosm seeded with a high concentration of zooplankton exhibited a net decrease in chlorophyll of approximately 20 ug L^{-1}. These tests also suggest that the consumption of algae by zooplankton results in a transformation of chlorophyll a to pheophytin a, and some of the pheophytin pigment survives the digestive processes of the zooplankton.

Figure 38 presents more results of microcosm tests performed on October 3, 2007. In this test the chlorophyll a and pheophytin a concentrations were monitored every 1.5 hours by removing 2 microcosm bottles (with and without zooplankton seed) from the water column and sampling for chlorophyll a and pheophytin a. For these tests algal productivity was inhibited by placing the bottle below the photic zone. These experiments indicated that the zooplankton were responsible for decreasing the chlorophyll a concentration from approximately 50 to 35 ug L^{-1} after 6 hours. During this time the pheophytin a concentration increased from 20 to 40 ug L^{-1}. These tests also support the observation that chlorophyll a is transformed to pheophytin when ingested and excreted by zooplankton.

Zooplankton grazing rates were estimated with the data collected from the microcosm experiments shown in Figures 37 and 38. A common equation for the chlorophyll *a* consumed by zooplankton is provided by Chapra, 1997,

$$k_{gz} = C_{gz} \cdot Zoo \cdot Chla$$

where, k_{gz} is the observed loss of chlorophyll a per time, C_{gz} is the grazing rate constant, *Zoo* is the zooplankton concentration, and *Chla* is the chlorophyll a concentration. After adjusting for growth and respiration in the microcosms, the zooplankton microcosm tests yielded grazing rates, C_{gz}, that ranged from approximately 0.8 to 1.4 $m^3 \cdot gC^{-1} \cdot d^{-1}$. The kinetic rates estimated with these experiments for zooplankton grazing were used later in the modeling efforts used to assess the relative contribution of grazing on the chlorophyll a decline below the HOR.

Algae kinetic decay experiments

Laboratory microcosm tests were also performed to assess chlorophyll a and pheophytin a decay when algae are subjected to darkness. These experiments were performed with water collected from Mossdale (MSD), Brandt Bridge (BDT), Stockton Brick Company (SBC), and the Outfall Pier (OP) on August 1, 2007. Each sample was maintained in darkness at 20°C for 13 days. Periodically, the samples were collected from the microcosms and measured for chlorophyll *a*, pheophytin *a* and algal fluorescence. The algal fluorescence was found to be best correlated to chlorophyll a and not total pigment concentrations (chlorophyll a plus pheophytin a concentrations). As such the chlorophyll fluorescence was calibrated with the extracted chlorophyll a concentrations and plotted in Figures 39 to 40 with the extracted pigment concentrations. These data show a rapid decline in chlorophyll *a* when subjected to extended darkness.

To assess the kinetic rates of chlorophyll *a* and pheophytin *a* a simple mass balance conceptual model for the water samples appears below for the concentration of chlorophyll *a* and pheophytin *a*. In box 1, chlorophyll *a* decays to pheophytin *a* according to an assumed first-order rate law. In box 2, the pheophytin *a* concentration is influenced by the rate of decay of chlorophyll *a* to pheophytin *a* (increases the pheophytin *a* concentration) and the decay of pheophytin *a*. Pheophytin *a* is also assumed to decay at a first-order rate.

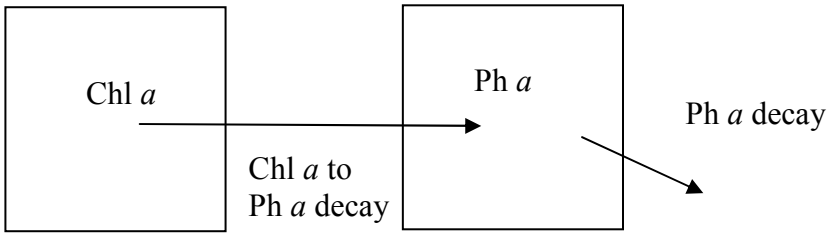

Governing Equations:

$$\frac{d(Chla)}{dt} = -k_c Chla \qquad \frac{d(Pha)}{dt} = A_{c \to p} \frac{d(Chla)}{dt} - k_p Pha$$

Solutions:

$$Chla = (Chla_0)e^{-k_c t} \quad \text{(eq. 1)}$$

$$Pha = (Chla_0)A_{c\to p}\frac{k_c}{k_p - k_c}[e^{-k_c t} - e^{-kpt}] + (Pha_0)e^{-k_p t} \quad \text{(eq. 2)}$$

Where:
$Chla$ = chlorophyll *a* concentration at time t
$Chla_0$ = initial concentration of chlorophyll *a*
Pha = pheophytin *a* concentration at time t
Pha_0 = initial concentration of pheophytin *a*
$A_{c\to p}$ = chlorophyll *a* to pheophytin *a* mass conversion factor (set to 1)
k_c = first-order decay rate of chlorophyll *a*
k_p = first-order decay rate of pheophytin *a*

Samples in excellent physiological conditions are considered to contain no pheophytin *a* (APHA 1998, 2005). Chlorophyll *a* is converted to pheophytin *a* upon loss of the magnesium atom. Regression expressions for the spectrophotometric determination of chlorophyll *a* indicate that 1 μg L^{-1} of pure chlorophyll *a* is converted to 1 μg L^{-1} of pure pheophytin *a* upon complete loss of its magnesium atom (APHA 1998, 2005). Therefore, $A_{c\to p}$, was set to 1 for the analysis presented here.

The samples collected from the San Joaquin River exhibited aging upon collection as indicated by the presence of pheophytin *a*. To adjust for this deterioration before reaching the DWSC, the time was adjusted by Δt, in the modified solutions for chlorophyll *a* and pheophytin *a* concentrations:

$$\text{Chl } a = \text{Chl } a_0^{\,a} \exp(-k_c t + \Delta t) \quad \text{(eq. 3)}$$

$$\text{Ph } a = k_c \text{ Chl } a_0^{\,a} A_{c\to p}/(k_p - k_c)[\exp(-k_c(t+\Delta t)) - \exp(-k_p(t+\Delta t))] \quad \text{(eq. 4)}$$

Where, Chl $a_0^{\,a}$ is the estimated concentration of chlorophyll *a* when the population was in excellent physiological condition. Under this condition the initial pheophytin *a* concentration, Ph a_0, is zero. The data for the two decay rate experiments performed with water collected from the San Joaquin River are shown in Figures 39 to 42. Decay constants of 0.55 d^{-1} for k_c and 0.27^{-1} for k_p, were found to provide a reasonable fit of the model to both sets of experimental data in past studies (Litton, 2002). These constants were subsequently used in modeling efforts presented later.

Task 8.3: BOD Decay and Nitrification Rates

During the tracer transport to the DWSC samples were also collected to assess the biochemical oxygen demand of the water. Nitrification rate kinetic experiments were also scheduled if ammonia concentrations exceeded 0.5 mg L^{-1} as N. All ammonia concentrations were measured below the detection limit of 0.05 mg L^{-1}, except at the City of Stockton outfall which is only one mile above the DWSC. Thus, nitrification rate tests

were not performed with the samples collected in 2005, 2006 and 2007, but instead the nitrogenous BOD associated with low ammonia concentrations was accounted for with the long-term BOD and CBOD tests.

Long-term BOD experiments were performed with samples collected from selected stations between Vernalis and the DWSC. The carbonaceous component of the BOD was measured by inhibiting nitrifying bacteria with 2-chloro-6-(trichloro methyl) pyridine (TCMP). The nitrogenous BOD was determined by subtracting the CBOD from the BOD. An example of the BOD test results are shown in Figure 44. The individual BOD and CBOD results from all three years are presented in Appendix A. Correlations with an approximate first-order fitting equation were generally excellent as most regression coefficients were greater than 0.95. A comparison of the BOD_{10} with the estimated BOD_{ult} is shown in Figure 44. Plots of the 20-d BOD measured from water samples collected between Vernalis and the DWSC during 2005 and 2006 are presented in Figure 45 and show little change in the 31-mile reach suggesting that the decay of algae below Mossdale has a limited effect on the exertion of the associated BOD. However, the relatively high flows encountered in the field investigation to date may best explain the uniformity of the BOD results. The 20-d BOD data for 2006 are also approximately twice the concentration measured in 2005.

The ultimate BOD results of the June, 2007 Lagrangian tracking indicate that the BOD is correlated to the chlorophyll a data as presented earlier in Figure 24. Between Vernalis and rm62 the BOD_{ult} increased from approximately 7.5 to 13 mg L^{-1} In this same reach chlorophyll *a* increased from about 40 to 80 mg L^{-1}. Therefore, the increase in BOD is largely associated with algal growth during the daylight hours of June 12 since common chemical representations for algae yield a theoretical oxygen demand of about 1.25 mg per mg of algal biomass. Beyond rm62, both the BOD_{ult} and the extracted chlorophyll reached a plateau at about 12 mg L^{-1} and 70 mg L^{-1}, respectively. Approaching the DWSC, the BOD and the chlorophyll declined sharply within 1 mile of the DWSC. This correlation is also evident in the longitudinal profiles shown earlier in Figures 26-30.

The data also suggest that about 30 percent of the BOD is nitrogenous as presented in Table 4 for the July, 2005 Lagrangian monitoring. However, total ammonia was undetected during the transport to the DWSC as shown in Table 4. These results were typical of BOD results observed throughout the study as shown in Appendix A. The NBOD appears to originate from the algae that decay during the BOD test. A common chemical expression of algae decomposition provides estimates of its associated CBOD and NBOD:

$$\underset{\text{(algae)}}{C_{106}H_{263}O_{110}N_{16}P} + 138\ O_2 \rightarrow 106\ CO_2 + 16\ NO_3^- + HPO_4^{2-} + 122\ H_2O + 18\ H^+.$$

Thus, each mg L^{-1} of algae will yield a theoretical oxygen demand of 1.2 mg L^{-1}. Of this 1.2 mg L^{-1}, approximately 25 percent is nitrogenous.

Task 8.4: Light-Dark Bottle Experiments

Light-dark bottle tests were conducted during the Lagrangian monitoring performed in 2005, 2006, and 2007 during daylight and night time periods and during the longitudinal monitoring conducted from July to September, 2007. The results of these experiments can be integrated into the water quality analytical model independently of Task 8. The data presented for July, 2005 is typical of other trials performed in subsequent months and years.

Light-dark bottle experiments were performed by suspending 2-L BOD bottles or 1-L polycarbonate bottles at depths of 1-ft intervals from a buoy. A dark bottle was also suspended to evaluate algal respiration. A filtered water sample was also placed in darkness to correct for the dissolved oxygen uptake associated with soluble oxygen demanding substances. Data collected in July for an experiment performed below Vernalis is presented in Table 5. The bottles were incubated for approximately 4.5 hours during midday. Chlorophyll *a* concentrations increased from 54 to 88 ug L^{-1} for the bottle placed at a depth of 1 ft. Photosynthesis occurring in this microcosm resulted in an increase of the dissolved oxygen from 8.6 to 14.3 mg L^{-1}. Consumption of carbonate minerals also increased the pH over 1 unit. In contrast, the bottle maintained in darkness exhibited a decrease in chlorophyll *a*, DO and pH due to algae respiration and decay.

The light intensity was also measured as a function of depth. Combining the light intensity measurements with the data presented in Table 5 yields a productivity-intensity (PI) curve that can be used to estimate DO production. Figure 47 presents the PI curve generated for the July, 2005 light-dark bottle trial. Similar curves were generated for the other experiments.

The production of chlorophyll *a* can also be estimated from the chemical representation for the growth of algae.

$$106\ CO_2 + 16\ NO_3^- + HPO_4^{2-} + 122\ H_2O + 18\ H^+ \rightarrow \underset{\text{(algae)}}{C_{106}H_{263}O_{110}N_{16}P} + 138\ O_2$$

The production of algae will yield an increase in dissolved oxygen and pH, and a decrease in the total carbonate species concentration. Total carbonates, $C_{T,CO3}$, is the sum of dissolved carbon dioxide gas (CO_2), carbonic acid (H_2CO_3), bicarbonate (HCO_3^-), and carbonate (CO_3^{2-}). The total carbonate concentration was calculated from the total alkalinity and the pH of the solution.

The change of the pH is also regulated by the following carbonate species that serve to buffer the pH of water when acids or bases are added. The sum of these species concentration is the total carbonate concentration, C_T.

$$C_T = [CO_{2(aq)}] + [H_2CO_3] + [HCO_3^-] - [CO_3^{2-}]$$

Since $CO_{2(aq)}$ is approximately 600 times greater than H_2CO_3 it is common to combine these species as $H_2CO_3^*$ yielding the following chemical equilibrium.

$$H_2CO_3^* \Leftrightarrow H^+ + HCO_3^- \qquad K_{a1}=10^{-6.35} \text{ at } 25^oC$$

$$HCO_3^- \Leftrightarrow H^+ + CO_3^{2-} \qquad K_{a2}=10^{-10.33} \text{ at } 25^oC$$

When alkalinity is dominated by the presence of carbonate species, the initial alkalinity and pH of the water can be used to calculate the initial total carbon concentration.

$$alkalinity = C_T(\alpha_1 + 2\alpha_2) + [OH^-] - [H^+] \qquad (2),$$

where, α_1 and α_2 are the ionization fractions for HCO_3^- and CO_3^{2-}:

$$\alpha_1 = \frac{K_{a1}[H^+]}{[H^+]^2 + K_{a1}[H^+] + K_{a1}K_{a2}},$$

$$\alpha_2 = \frac{K_{a1}K_{a2}}{[H^+]^2 + K_{a1}[H^+] + K_{a1}K_{a2}}.$$

The equilibrium constants, K_{a1} and K_{a2}, are dependent on the ionic strength and temperature of the water. Temperature correction for the equilibrium constants were performed with Van't Hoff's equation.

$$\ln\frac{K_{25}}{K_i} = \frac{\Delta H^\circ}{R}\left(\frac{1}{T_i} - \frac{1}{T_{25}}\right)$$

Where, ΔH° is the standard change of enthalpy for the specific chemical reaction, R is the universal gas constant, T_i and T_{25} are the absolute temperatures at temperature i and 25ºC, and K_{25} and K_i are the equilibrium constants at 25ºC and temperature i.

The salinity of water will also affect chemical equilibrium. The ionic strength, μ, of water can be estimated from the specific conductance (SC, conductivity at 25°C) or total dissolved solids (TDS), Russell, 1976; Lind, 1970).

$$\mu = 1.6 \times 10^{-5} \times \text{SC } (\mu\text{mho/cm})$$

$$\mu = 2.5 \times 10^{-5} \times \text{TDS } (\text{mg L}^{-1})$$

The SC of the San Joaquin River typically ranges from 400 to 900 µmho/cm and the TDS varies from approximately 150 to 650 mg L^{-1}. A value of 600 µmho/cm yields an ionic strength of approximately 0.01, a level at which the equilibrium constants should be adjusted. For ionic strengths less than 0.1, the Güntelberg approximation provides reasonable estimates for the activity coefficient,

$$-\log \gamma_i = \frac{0.5 Z_i^2 \mu^{1/2}}{1 + \mu^{1/2}},$$

where, Z_i is the valance of ion i. Ionic strength effects can be incorporated into chemical equilibrium calculations by developing a corrected equilibrium constant.

Aqueous solutions are electrically neutral. This balance of positive and negative charges yields the following equation for the San Joaquin River:

$$\text{alkalinity} + [H^+] = [HCO_3^-] + 2[CO_3^{2-}] + [OH^-],$$

and after substitution, the concentration of carbonate minerals, $C_{T,CO3}$, before and after the light-dark bottle incubation period is computed from:

$$\text{alkalinity} + [H^+] = \alpha_1 C_{T,CO3} + 2\alpha_2 C_{T,CO3} + [H^+]/K_w^c$$

These chemical equations and calculations were used to estimate chlorophyll *a* production based on increases in DO and pH. The alkalinity was also measured before and after the light exposure. The predictions for the each of the bottles are shown in Figure 48. Estimations of chlorophyll *a* production from DO or pH data are reasonably good and exhibit the same trend as the measured chlorophyll a values. These analyses suggest that common chemical representations of algae and equilibrium calculations may be adequate to describe algal productivity and decay in the San Joaquin River. Dissolved oxygen uptake and pH response associated with algal processes could be incorporated in the algae-zooplankton models independent of Task 8.

Data interpretation with a numerical model

A number of causes for the decline of the algal community below Mossdale have been identified by inspecting the data sets. These appear to include zooplankton grazing, the reduction of available light associated with increased river depth below Mossdale, and dispersion associated with tidal flows. No single mechanism is dominant in the 2005, 2006 and 2007 data sets; however, light limitation and zooplankton grazing appear to be the primary causes for the decline in chlorophyll a concentrations below the HOR. Light has been identified as the limiting factor for algal productivity in the San Joaquin River because available nutrient concentrations are typically very high (Lehman, 2002). Figure 49 shows the approximate thalweg bathymetry of the San Joaquin River from Vernalis to the DWSC and illustrates the relative depth of the river above and below Mossdale. Above Mossdale the average river depth is almost entirely within the photic zone. However, below Mossdale the average depth increases from 5 to 20 ft. Thus algae in the well-mixed San Joaquin River above the DWSC may be in then 5 ft thick photic zone only 25 percent of time for a river depth of 20 ft. A more comprehensive analysis follows.

The development of a numerical water quality model was initiated to assess the contribution of depth and zooplankton grazing on the algae concentrations. Below Mossdale, the depth of the San Joaquin River increases steadily from about 5 ft to 20 ft at the Port of Stockon (rm39.0) as shown in Figure 49. The dyed parcel of water tracked during the Lagrangian measurements (Task 8.2) was considered to be well-mixed from Vernalis to the DWSC, a characteristic supported by water quality parameter vertical profiles. Except during brief 15 to 30-minute periods when tidal flows reverse direction a well-mixed water profile appears valid.

A relatively simple numerical model was developed to assist with the interpretation of the Lagrangian monitoring results. The concentration of chlorophyll *a,* pheophytin *a*, and zooplankton were simulated along the 31 mile reach between Vernalis and the DWSC. The governing ordinary differential equations appearing below were solved simultaneously with Matlab (The Mathworks, Inc.).

$$\frac{dChla}{dt} = k_g Chla - k_{da} Chla - k_{gz} Chla$$

$$\frac{d(Pha)}{dt} = -A_{c\to p} k_{da} Chla - k_{gz} Pha - k_{dp} Pha$$

$$\frac{dZoo}{dt} = A_{ca}\eta \frac{Chla}{k_{sa} + Chla} C_{gz} (Chla + Pha) \cdot Zoo - k_{dz} Zoo$$

Where:

$Chla$	= the chlorophyll *a* concentration,
Pha	= the pheophytin *a* concentration,
Zoo	= the zooplankton concentration in the dyed water,
k_g	= the algal growth rate, a function of temperature, light and nutrients,
k_{da}	= the algal decay rate,
k_{gz}	= the zooplankton grazing rate on the algae,
$A_{c\rightarrow p}$	= the conversion factor of chlorophyll *a* decay to pheophytin,
k_{dp}	= the pheophytin *a* decay rate,
A_{ca}	= is the ratio of carbon to chlorophyll *a,*
η	= is the grazing efficiency,
C_{gz}	=zooplankton grazing rate, and
k_{dz}	=the zooplankton decay rate.

The algal growth rate constant is a function of temperature, light, and nutrients. Temperature corrections to k_g were performed with:

$$k_{g,T}(temp, nutrients, light) = k_{g,20}\phi_{nutrients}\phi_{light},$$

$$k_{g,T} = k_{g,20}1.066^{T-20},$$

and $\phi_{nutrients}$ and ϕ_{light} are attenuation factors associated with nutrient and light inhibition on the growth rate. For nutrients, a Michaelis-Menten term is used to reduce growth relative to the limiting nutrient of the system,

$$\phi_{nutrients} = \frac{C_{LN}}{k_{s,LN} + C_{LN}},$$

where C_{LN} and $k_{s,LN}$ are the concentration of the limiting nutrient and half-saturation constant for the limiting nutrient (e.g., carbon, nitrogen (5-20 µgN L^{-1}), phosphorus (1-5 µgP L^{-1}), silica(20-80 µgSi L^{-1})), respectively. For the simulations presented here, measured concentrations in the San Joaquin River between Vernalis and the DWSC are generally well above the half-saturation concentrations (Lehman, 2001) and therefore are not expected to significantly limit algal growth in the study reach. Monitoring of these nutrients during 2007 again exhibited high non-limiting concentrations.

The influence of light was simulated to be dependent on the,

1. growth rate dependence on light intensity,
2. diurnal surface-light variation,
3. light attenuation with depth.

To account for algal growth inhibition at high intensities, the light intensity attenuation factor, ϕ_{light} is expressed in terms of the intensity I (Steele, 1965),

.

$$\phi\{I(z,t)\} = \frac{I(z,t)}{I_s} e^{-\frac{I(z,t)}{I_S}+1},$$

where I_s is the optimal light level. The intensity, I, is a function of the time and the depth in the water column, z.

Suspended particles, including algae, attenuate the light intensity exponentially with depth,

$$I(z) = I_0 e^{-k_e h},$$

where, I_0 is the light intensity at the water surface, and k_e is the exponential extinction coefficient, which can be approximated by the Secchi-disk depth (SD),

$$k_e = \frac{1.8}{SD}.$$

Substituting the light extinction equation into the growth equation:

$$\phi\{I(h,t)\} = \frac{I_0(t)e^{-k_e h}}{I_s} e^{-\frac{I_0(t)e^{-k_e h}}{I_S}+1},$$

A plot of $\phi\{I(z,t)\}$ is presented in Figure 50 and exhibits the sensitivity of the algal growth attenuation factor, and therefore, the algal growth rate, to the depth in the water. This profile was generated with a Secchi-disk depth of 2 ft; measurements are frequently less than 2 ft in the Task 8 study reach. The plot suggests that the algal growth rate is less than 5 percent of the optimum rate at depths below 5 ft between Vernalis and the DWSC.

Integrating with respect to the total water depth, H,

$$\phi_L = \frac{2.718}{k_e H}(e^{-\alpha_1} - e^{-\alpha_0})$$

$$\alpha_0 = \frac{I_0(t)}{I_s}$$

$$\alpha_0 = \frac{I_0(t)}{I_s} e^{-k_e H}$$

yields an expression for evaluating the influence of the attenuated light in the water column (Chapra, 1997). The effect on the growth rate with respect to the total water depth is presented in Figure 51.

The light intensity, I, will also vary during the day, and was characterized with the half-sinusoid,

$$I(t) = I_{\max} \sin[w(t - t_r)]$$
$$t_r \le t \le t_s \quad ,$$

where t_r is the time of sunrise and t_s is the time of sunset. I(t) = 0 during the night. The angular frequency is a function of the photoperiod and the daily period,

$$w = \frac{\pi}{fT_p},$$

where f is fraction of the photoperiod for the day and T_p is the daily period (e.g., 24 hr, 1 d). An approximation for the half-sinusoid was represented using a Fourier series (O'Connor and Di Toro, 1970)

$$I(t) = I_m\left(\frac{2f}{\pi} + \sum_{n=1}^{\infty} b_n \cos\left[\frac{2\pi n}{T_p}\left(t - \frac{fT_p}{2}\right)\right]\right)$$
$$b_n = \cos(n\pi f)\frac{4\pi / f}{(\pi / f)^2 - (2\pi n)^2}.$$

The advantage of using the Fourier series was that it was not necessary to manually turn the light on and off when solving the three governing equations simultaneously. Twenty terms were used to calculate the Fourier series approximation. An example of the series used in the simulations is shown in Figure 52 for a 24-hr day with a photoperiod fraction of 0.6.

Grazing

Losses due to zooplankton grazing are a function of the algae and zooplankton concentrations,

$$k_{gz} = C_{gz} Zoo,$$

where, C_{gz} and Zoo, are the grazing rate and zooplankton concentration respectively. Adjusting for temperature,

$$k_{gz} = k_{gz,20^\circ C}\theta_{gz}^{T-20},$$

adding a Michaelis-Menten term to account for the observed leveling off of the grazing rate at high chlorophyll *a* concentrations (Chapra, 1997) yields and adjusting for temperature yields,

$$k_{gz} = \frac{Chla}{K_{sa} + Chla} C_{gz} \theta_{gz}^{T-20} ZooChla$$

The overall formulation for the zooplankton grazing rate incorporates the grazing efficiency, η, zooplankton decay, k_{dz}, and algal biomass carbon to chlorophyll *a* mass ratio, A_{ca}, yielding a final equation for simulating the effect of zooplankton grazing on algae,

$$\frac{dz}{dt} = A_{ca} \eta \frac{Chla}{k_{sa} + Chla} C_{gz} ZooChla - k_{dz} Zoo \, .$$

Table 6 contains the parameters introduced above and representative values.

Figure 53 shows the sensitivity of algal productivity as a function of river depth in the absence of zooplankton grazing. The simulation was conducted for a 50-hour travel time from Vernalis to the DWSC, similar to flow conditions observed in September, 2005. The initial concentrations of chlorophyll a, pheophytin a and zooplankton were assumed to be 100 μg L^{-1}, 0 μg L^{-1}, and 3.0 μgC L^{-1}, respectively. Two of the simulations assume the river is of fixed depth at either 5 or 20 ft. At a constant 5 ft depth, chlorophyll a concentrations remain high, with growth during the day and decay during the night. However, if the San Joaquin River were of a constant 20 ft depth, chlorophyll *a* concentrations continue to decline from Vernalis to the DWSC. Using the actual mid-river depth for the simulation yields an increase in the chlorophyll *a* concentration for the first 9 hours of daylight. As shown previously in Figure 49, the average river depth is about 5 ft during this time. After 20 hours, the water parcel is beyond Mossdale, CA, the point at which river depth increases and tidal flows become more significant. From 20 to 50 hours the chlorophyll *a* continues to decline due to the effect of increased river depth on the algal growth rate.

The potential effect of zooplankton grazing is shown in Figure 54. The two upper curves simulate depth effects without grazing as shown previously in Figure 53. The lower curve simulates the additional reduction in chlorophyll *a* associated with zooplankton grazing. These simulations suggest that river depth and zooplankton effects can account for the 50 percent reduction in chlorophyll *a* that is commonly observed between Mossdale and the DWSC during periods of low net flow. Measurements presented in the Task 9 interim report indicate that relatively low concentrations of zooplankton are present above Mossdale, but populations were observed to increase significantly as the water approached the DWSC. The zooplankton population growth is also simulated by the model as shown in Figure 55. These modeling efforts appear to support the general observed trends in chlorophyll *a*, pheophytin *a* and zooplankton shown earlier for the Lagrangian monitoring conducted in 2005, 2006, and 2007.

The observed concentrations of extracted chlorophyll a and pheophytin a, and zooplankton are presented in Figure 56 for August, 2005 Lagrangian monitoring. The model simulations are superimposed as solid lines on the graph. Simulations yield reasonable but not perfect fits to the observed data. Algal concentrations increase during

daylight hours, and decrease at night. However, beyond 25 hours (rm50) the chlorophyll *a* concentrations attenuate from approximately 40 to 20 $\mu g\ L^{-1}$. The last sharp decline in chla is probably associated with dispersion of low chlorophyll *a* water from the DWSC mixing with higher chlorophyll *a* water entering from the San Joaquin River. The model developed here doesn't consider dispersion and therefore, may be incapable of accurately simulating algal pigment concentrations with approximately 1 mile of the DWSC. A corresponding increase in pheophytin *a*, the degradation product of chlorophyll *a*, occurs during this decline. Zooplankton concentrations also increase dramatically below rm50, suggesting that grazing is a significant mechanism for algal decline.

Measured concentrations of algal pigments and zooplankton are again compared with model simulations for the June, 2007 Lagrangian tracking in Figure 57. The simulation yields good fits to the observed chlorophyll a and pheophytin a concentrations, and a reasonable simulation to most of the zooplankton measurements. The numerical model presented here was not developed as a predictive tool, but instead to quantitatively estimate the contribution of light attenuation and zooplankton grazing to the behavior of algae being transported by flow to the DWSC. The simulations shown here support the conclusion that light attenuation and zooplankton grazing can account for most of the algal dynamics above the DWSC. This exercise may also assist in developing accurate algorithms for a more comprehensive model of the San Joaquin River. These algorithms could be incorporated into a comprehensive water quality management model to evaluate land use practices, pollutant control strategies, and water routing operations in the San Joaquin River watershed.

Summary and Conclusions

A three-year field study has been completed to evaluate algal productivity and decay between Vernalis and the Stockton DWSC. The monitoring approach relied on measuring parameters at fixed locations while simultaneously tracking water quality and algal changes in a dyed parcel of water flowing to the DWSC. Oxygen demands, algal productivity and decay, and zooplankton grazing were also characterized with isolated batch microcosm experiments. Task 9 augments this work by identifying and enumerating phytoplankton populations for assessing changes in species composition within the study reach. In addition, Task 9 identifies and quantifies zooplankton and bi-valve populations to evaluate the impacts of grazing on algae flowing to the DWSC and South Delta.

High flows in the San Joaquin River during 2005 and 2006 delayed the start of major field components until July of these years. The resources originally assigned for May and June were rescheduled to later months when lower, more representative flows occurred. Eight dye tracking field trials were performed in 2005, 2006 and 2007. When the net flow entering the DWSC approached zero, the Lagrangian monitoring approach was no longer feasible and as part of an adaptive management plan an additional six longitudinal monitoring events were conducted in July, August, and September of 2007.

The causes for the decline of the algal community below Mossdale were identified by inspecting data sets, estimating losses of chlorophyll *a* associated with zooplankton grazing using microcosm experiments, and developing an algal growth and decay model and conducting model simulations. Inspection of the data indicated that several different mechanisms are responsible for the decline in algae between Mossdale and the DWSC. These include dispersion, settling, light limitation, and zooplankton grazing. Nutrient limitation did not appear to be significant as concentrations of available phosphorus, nitrogen and silica were relatively high and constant between Vernalis and the DWSC.

Settling and dispersion become more significant within 1 or 2 miles above the DWSC. High resolution vertical profiles of turbidity, chlorophyll a, temperature and other perimeters indicate that tidal velocities are sufficiently high to provide a vertically mixed water column above the DWSC under most conditions. Review of tidal flows above the DWSC show that the flow direction reverses quickly from flood to ebb tide. As such, settling is possible during brief periods of the tidal cycle, but tidal flows quickly reestablish a vertically-mixed profile and permanent deposition is limited. Some data do suggest that zooplankton grazing may increase during short durations of low river velocity, but evidence for this phenomenon is limited and requires further investigation. However, zooplankton grazing was found to be important, but quantification of grazing rates during brief periods during tidal flow reversals was not attempted, but instead averaged into an overall grazing mechanism.

The Lagrangian dye tracking and rhodamine dye releases that were monitored at fixed locations in the tidal reach above the DWSC showed that the front of a dyed plume

remained relatively sharp even though the peak concentration in the plume was well attenuated. Dispersion appeared to have the greatest effect on the chlorophyll *a* concentration when a tracked plume actually entered the DWSC on an ebb tide, mixed with water of the DWSC, and then returned to the upper river during the flood tide. Model simulations of a dye plume moving down the San Joaquin River from Vernalis were also consistent with experimental observations, exhibiting a sharp-front plug driven by advective river or tidal flow (see Appendix B). Chlorophyll *a* decreases near the DWSC due to dispersion is evident in some of the Lagrangian data sets, but it was not quantified. However, data sets of rhodamine dye plumes are available for future model calibration efforts.

The two dominant mechanisms for the decline of chlorophyll *a* in the San Joaquin River below Mossdale are associated with the reduction of available light associated with increased river depth and zooplankton grazing. Above Mossdale, the average depth of the San Joaquin River is approximately 5 feet under low flow conditions. Suspended particles, including sediments and algae, rapidly attenuate the light penetrating the water column. Between Vernalis and the DWSC one percent of the ambient light is measured at a depth of 4 to 5 feet. Below this light threshold, little algal photosythesis occurs. As such, above Mossdale where shallow reaches prevail, algae are usually in the photic zone of the water column and production associated with photosynthesis is sufficient to maintain a physiologically viable community. However, below Mossdale, the San Joaquin River increases in depth, to approximately 20 ft at Navy Bridge. The photic zone remains limited to the upper 4 or 5 feet by suspended, light-scattering matter, but in the vertically mixed San Joaquin River above the DWSC, the algae reside for a portion of the daytime in darkness. As a simple example, for a river depth of 15 feet and a photic zone of 5 ft, the algae will spend approximately one-third of the daylight hours in darkness. An analytical model was developed to quantify the effect on algae in the San Joaquin River flowing to the DWSC. Using measured and common modeling parameters, the effect on the algae associated with the reduction of light due to river deepening was estimated to reduce chlorophyll *a* by 20 to 50 percent. Low net flows to the DWSC yield long travel times from Mossdale to the DWSC and increase the effect of light limitation associated with increased river depth. At extremely low net flows, model simulations indicate that algae species common to the San Joaquin River above Mossdale are not sustainable below Mossdale.

Zooplankton grazing on algae was also found to be a significant cause for the decline in chlorophyll *a* below Mossdale. Zooplankton populations were observed to increase dramatically between the HOR and the DWSC if net flows were sufficiently low to provide enough residence time for community development. Microcosm experiments estimated that zooplankton grazing rates were consistent with literature values. At these rates and sufficient residence time, zooplankton grazing alone could deplete an algal community. Depending on the net flow to the DWSC, zooplankton grazing could reduce chlorophyll *a* concentrations by 20 to over 80 percent while the algae are transported from the HOR to the DWSC. Similar to the light limiting effects on algae associated with increased river depth, at extreme low net San Joaquin River flows to the DWSC zooplankton grazing can dramatically reduce algal communities. This was observed in

July, August, and September of 2007 when net flow to the DWSC was approximately zero. Chlorophyll *a* concentrations were observed to decline by 80 to 90 percent between the HOR and the DWSC. Using residence time, measured zooplankton grazing rates, and observed zooplankton concentrations, simple grazing calculations can explain most of the loss of algae in this reach.

Biochemical oxygen demands entering the DWSC were correlated to the chlorophyll *a* concentration in 2007, but not in 2005 and 2006. Net flows to the DWSC in 2005 and 2006 were abnormally high and may be one of the causes for the poor correlation of algal biomass to the BOD. Improved treatment of wastewater effluent discharged to the San Joaquin River from the City of Stockton in 2007 may also influence the improved BOD correlation to chlorophyll a for 2007 by reducing non-algal oxygen demanding substances. The monitoring performed for 2007 captured data during a 2 month period in which the net flow entering the DWSC was approximately zero. During this time, it appears that the most concentrated zooplankton community developed approximately 8 miles upstream of the DWSC to feed on fresh algae carried below the HOR during ebb tidal flows. Measurements of ultimate BOD from HOR to the DWSC also show a dramatic decline that is well correlated with algal pigment concentrations. During July and August of 2007 when there was no net flow to the DWSC, the ultimate BOD decrease from approximately 20-25 mg L^{-1} to 5 mg L^{-1} at the DWSC. Thus, approximately 75 to 80 percent of the oxygen demand was exerted above the DWSC and not in the DWSC. During this time the dissolved oxygen concentration in the DWSC remained above the water quality objective of 5 mg L^{-1} during most of July and August. These observations may support the idea that control gates at the HOR could be used to effectively to reduce oxygen demanding loads from entering the DWSC at critical times.

In addition, the light-dark bottle experiments suggest that algal productivity can be predicted with either pH or dissolved oxygen measurements using chemical stoichiometry and equilibrium calculations. This approach could be applied to the river data and combined with light intensity measurements to simulate the algal productivity and respiration between Vernalis and the DWSC. A simple numerical model was developed for evaluating the coupled behavior of chlorophyll *a*, pheophytin *a*, and zooplankton populations between Vernalis and the DWSC. Simulations are generally consistent with the observed data and support the conclusions that the light limiting effect on algal growth increases significantly with river depth and zooplankton grazing can effectively clear algae from the water column. The simulations also suggest that the algae community can experience a continued state of decline with either mechanism. Under this condition, the algae community entering the DWSC is not sustainable and the degree to which algae decreases between the HOR and the DWSC is controlled by the travel time in this reach. These observations suggest that it is important to include light limiting algorithms associated with increased river depth and zooplankton grazing in dissolved oxygen simulation models of the San Joaquin River below Mossdale in order to successfully predict dissolved oxygen concentration in and oxygen demands to the DWSC.

Acknowledgements

The study team gratefully acknowledges the California Bay-Delta Authority for project funding. Special thanks are extended to Dr. William Stringfellow for his interest and support in extending the zooplankton monitoring work through 2007. Also important to this project was the nutrient analyses performed by Remie Burks and Chelsea Spier with subsequent data review by Dr. Sharon Borglin of the Environmental Engineering Research Program at the University of the Pacific.

References

APHA, 2005. Standard Methods of the Examination of Water and Wastewater, 21th Edition. 2005. American Public Health Association, Washington, DC.

APHA, 1998. Standard Methods of the Examination of Water and Wastewater, 20th Edition. 1998. American Public Health Association, Washington, DC.

Bowie, G.L., Mills, W.B., Porcella, D.B., Campbell, C.L., Pagenkopf, J.R., Rupp, G.L., Johnson, K.M., Chan, P.W.H., Gherini, S.A. and Chamberlin, C.E. 1985. Rates, Constants, and Kinetic Formulations in Surface Water Quality Modeling. U.S. Environmental Protection Agency, ORD, Athens, GA, ERL, EPA/600/3-85/040.

Chapra, 1997. *Surface Water–Quality Modeling*, McGraw-Hill: New York.

Foe, C., M. Gowdy, and M. McCarthy, 2002. Draft Strawman Allocation of Responsibility Report, California Regional Water Quality Control Board, Central Valley Region, January, Sacramento, CA.

Jones & Stokes, 2002. Evaluation of Stockton Deep Water Ship Channel Model Simulations of 2001 Conditions: Loading Estimates and Model Sensitivity, Prepared for the CALFED Bay-Delta Program 2001 Grant 01-N61, Sacramento, CA

Jones & Stokes, 2001. "City of Stockton Year 2000 Field Sampling Program Data Summary", Prepared for the City of Stockton, Sacramento, CA.

Jones & Stokes, 1998. *Potential solutions for achieving the San Joaquin River dissolved oxygen objectives*. Prepared for the City of Stockton Department of Municipal Utilities, Sacramento, CA.

Lehman, P. 2001. "The Contribution of Algal Biomass to Oxygen Demand in the San Joaquin River Deep Water Channel", Final Draft Report, San Joaquin River Dissolved Oxygen TMDL Steering Committee, Department of Water Resources, Central District, Sacramento, CA.

Lehman, P. W., Sevier, J., Giulianotti, J., and Johnson, M. (2004) Sources of Oxygen Demand in the Lower San Joaquin River, California. *Estuaries* **27**(3), 405-418.

Lind, C.J. 1970. U.S. Geological Survey Professional Paper 700D, pp. D272-D280.

Litton, G.M., 2002. "Sediment Deposition Rates and Oxygen Demands in the Deep Water Ship Channel of the San Joaquin River, Stockton, CA", Prepared for CALFED Bay-Delta Program 2001 Grant 01-N61-005, University of the Pacific, Stockton, CA.

Pace, M. L. and Orcutt, Jr., J. D. (1981) The relative importance of protozoans, rotifers, and crustaceans in a freshwater zooplankton community. *Limnology and Oceanography* **26**(5), 822-830.

O'Connor, D.J. and Di Toro, D.M. 1970. Photosynthesis and Oxygen Balance in Streams. *J. San. Engr. Div. ASCE* 96(2), 547-571.

Quinn N. W. T. and A. Tullock, 2002. "San Joaquin River Diversion Data Assimilation, Drainage Estimation and Installation of Diversion Monitoring Stations. Prepared for the CALFED Bay-Delta Program 2001 Grant 01-N61.

Russell, L.L. 1976. Chemical Aspects of Groundwater Recharge with Wastewaters, Ph.D. Thesis, University of California, Berkeley, December.

Snoeyink, V.L. and D. Jenkins, 1980. *Water Chemistry*. Wiley & Sons, New York, 463p.

Steele, J.H. 1965. Notes on Some Theoretical Problems in Production Ecology. In *Primary Production in Aquatic Environments,* C.R. Goldman, ed., University of the California Press, Berkeley, CA.

Stumm W. and J.J. Morgan, 1996. Aquatic Chemistry, 3rd ed., Wiley & Sons: New York.

Task 8 Tables

Table 1: Dates and locations of the Lagrangian tracking trials performed during 2005, 2006 and 2007.

Dates	Start Location/ Time	End Location/Time	Total Travel Time (hr)
July 13-14, 2005	VNS 12:12	DWSC 18:30	30.5
August 16-18, 2005	VNS 13:35	DWSC 13:58	48.4
Sept. 15-17 , 2005	VNS 9:39	DWSC 11:54	50.2
October 13-15, 2005	VNS 9:10	DWSC 00:15	38.6
July 19-21, 2006	VNS 18:10	DWSC 10:06	40.0
August 9-10, 2006	HOR 9:04	DWSC 10:48	25.8
June 12-15, 2007	VNS 8:39	DWSC 2:15	65.5
July 19-20, 2007	VSN 10:45	MSD 9:30	22.8

VRN: Vernalis (SJR River Mile 71.9)
MSD: Mossdale boatramp (SRJ River Mile 56.7)
HOR: Head of Old River (SJR River Mile 54.0)
DWSC: Stockton Deep Water Ship Channel (SJR River Mile 39.8)

Table 2. Schedule of longitudinal monitoring runs and lagrangian tracking or tracer release events for 2007.

Date	Vernalis Flow (cfs)	Net Flow to DWSC[1] (cfs)	Range of Longitudinal Profiles SJR River Miles	Tide conditions	Zooplankton collected	Date and time of dye release
6/12/2007 to 6/15/2007	2223 1858	873 652	Lagrangian tracking from rm71.9 (Vernalis) to rm 39.8 (DWSC)	n/a	yes	6/12/2007 (8:37)
7/16/2007 7/17/2007	1100 997	15 7.3	rm39.8 (7/16 22:49) to rm 54 (0:51) rm39.8 (7/17 3:49) to rm 54 (7/17 6:00) rm39.8 (7/17 8:45) to rm 54 (7/17 10:52) rm39.8 (7/17 15:36) to rm 54 (7/17 17:55)	flood ebb flood ebb	yes yes yes yes	n/a
7/19/2007 7/20/2007	989 968	0	Lagrangian tracking rm71.9(Vernalis) to rm56.7 (Mossdale)	n/a	yes	7/19/2007 10:45
8/14/2007 8/15/2007	1002 919	60 -51	rm39.8 (8/14 21:12) to rm 56.7 (23:45) rm39.8 (8/15 1:07) to rm 56.7 (8/15 3:10) rm39.8 (8/15 8:47) to rm 56.7 (8/15 11:08) rm39.8 (8/15 15:27) to rm 56.7 (8/15 17:53)	flood ebb flood ebb	yes yes yes yes	n/a
9/6/2007	993	21	rm34 (8:32) to rm56.7 (11:23)	ebb	no	n/a
9/19/2007 9/20/2007	939 926	246	rm34 (9/19 21:20) to rm56.7 (9/20 1:45) 39.6 (9/20 7:45) to 56.7 (9/20 10:30)	flood ebb	yes	9/20/2007 2:05

[1]Measured at the USGS Garwood Bridge Station (CDEC Station: SJG)

Table 3: BOD results for July 13-14, 2005 along the San Joaquin River.

Location River Mile	Sample No.	20 day results		
		BOD	CBOD	NBOD
68.4	SJR 1	6.0	4.0	2.0 / 33%
61.4	SJR 3	7.0	4.5	2.5 / 36%
55.6	SJR 5	7.0	4.5	2.0 / 29%
53.1	SJR 6	7.0	4.8	2.2 / 31%
46.7	SJR 9	6.2	4.3	1.9 / 31%
42.9	SJR 11	7.0	4.6	2.4 / 34%

Table 4: Initial and final DO, pH, and chlorophyll a July light-dark bottle experiment results.

Depth (ft)	Elapsed Time (hr)	DO (mg/L)		pH		Chlorophyll *a (ug/L)*	
		Start	End	Start	End	Start	End
1	4:45	8.63	14.32	7.92	9.05	54.1	88.0
2	4:40	8.60	13.38	7.92	8.94	54.1	85.4
3	4:30	8.59	10.5	7.97	8.43	54.1	70.9
dark	4:55	8.50	8.03	7.94	7.91	54.1	51.9

Table 5: Parameters used for numerical model simulations (Bowie, 1985, Chapra, 1997).

Parameter	Description	Units	Range	Common values	Simulation value
$k_{g,20}$	maximum algal growth rate	d^{-1}		2	2
k_{da}	algal decay rate	d^{-1}	0.01-0.5	0.1-0.2	0.36
A_{ca}	carbon-chlorophyll a ratio	gC $gChl^{-1}$	10-100	40	40
k_{dp}	pheophytin decay rate	d^{-1}	NR	NR	0.27
$A_{c \rightarrow p}$	Chlorophyll pheophytin ratio		NR	NR	1
C_{gz}	zooplankton grazing rate	L mgC^{-1} d^{-1}	0.5-5	1 - 2	0, 1.5
k_{dz}	zooplankton decay rate	d^{-1}	0.001-0.1	0.01-0.05	0.1
K_{sa}	zooplankton half-saturation	µgChl L^{-1}	2-25	5-15	10
η	grazing efficiency		0.4-0.8		0.5
I_s	optimal light intensity	ly d^{-1}		100-400	100

NR: none reported, simulation value based on measured losses and model fit by Litton (2002).

Task 8 Figures

Figure 1: The San Joaquin River between Vernalis and the Stockton Deep Water Ship

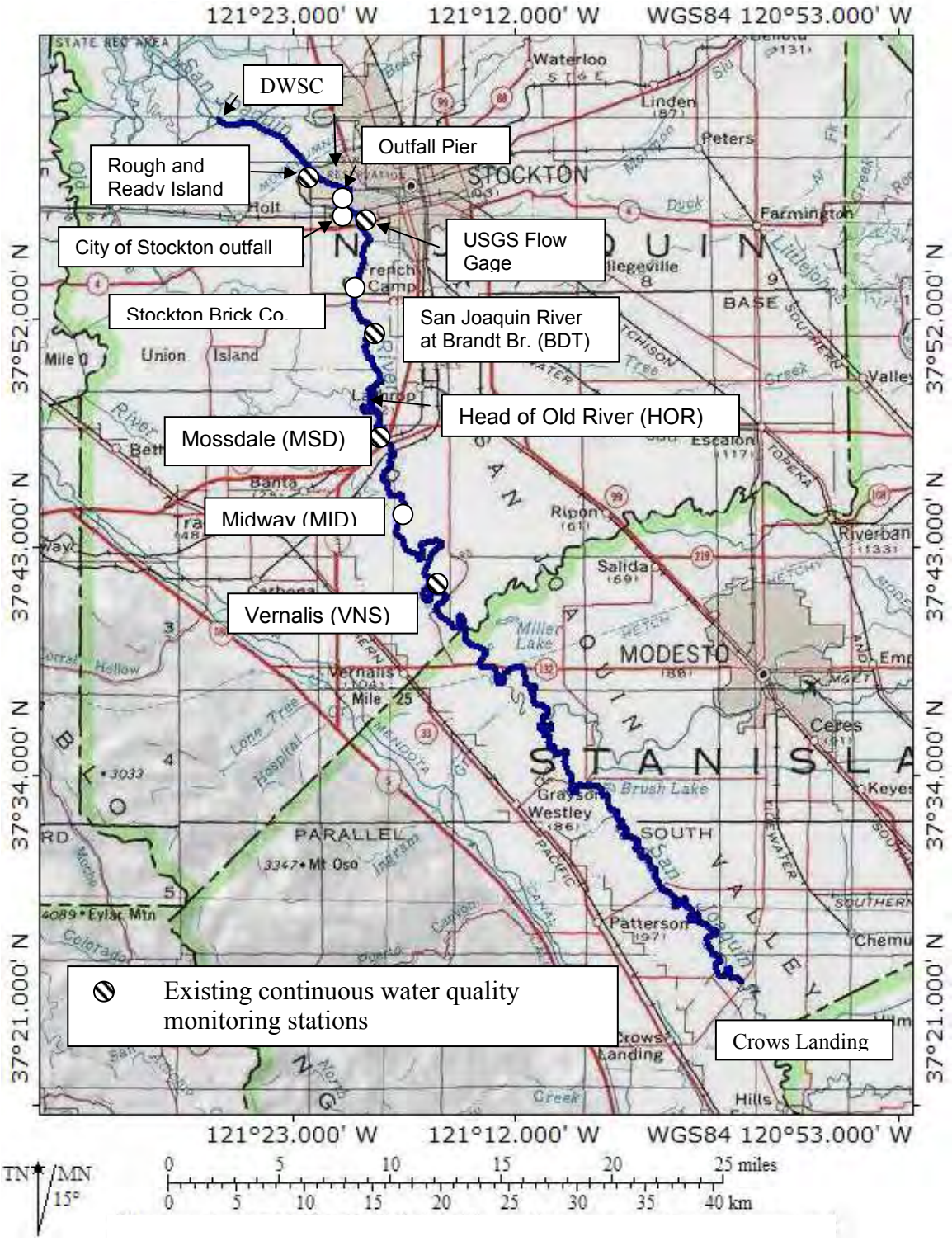

Figure 2: Monitoring boat and data acquisition system.

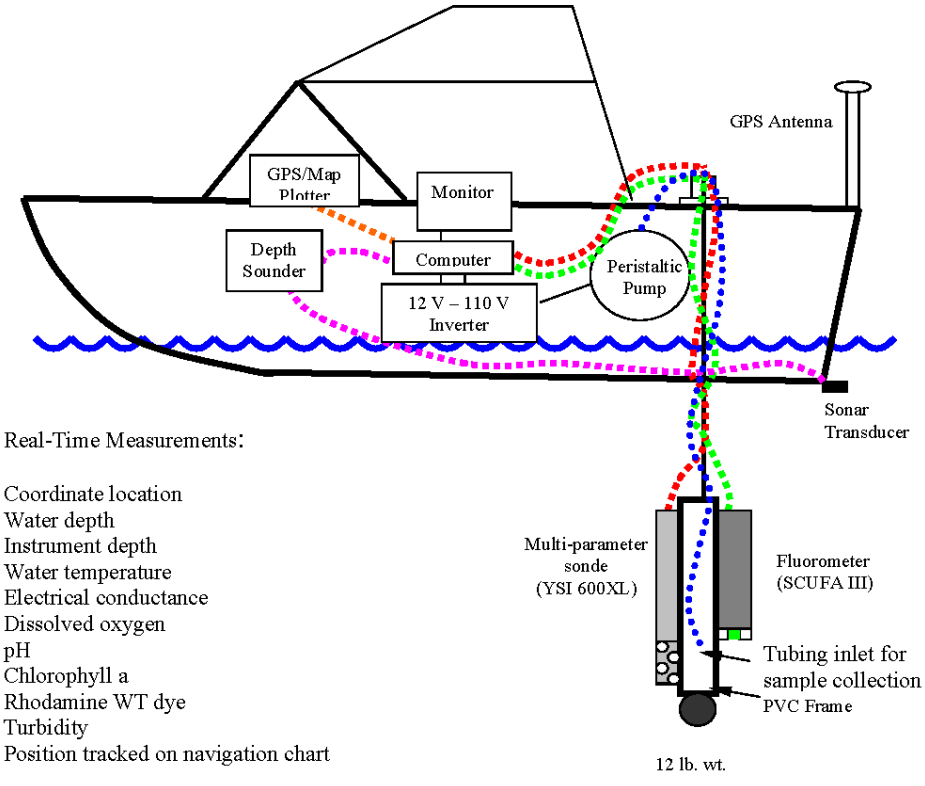

Real-Time Measurements:

Coordinate location
Water depth
Instrument depth
Water temperature
Electrical conductance
Dissolved oxygen
pH
Chlorophyll a
Rhodamine WT dye
Turbidity
Position tracked on navigation chart

Figure 3: San Joaquin River Flow at Vernalis for 2004 through 2007, and the Task 8 lagrangian monitoring trials performed during 2005, 2006, and 2007.

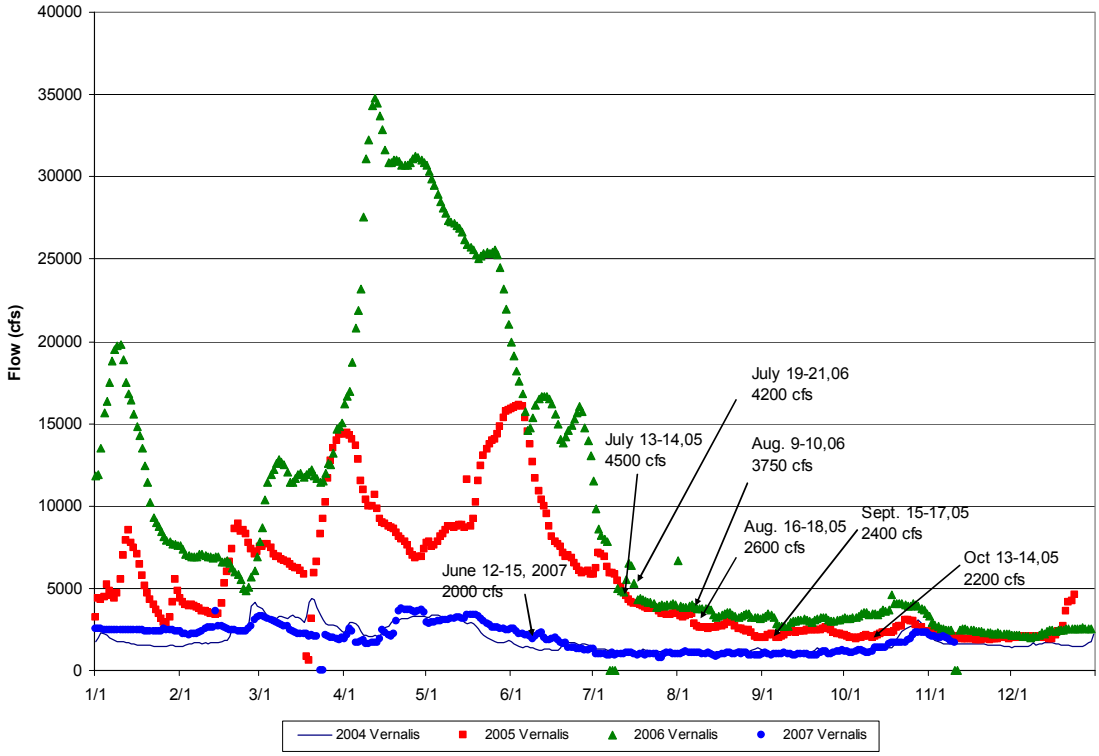

Figure 4: San Joaquin River flow at Vernalis and entering the DWSC (San Joaquin River at Garwood Bridge) during the 2005 monitoring.

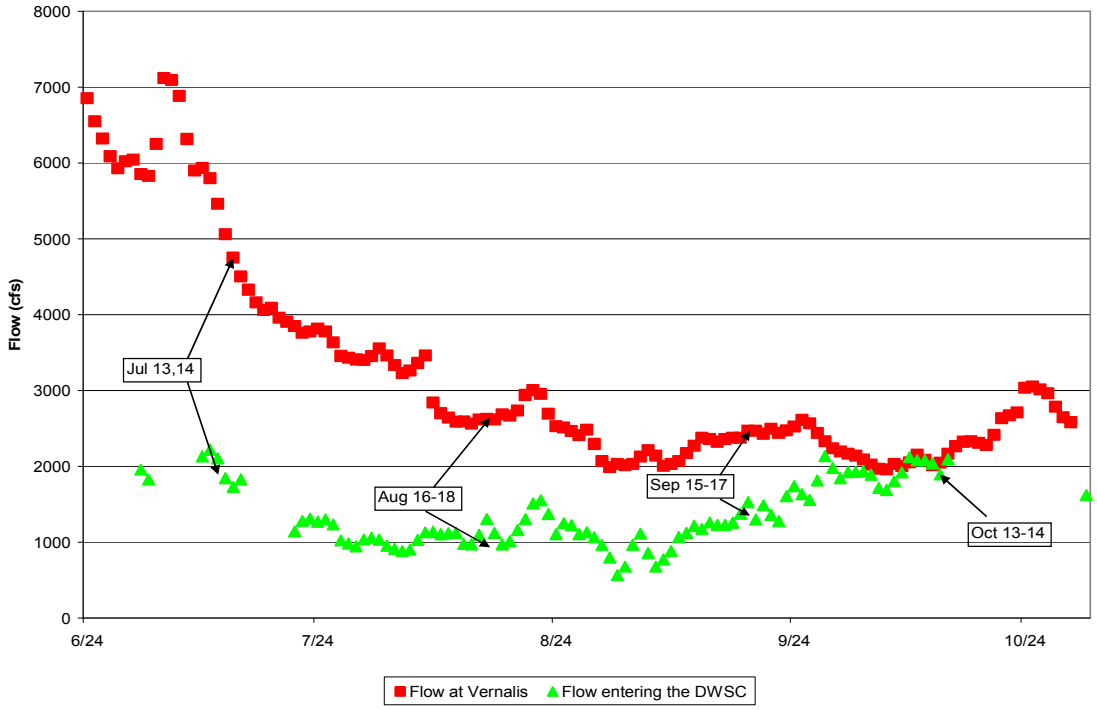

Figure 5: Flows at Vernalis and entering DWSC (measured at the Garwood Bridge station) during the 2006 monitoring.

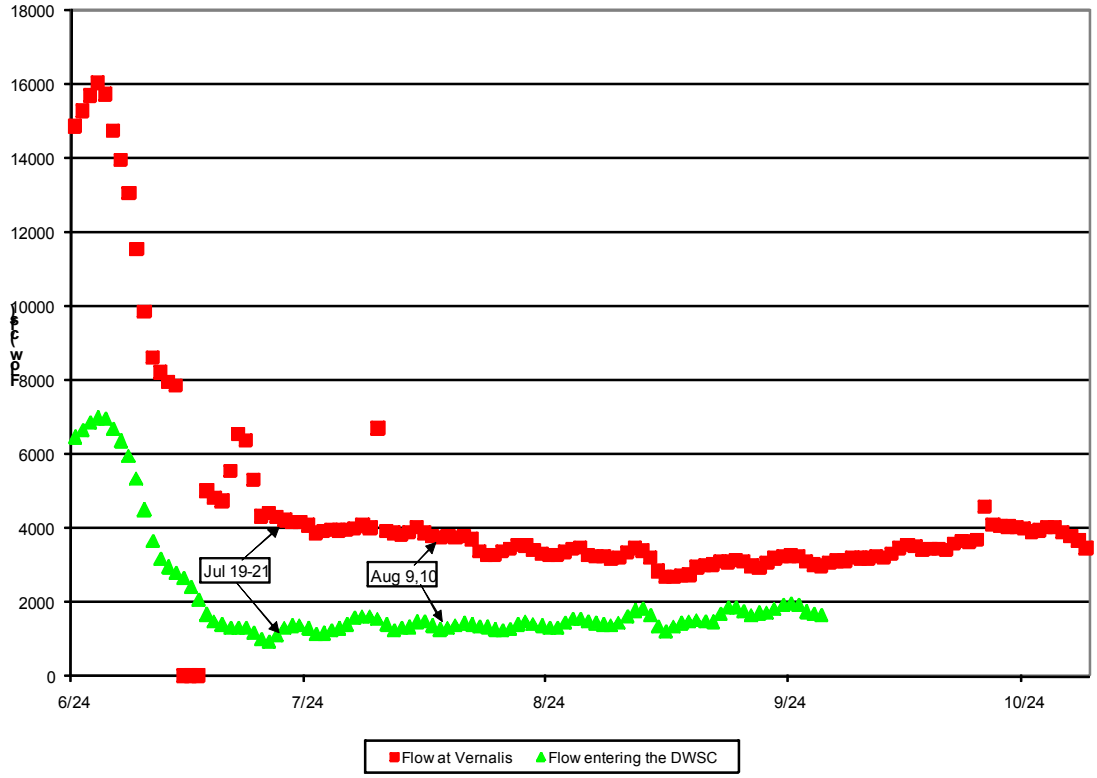

Figure 6: Flows at Vernalis and entering DWSC (measured at the Garwood Bridge station) during the 2007 monitoring. Lagrangian and longitudinal monitoring trails are also shown.

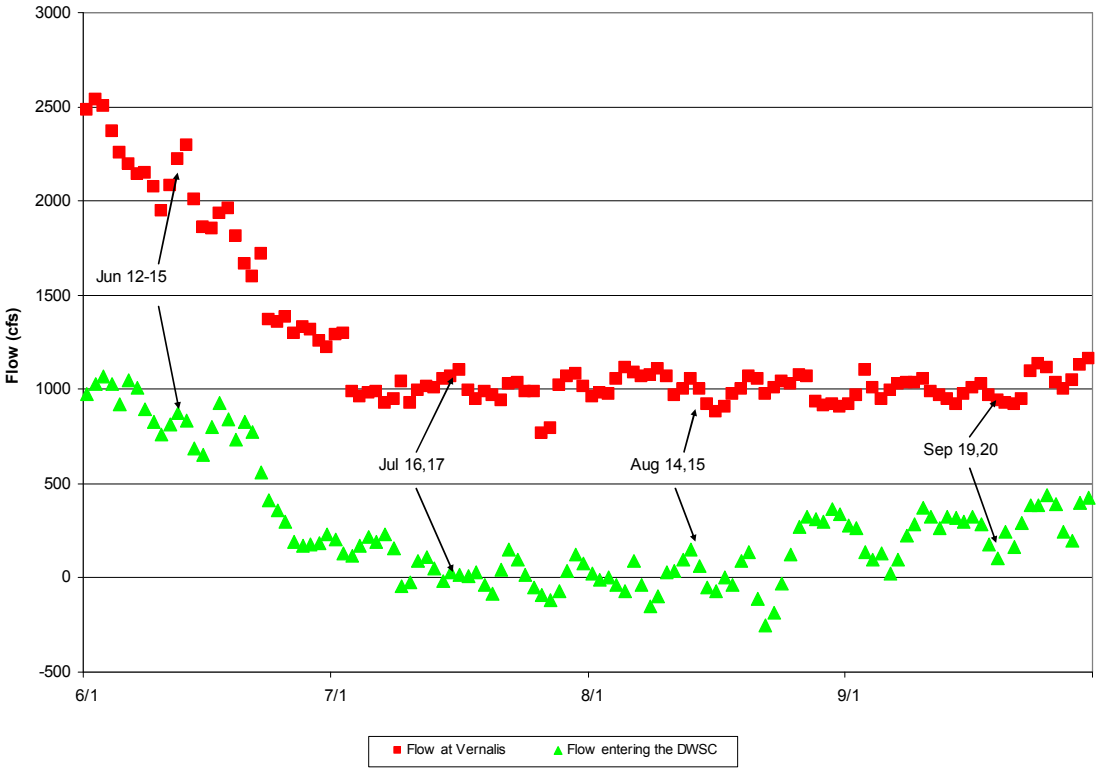

Figure 7: Dissolved oxygen, pH, and chl a measured midway between Vernalis and Mossdale on the San Joaquin River, July 11-15, 2005.

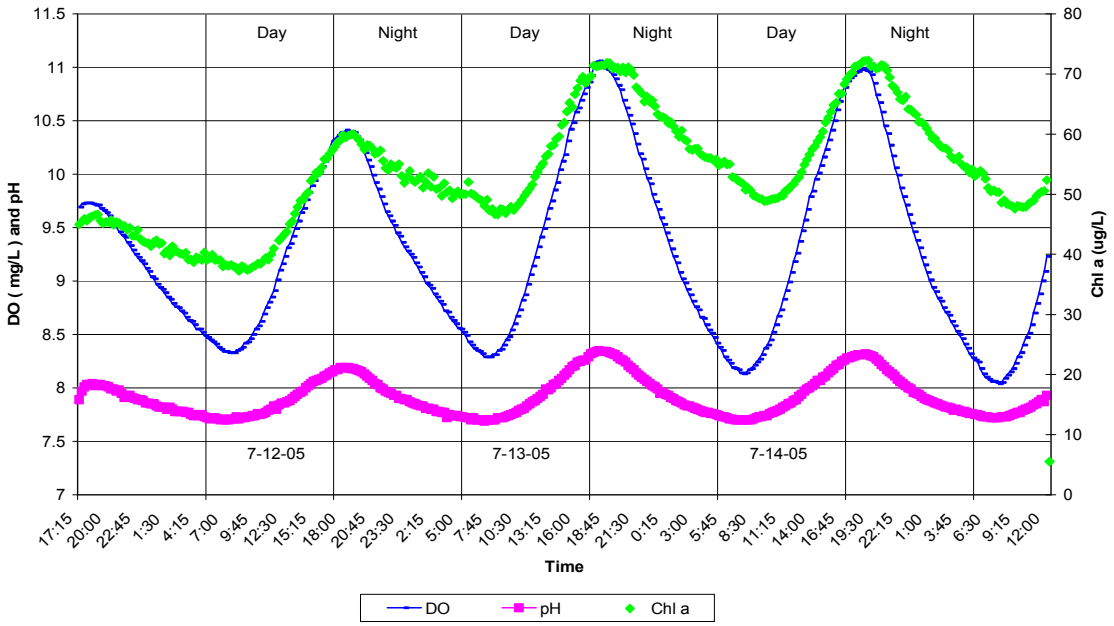

Figure 8: Dissolved oxygen, pH, and Chl a measured at Brandt Bridge on the San Joaquin River, July 11-15, 2005.

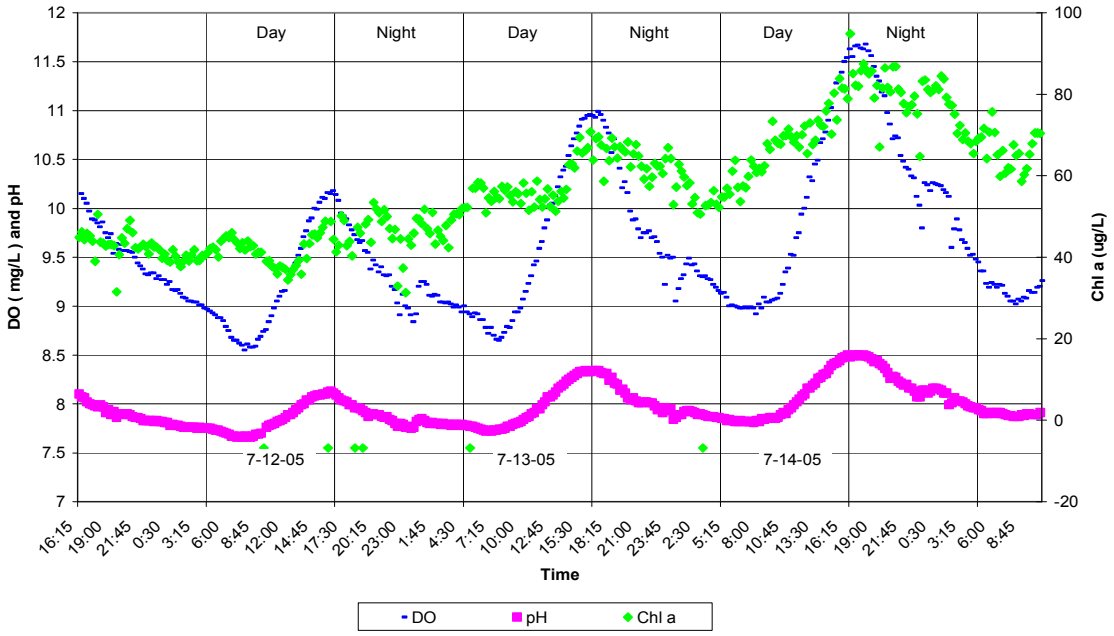

Figure 9: Pigment concentrations, dissolved oxygen, and pH within the rhodamine WT plume flowing from Vernalis to the DWSC, July 13-14, 2005.

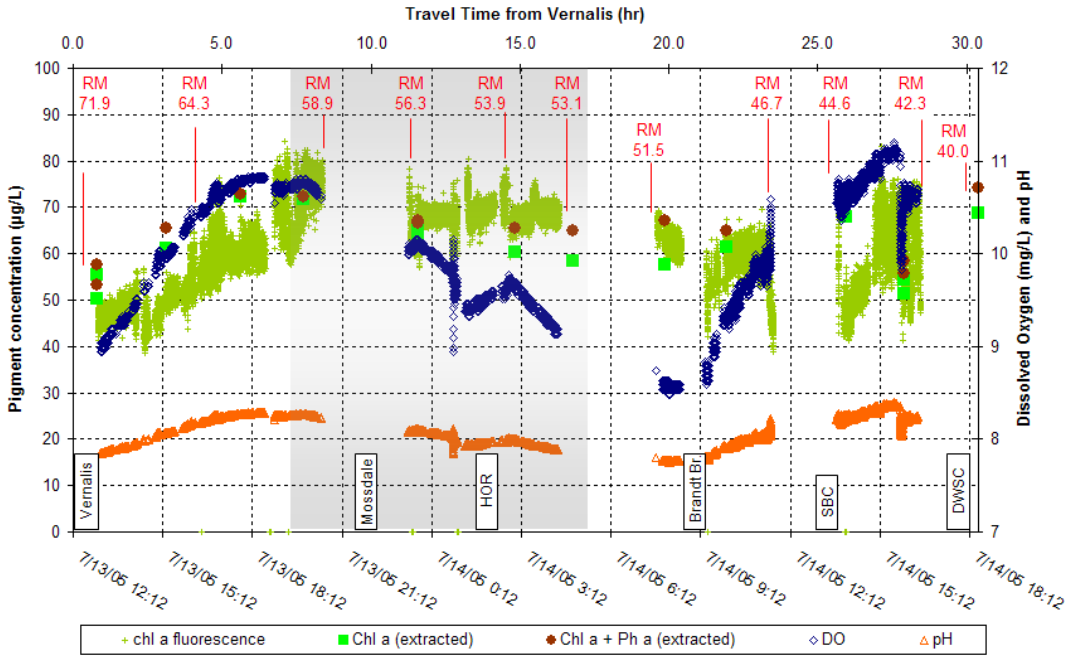

Figure 10: Extracted pigment concentration and the ch a/(chl a + ph a) fraction within the rhodamine WT plume flowing from Vernalis to the DWSC, July 13-14, 2005.

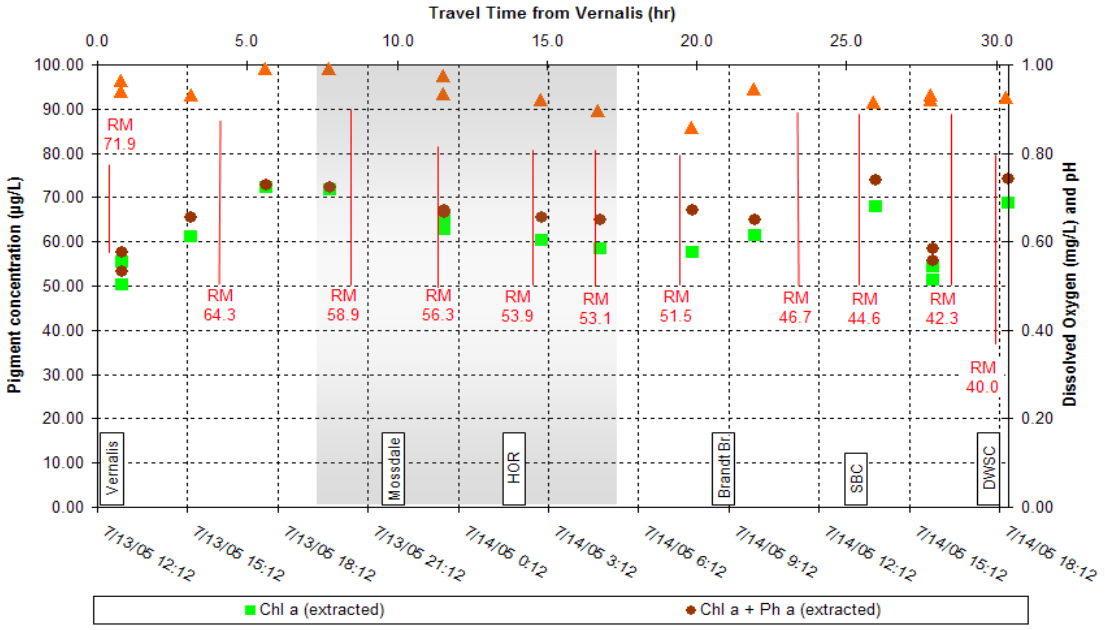

Figure 11: Pigment concentrations, dissolved oxygen, and pH within the rhodamine WT plume flowing from Vernalis to the DWSC, August 16-18, 2005.

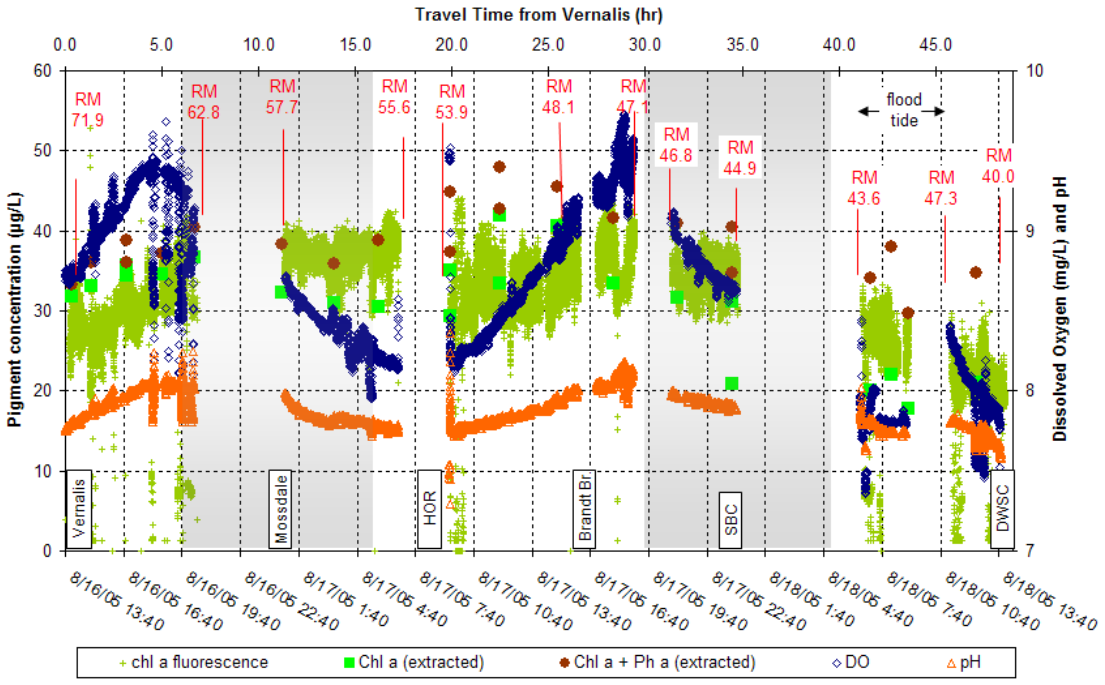

Figure 12: Extracted pigment concentration and the ch a/(chl a + ph a) fraction within the rhodamine WT plume flowing from Vernalis to the DWSC, August 16-18, 2005.

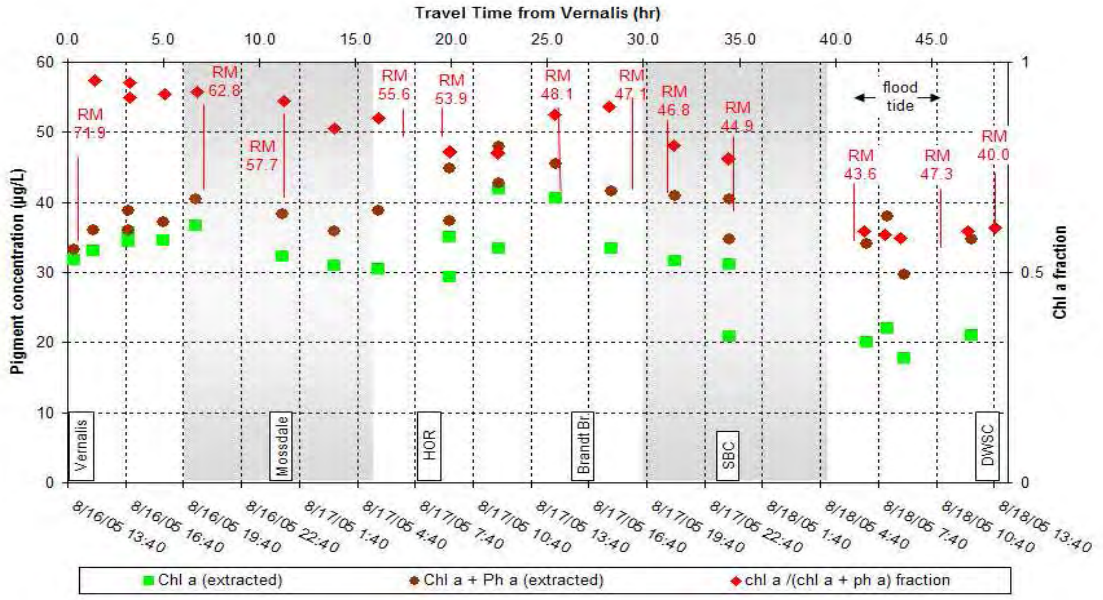

Figure 13: Pigment concentrations, dissolved oxygen, and pH within the rhodamine WT plume flowing from Vernalis to the DWSC, September 15-17, 2005.

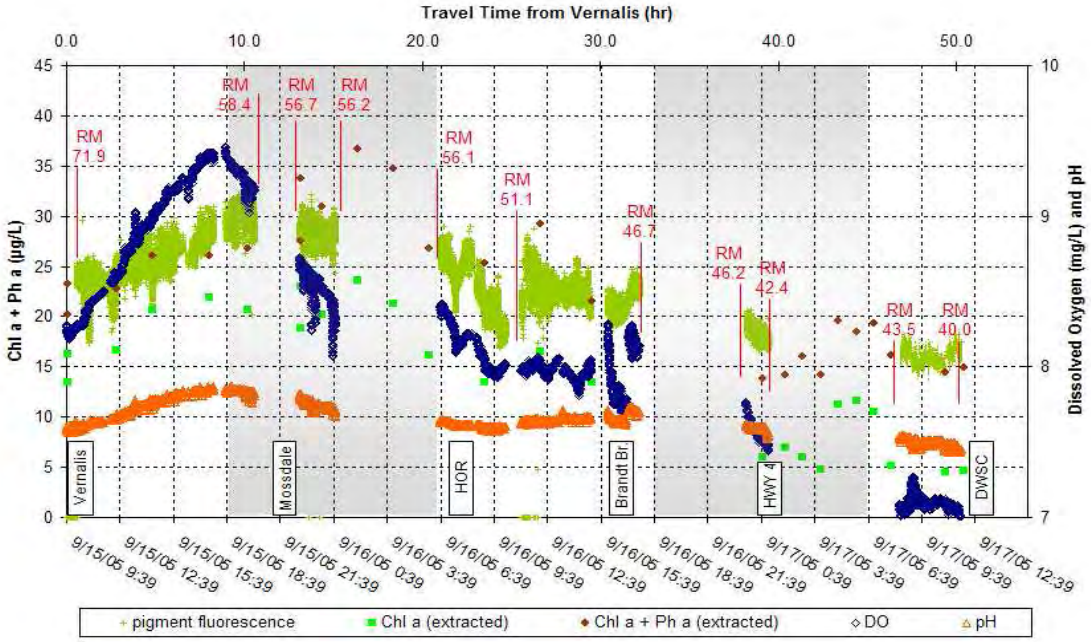

Figure 14: Extracted pigment concentration and the ch a/(chl a + ph a) fraction within the rhodamine WT plume flowing from Vernalis to the DWSC, September 15-17, 2005.

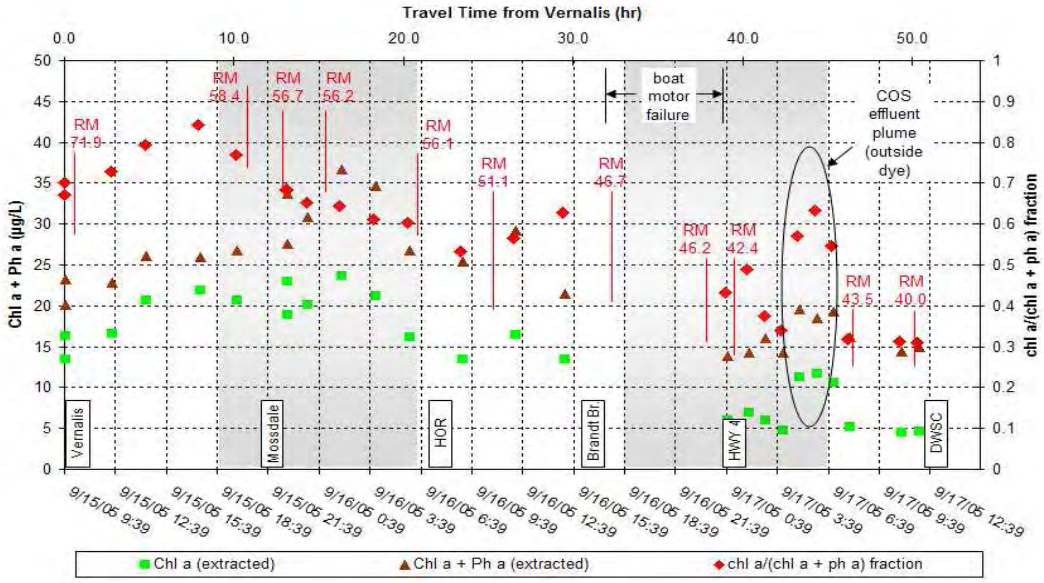

Figure 15: Pigment concentrations, dissolved oxygen, and pH within the rhodamine WT plume flowing from Vernalis to the DWSC, October 13-14, 2005.

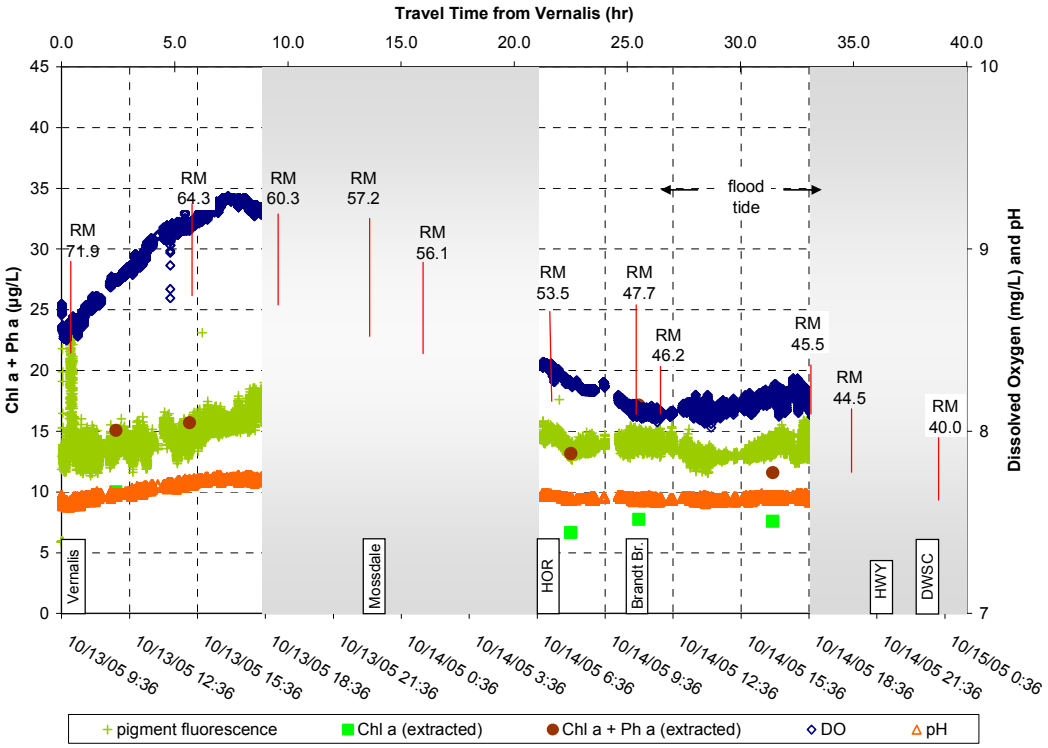

Figure 16: Extracted pigment concentration and the ch a/(chl a + ph a) fraction within the rhodamine WT plume flowing from Vernalis to the DWSC, October 13-14, 2005.

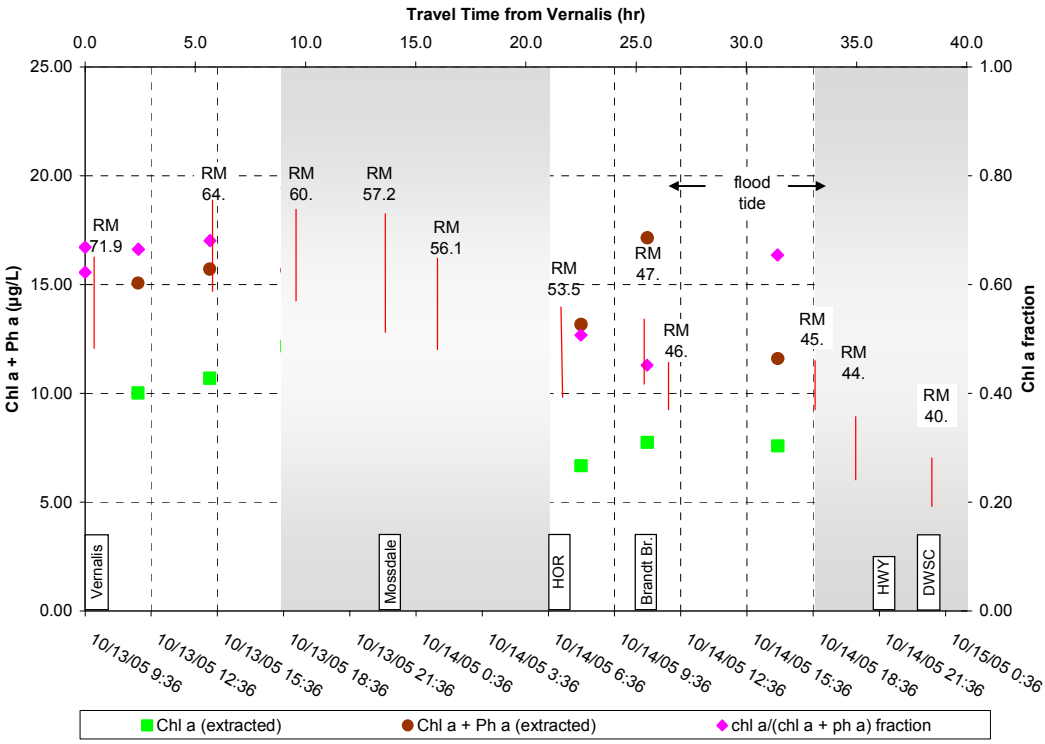

Figure 17: Pigment concentrations, dissolved oxygen, and pH within the rhodamine WT plume flowing from Vernalis to the DWSC, July 19-21 2006.

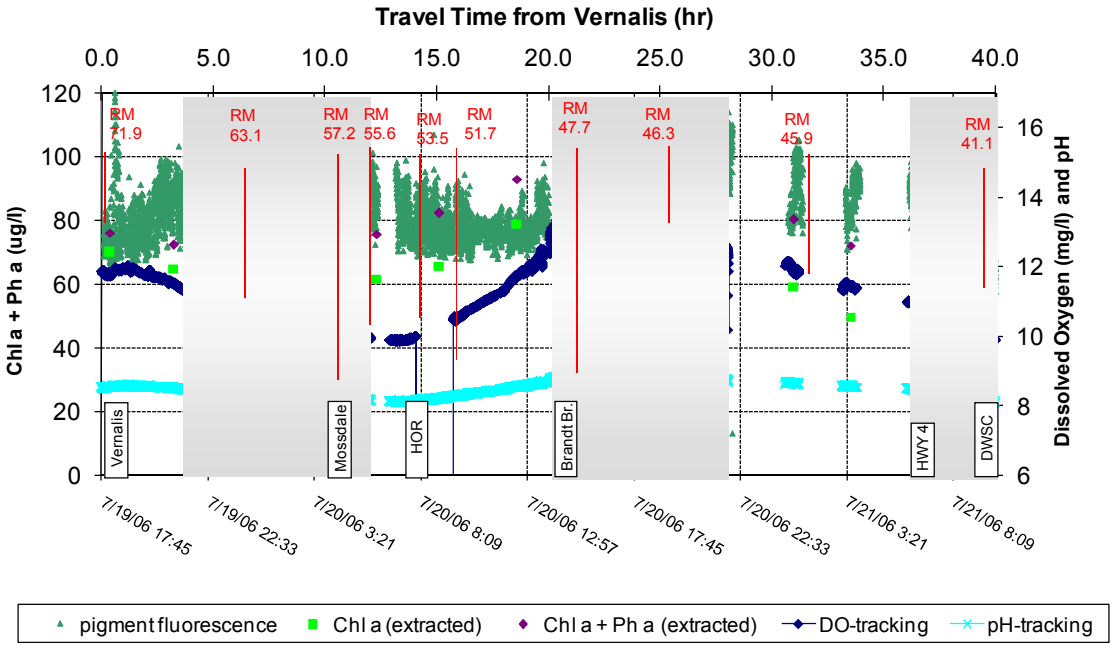

Figure 18: Extracted pigment concentration and the ch a/(chl a + ph a) fraction within the rhodamine WT plume flowing from Vernalis to the DWSC, July 19-21 2006.

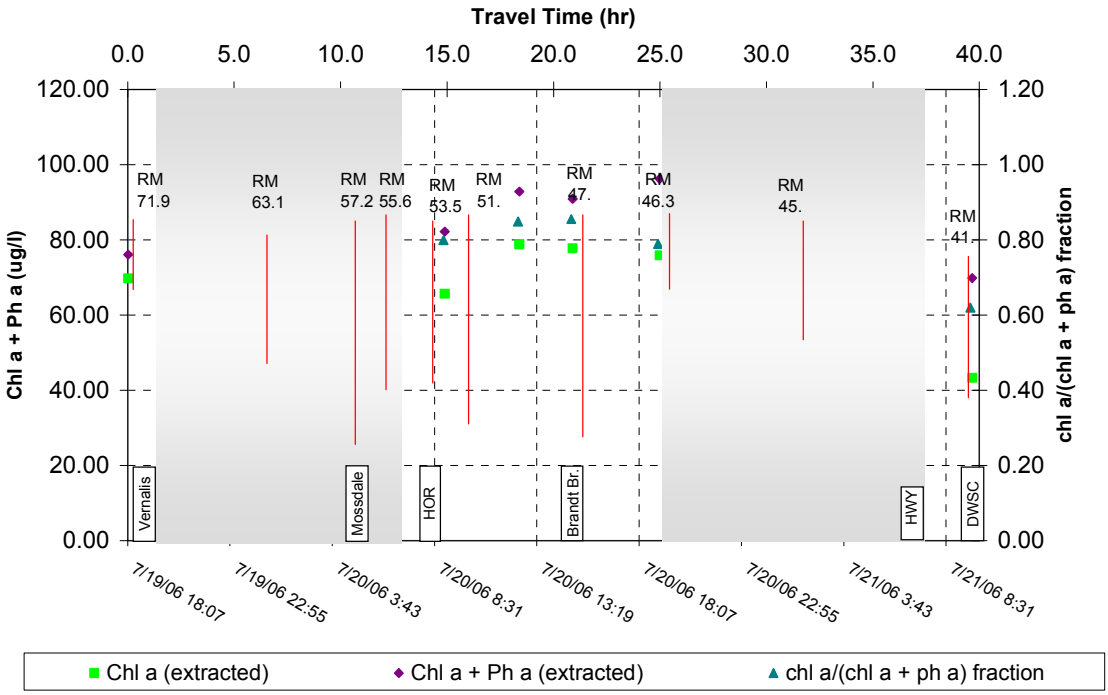

Figure 19: Pigment concentrations, dissolved oxygen, and pH within the rhodamine WT plume flowing from Vernalis to the DWSC, August 9, 10 2006.

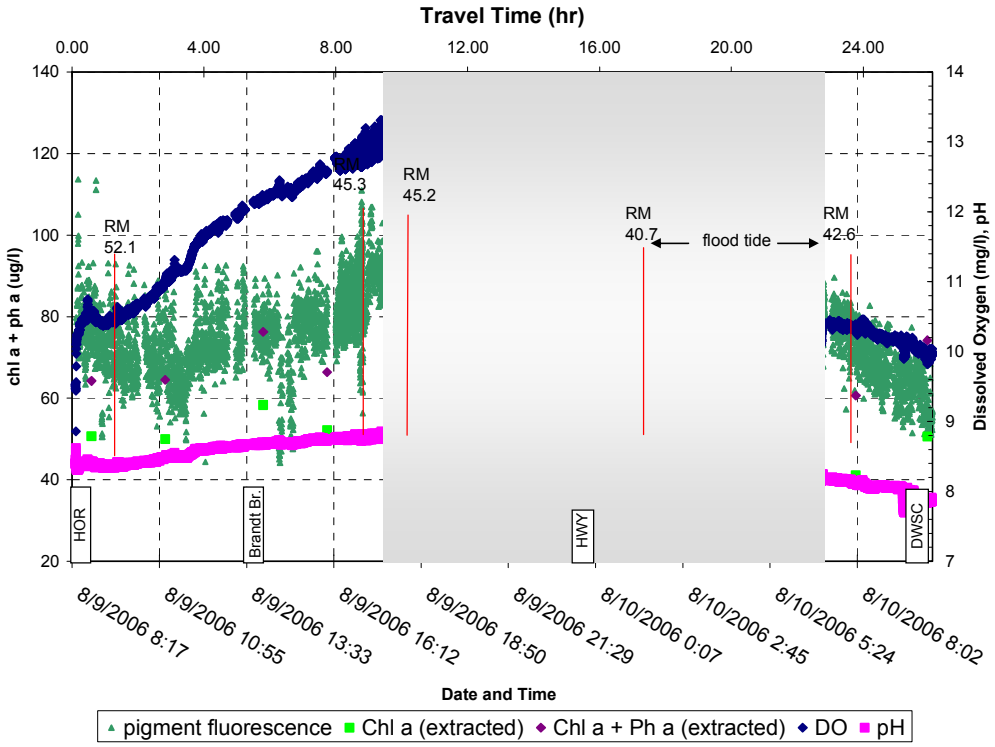

Figure 20: Extracted pigment concentration and the ch a/(chl a + ph a) fraction within the rhodamine WT plume flowing from Vernalis to the DWSC, August 9, 10 2006.

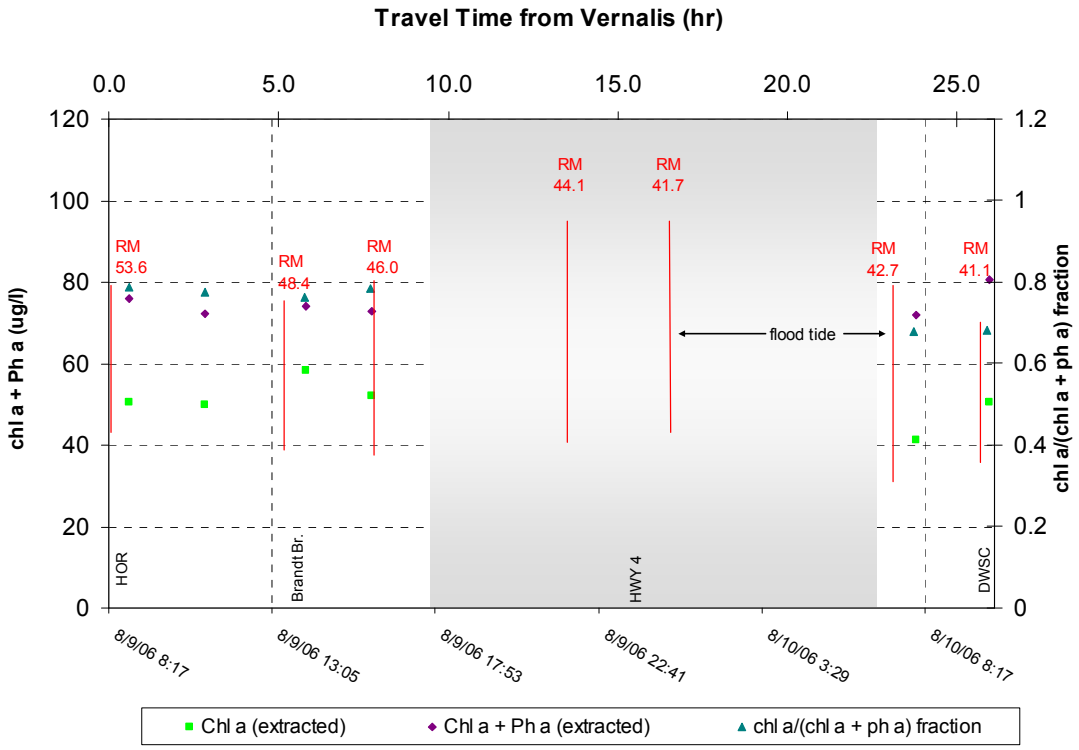

Figure 21: Extracted chlorophyll a, chlorophyll fluorescence and dissolved oxygen for the June 12-15, 2007 lagrangian tracking event.

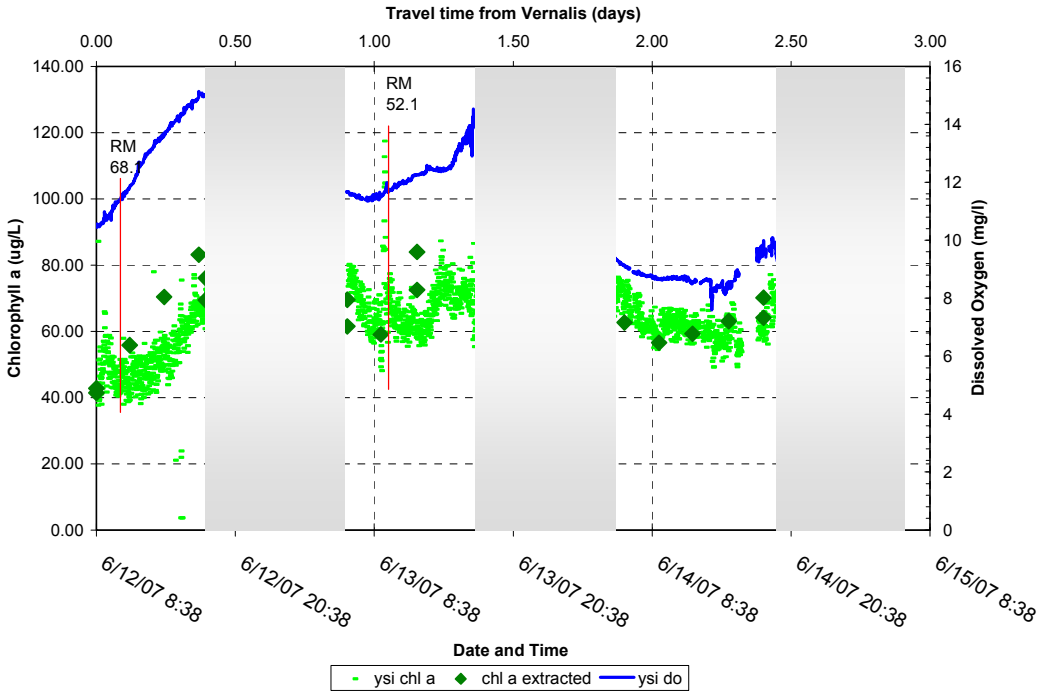

Figure 22: Extracted chlorophyll a and pheophytin a concentrations during lagrangian tracking performed on June 12-15, 2007.

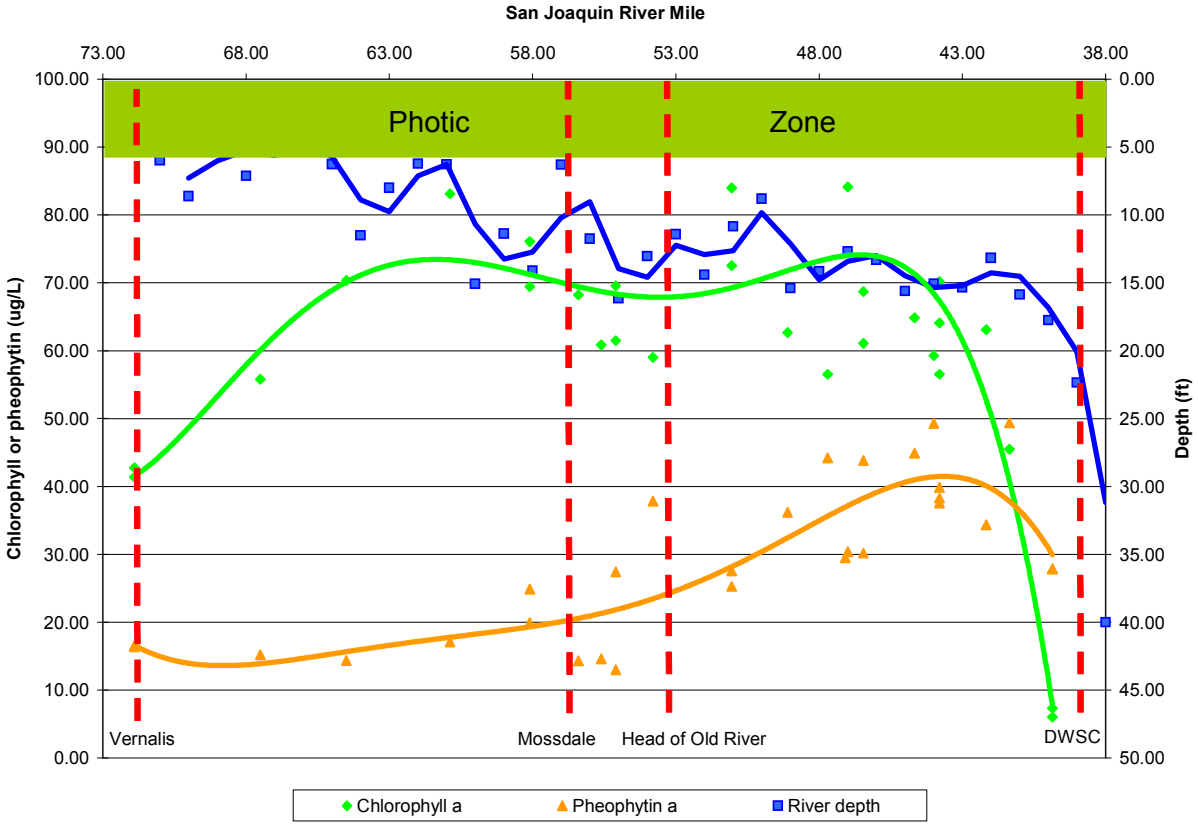

Figure 23: Chlorophyll a to total pigment ratio compared with the water depth during the June 12-15, 2007 lagrangian tracking.

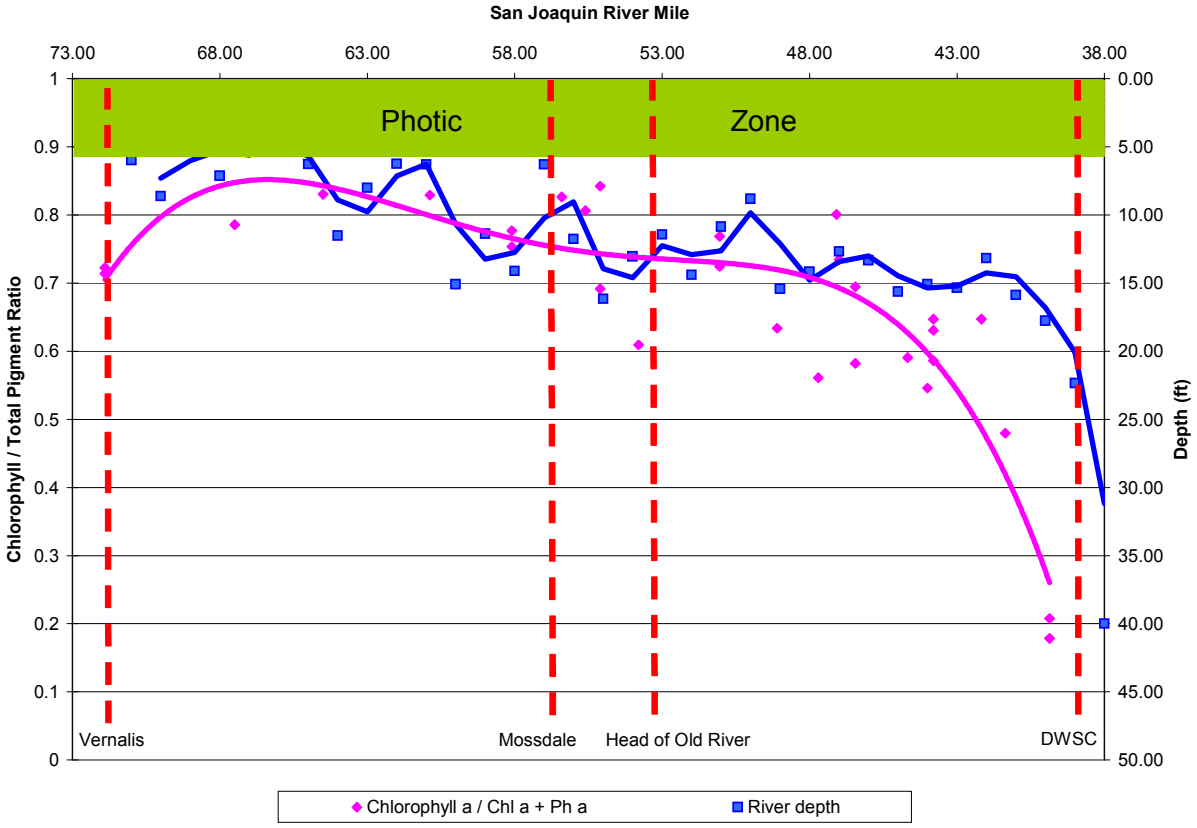

Figure 24: Chlorophyll a, pheophytin a, and zooplankton concentrations during the June 12-15, 2007 lagrangian tracking from Vernalis to the DWSC.

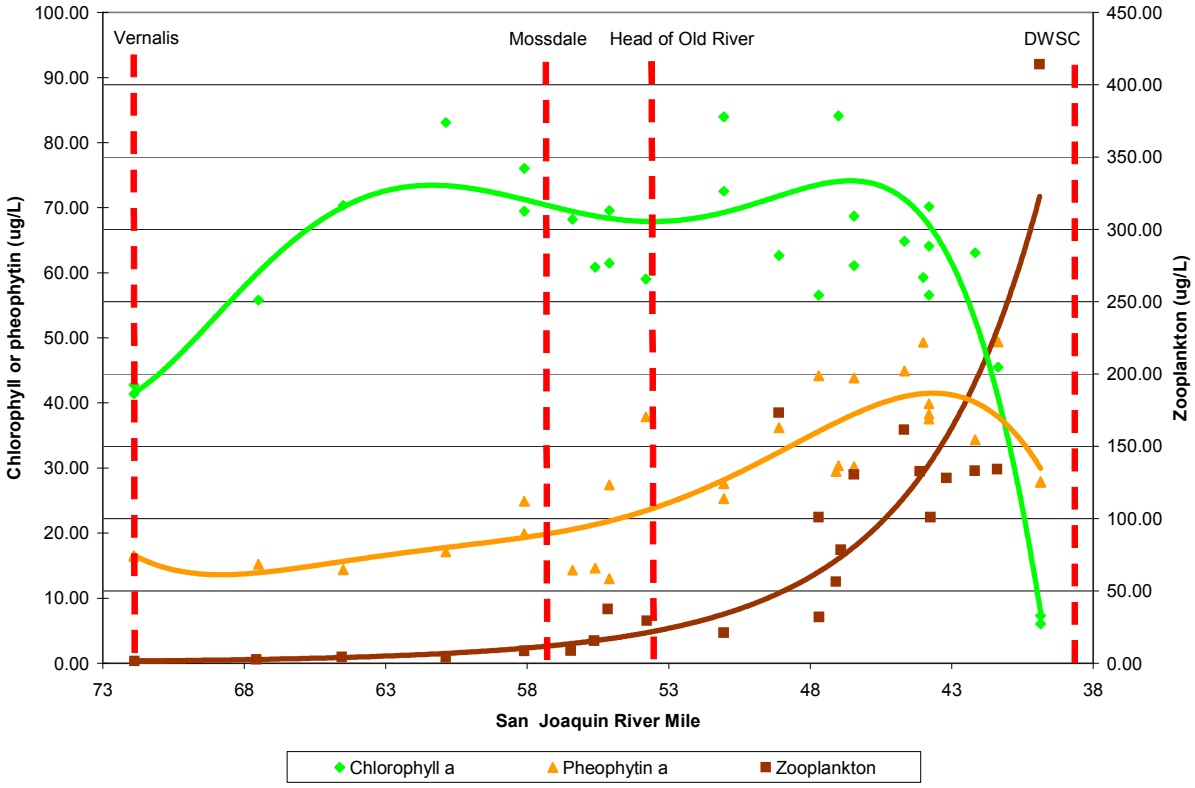

Figure 25: Longitudinal profiles of dissolved oxygen and ultimate BOD during slack tides on July 14 and 15, 2007.

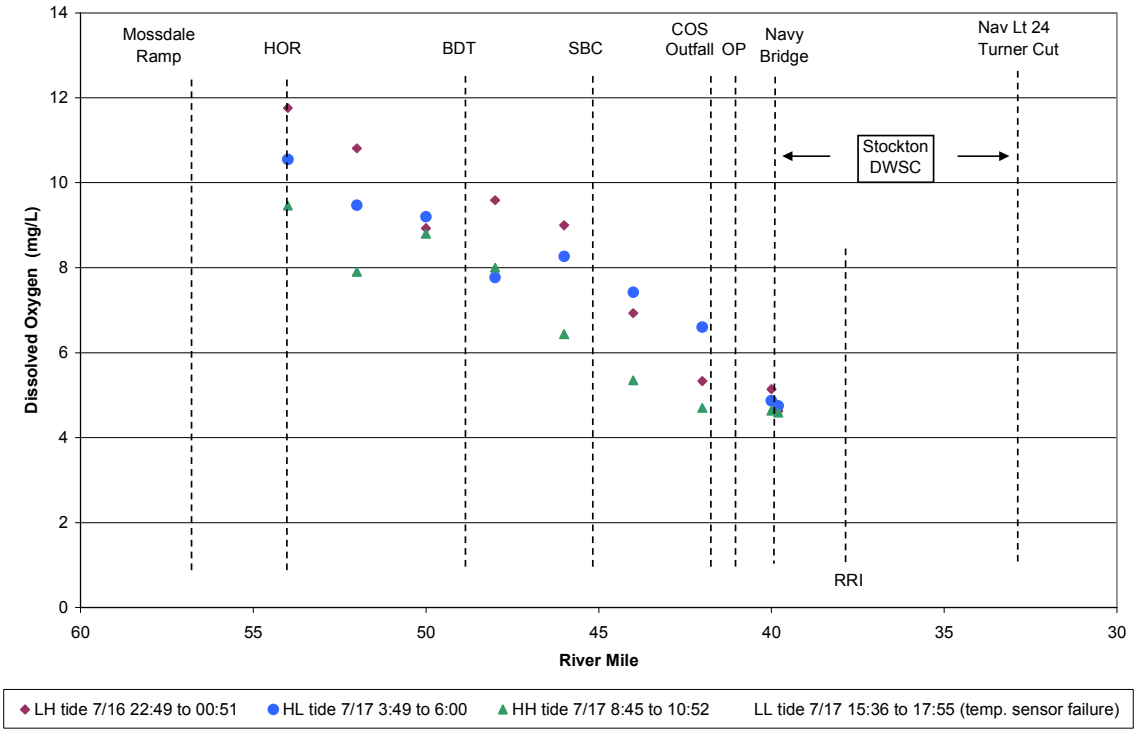

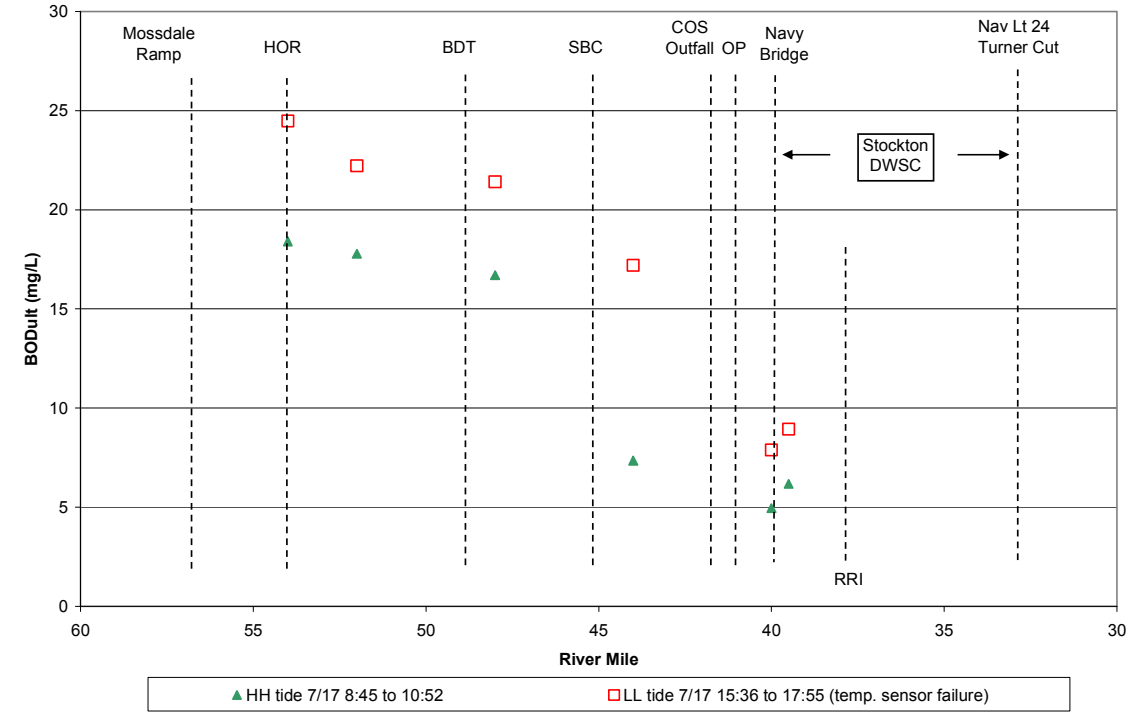

Figure 26: Longitudinal profiles of extracted chlorophyll a and and pigment ratio during slack tides on July 14 and 15, 2007.

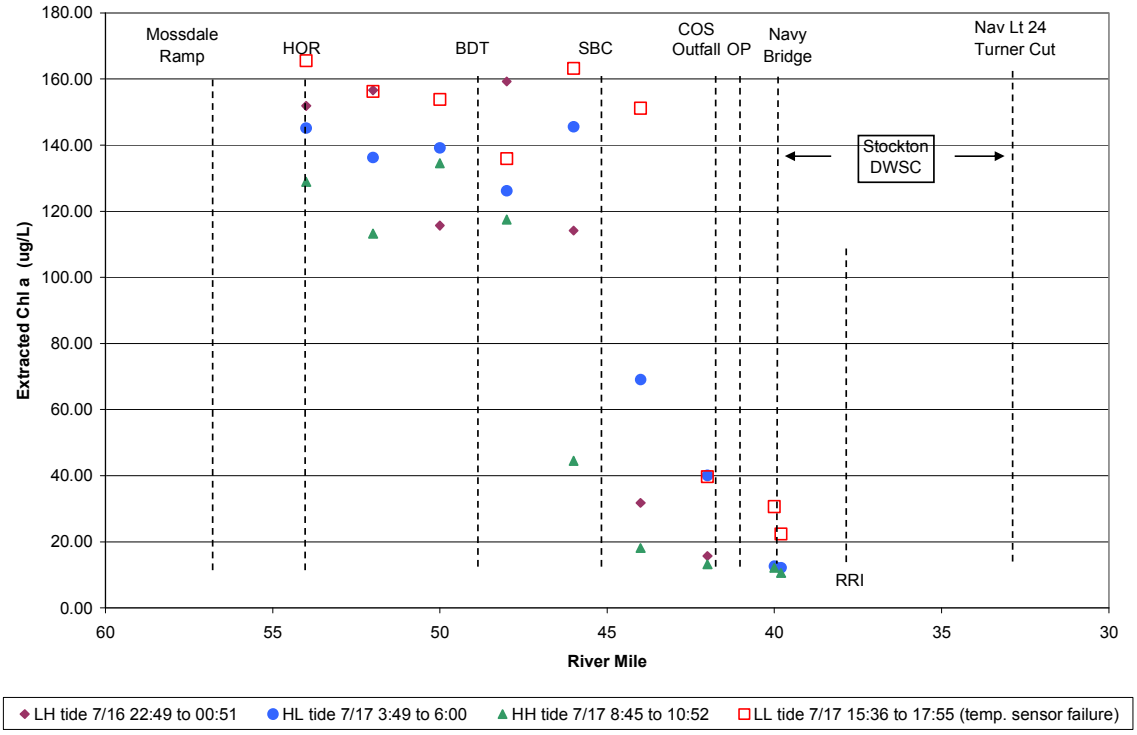

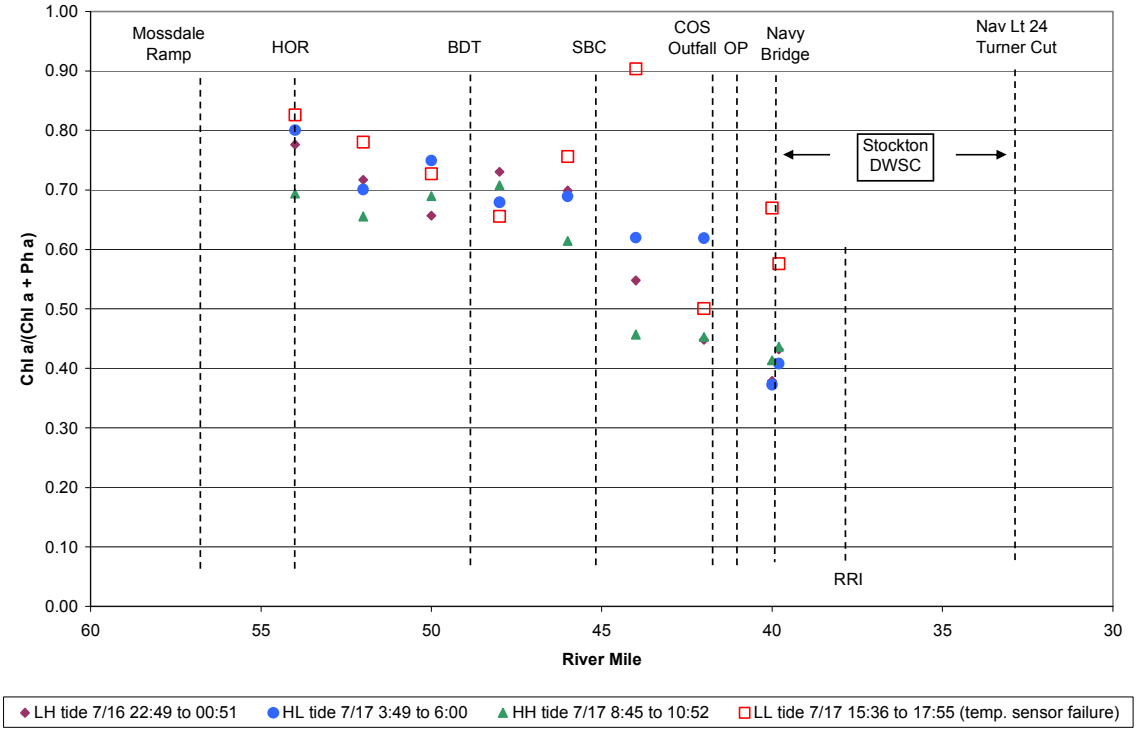

Figure 27: Longitudinal profiles of dissolved oxygen and ultimate BOD during slack tides on August 14 and 15, 2007.

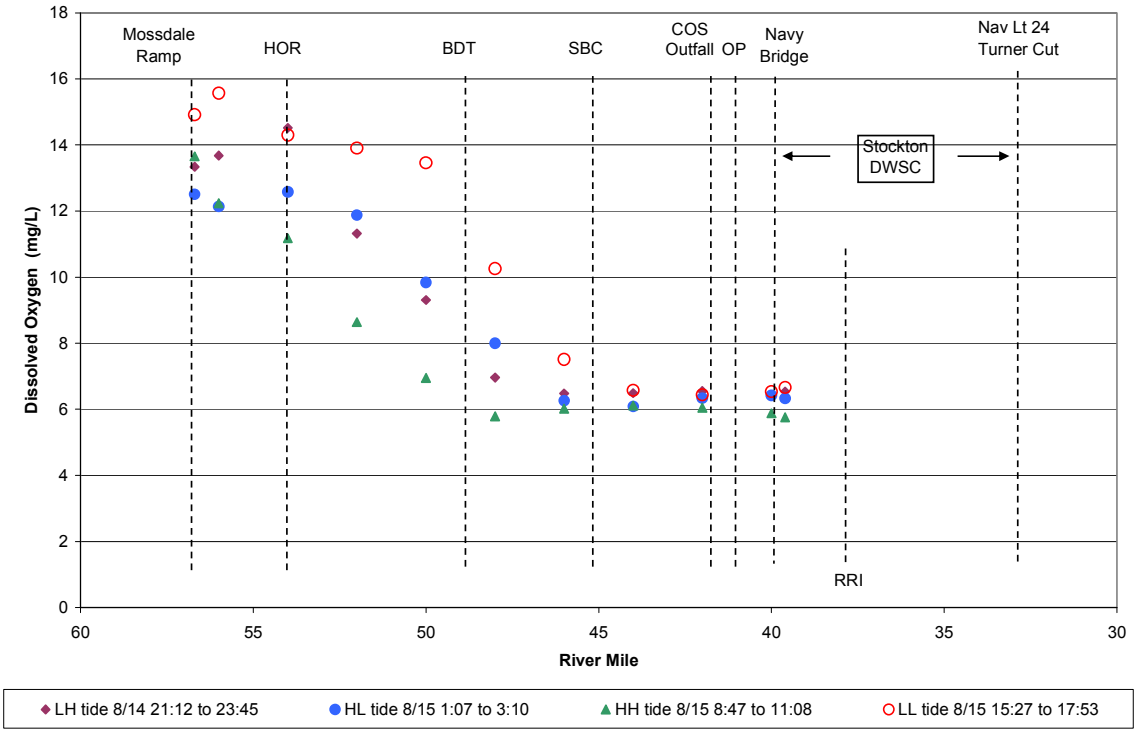

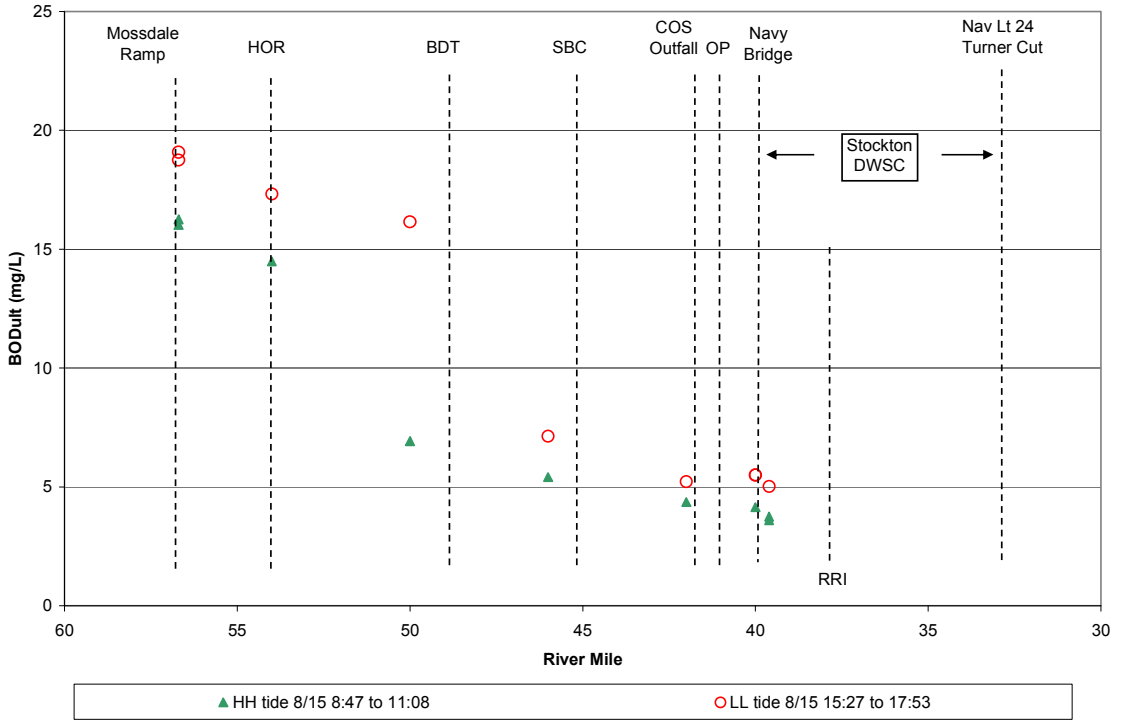

Figure 28: Longitudinal profiles of extracted chlorophyll a and and pigment ratio during slack tides on August 14 and 15, 2007.

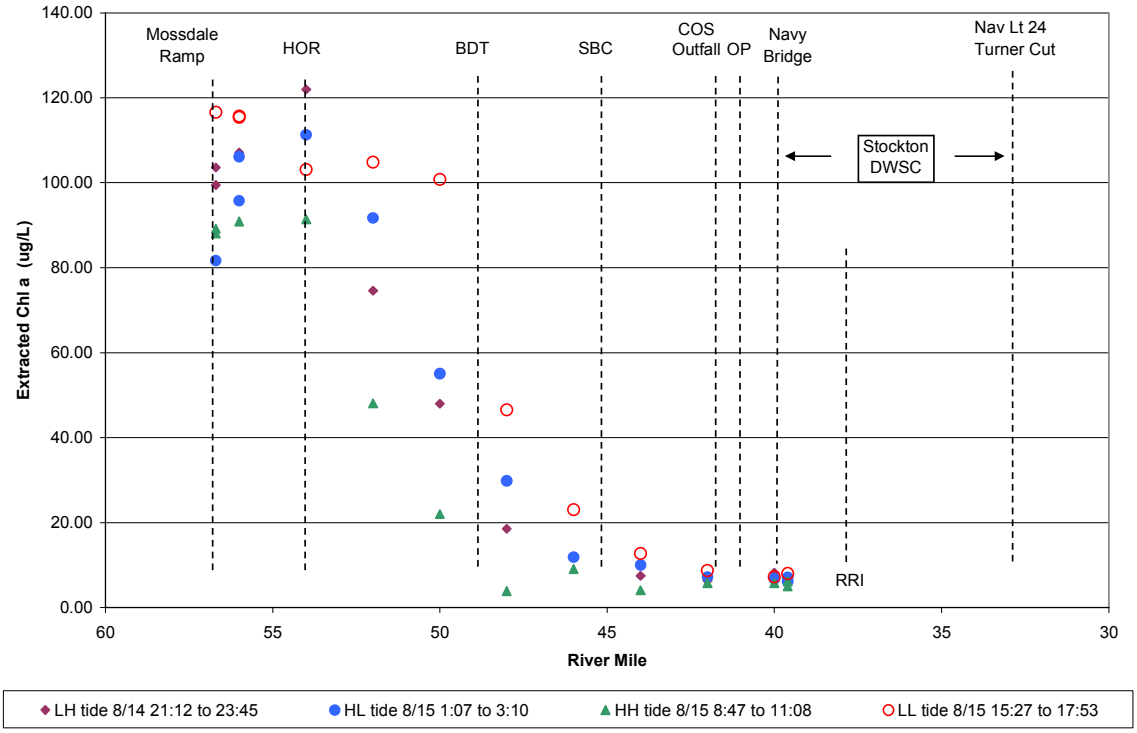
Mossdale Ramp
HOR
BDT
SBC
COS Outfall
OP
Navy Bridge
Nav Lt 24 Turner Cut
Stockton DWSC
RRI
Extracted Chl a (ug/L)
River Mile
LH tide 8/14 21:12 to 23:45
HL tide 8/15 1:07 to 3:10
HH tide 8/15 8:47 to 11:08
LL tide 8/15 15:27 to 17:53

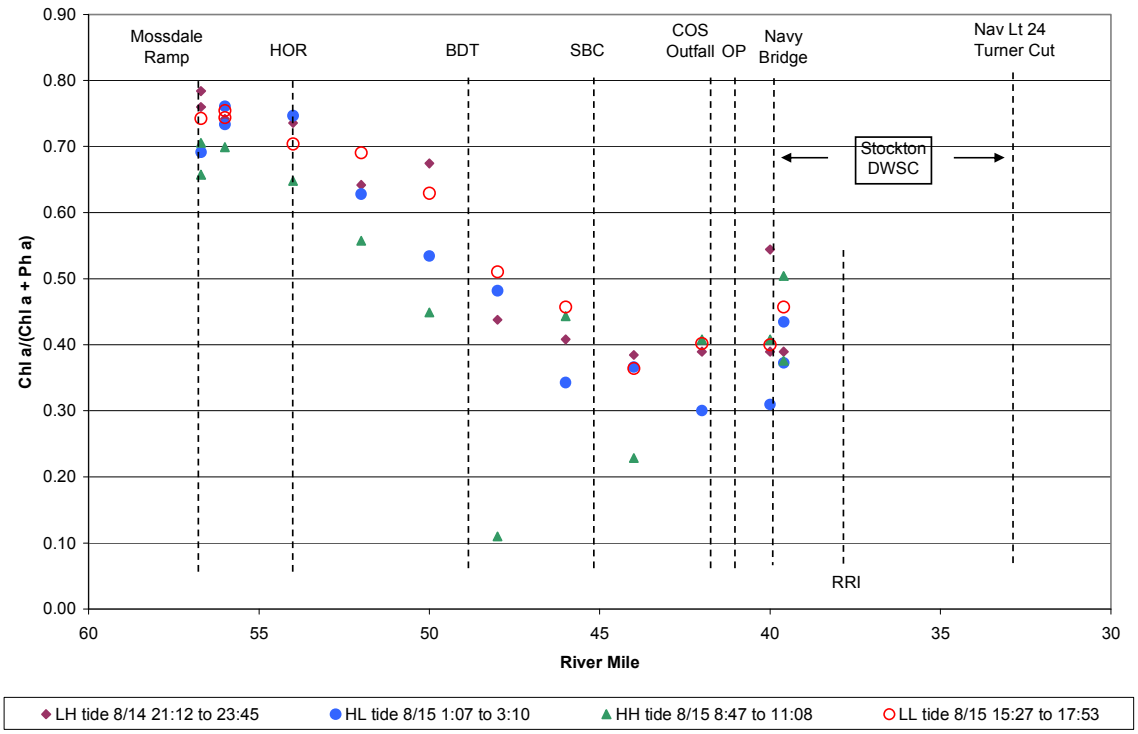
Mossdale Ramp
HOR
BDT
SBC
COS Outfall
OP
Navy Bridge
Nav Lt 24 Turner Cut
Stockton DWSC
RRI
Chl a/(Chl a + Ph a)
River Mile
LH tide 8/14 21:12 to 23:45
HL tide 8/15 1:07 to 3:10
HH tide 8/15 8:47 to 11:08
LL tide 8/15 15:27 to 17:53

Figure 29: Longitudinal profiles of extracted chlorophyll a and and pigment ratio during slack tides on September 19 and 20, 2007.

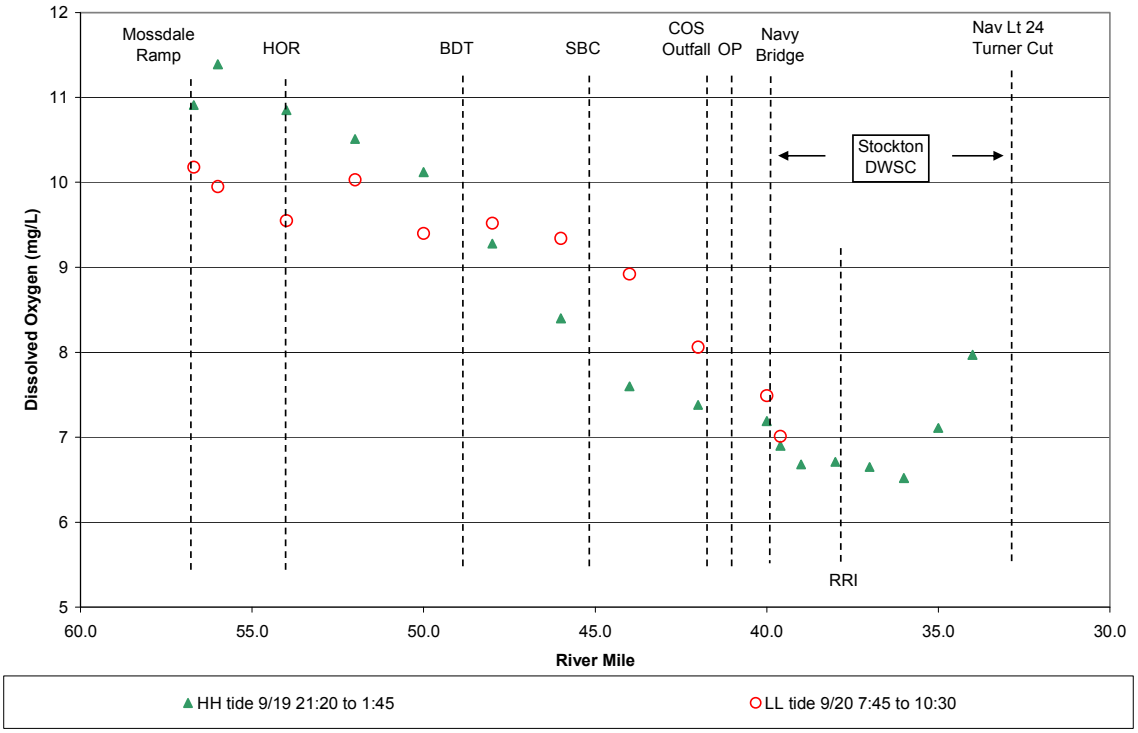

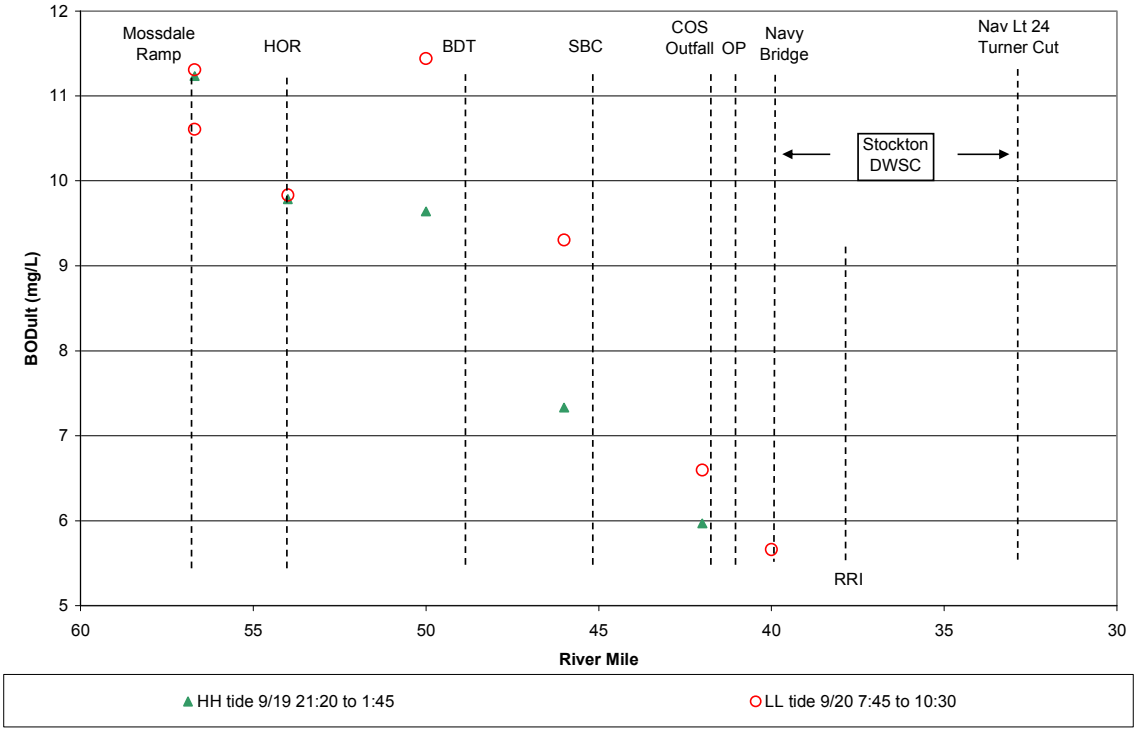

Figure 30: Longitudinal profiles of extracted chlorophyll a and and pigment ratio during slack tides on September 19 and 20, 2007.

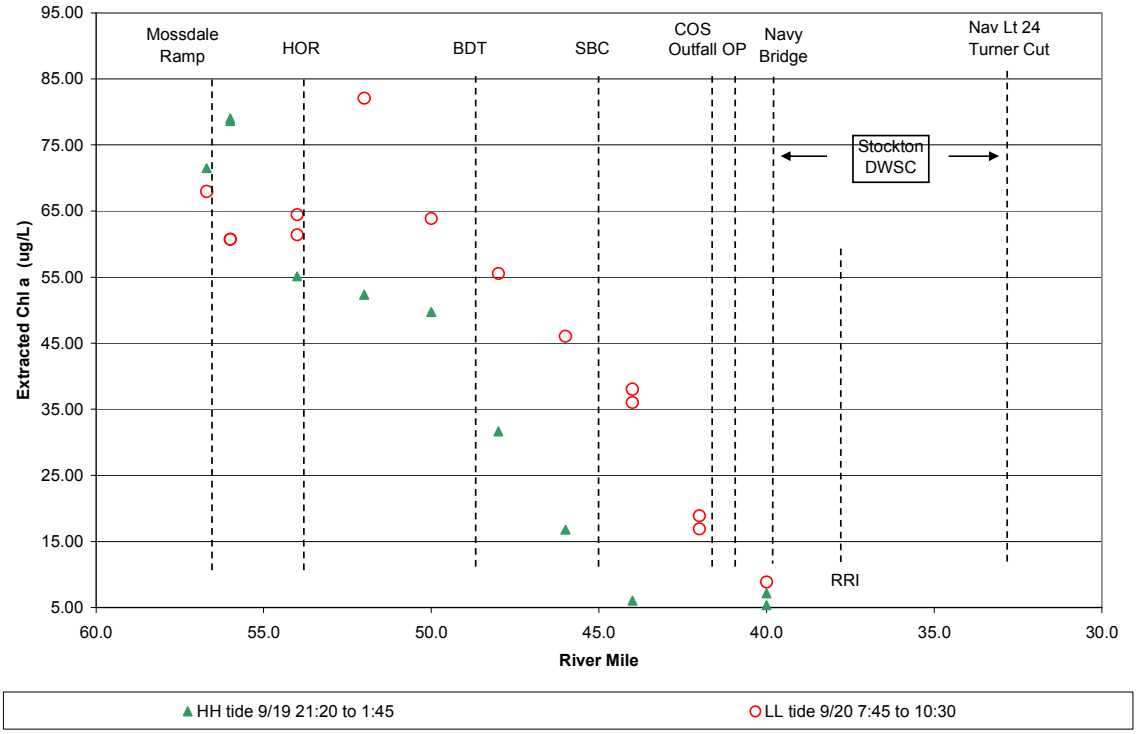
Mossdale Ramp
HOR
BDT
SBC
COS Outfall
OP
Navy Bridge
Nav Lt 24 Turner Cut
Stockton DWSC
RRI
Extracted Chl a (ug/L)
95.00
85.00
75.00
65.00
55.00
45.00
35.00
25.00
15.00
5.00
60.0
55.0
50.0
45.0
40.0
35.0
30.0
River Mile
HH tide 9/19 21:20 to 1:45
LL tide 9/20 7:45 to 10:30

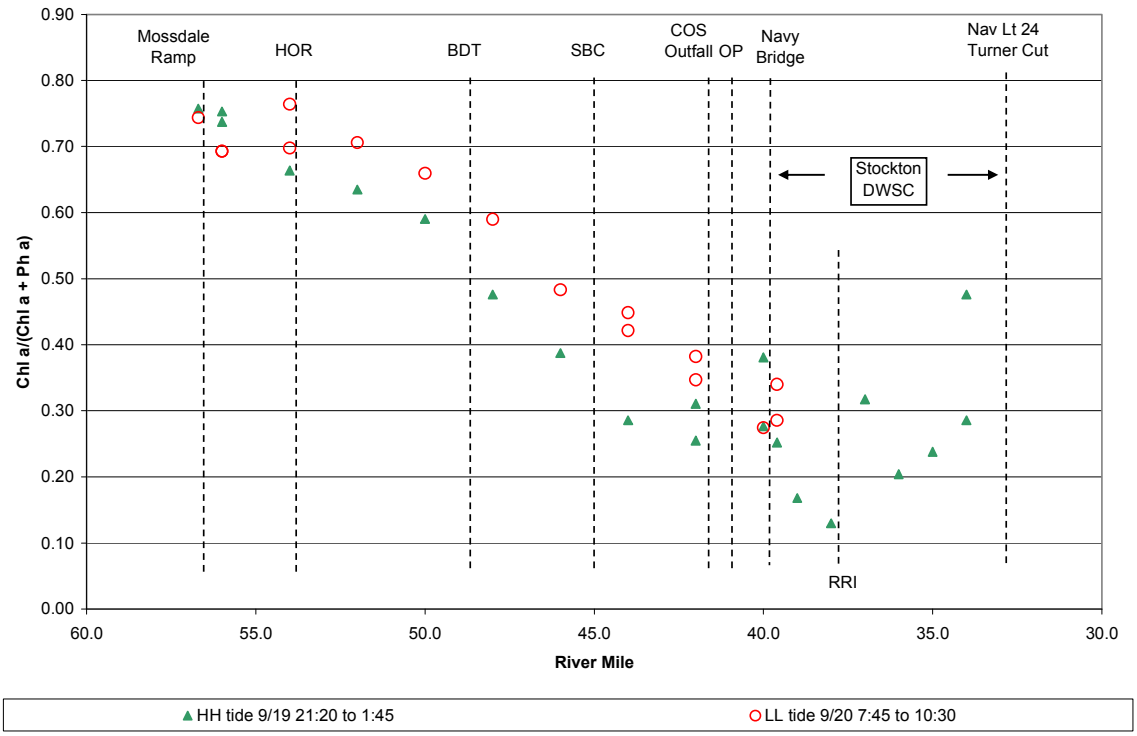
Mossdale Ramp
HOR
BDT
SBC
COS Outfall
OP
Navy Bridge
Nav Lt 24 Turner Cut
Stockton DWSC
RRI
Chl a/(Chl a + Ph a)
0.90
0.80
0.70
0.60
0.50
0.40
0.30
0.20
0.10
0.00
60.0
55.0
50.0
45.0
40.0
35.0
30.0
River Mile
HH tide 9/19 21:20 to 1:45
LL tide 9/20 7:45 to 10:30

Figure 31: Zooplankton and extracted chlorophyll a concentrations in the San Joaquin River above the DWSC for the longitudinal monitoring at low-low slack tide on July 17, 2007.

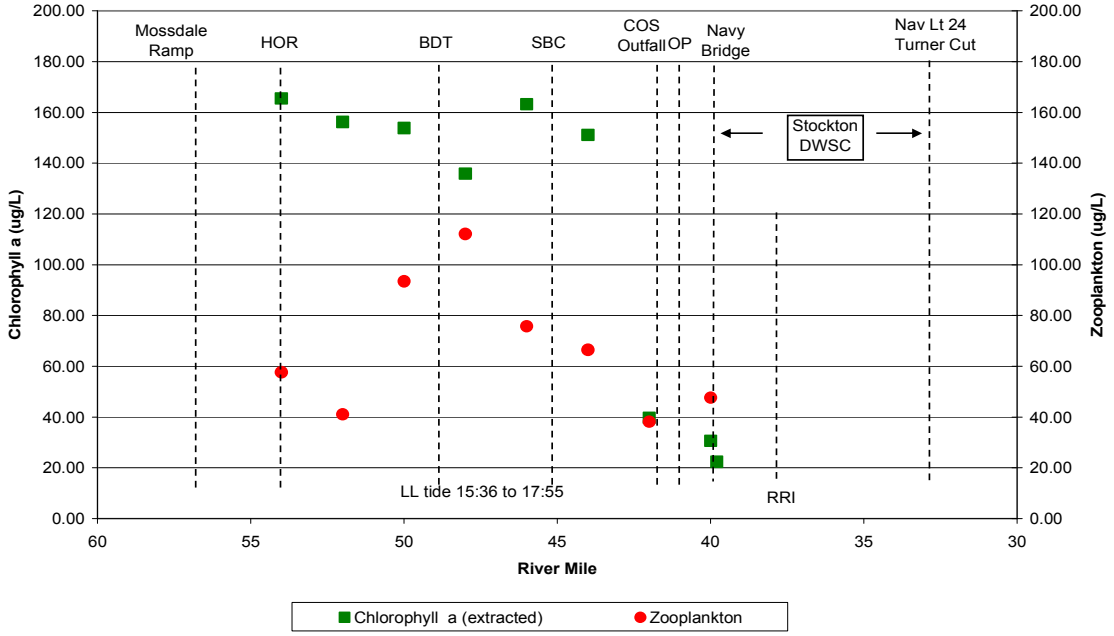

Figure 32: Longitudinal profile of zooplankton and extracted chlorophyll a concentrations in the San Joaquin River above the DWSC at low-low slack tide on July 24, 2007.

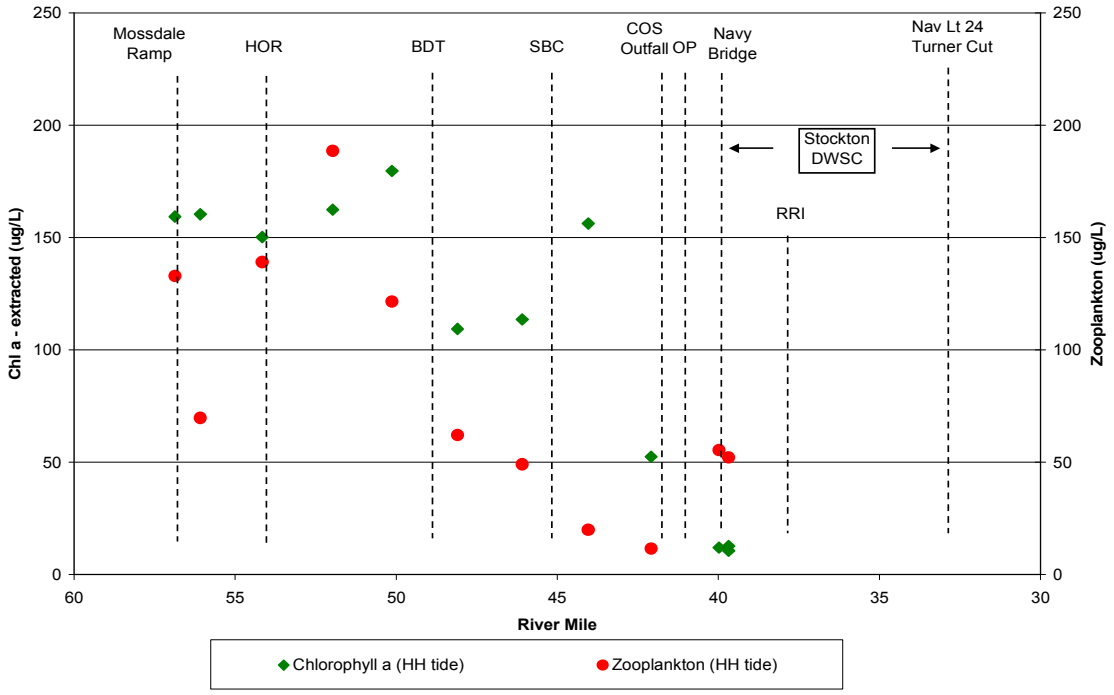

Figure 33: Longitudinal profiles of zooplankton and extracted chlorophyll a concentrations in the San Joaquin River above the DWSC near low-high slack tide on August 14, 2007.

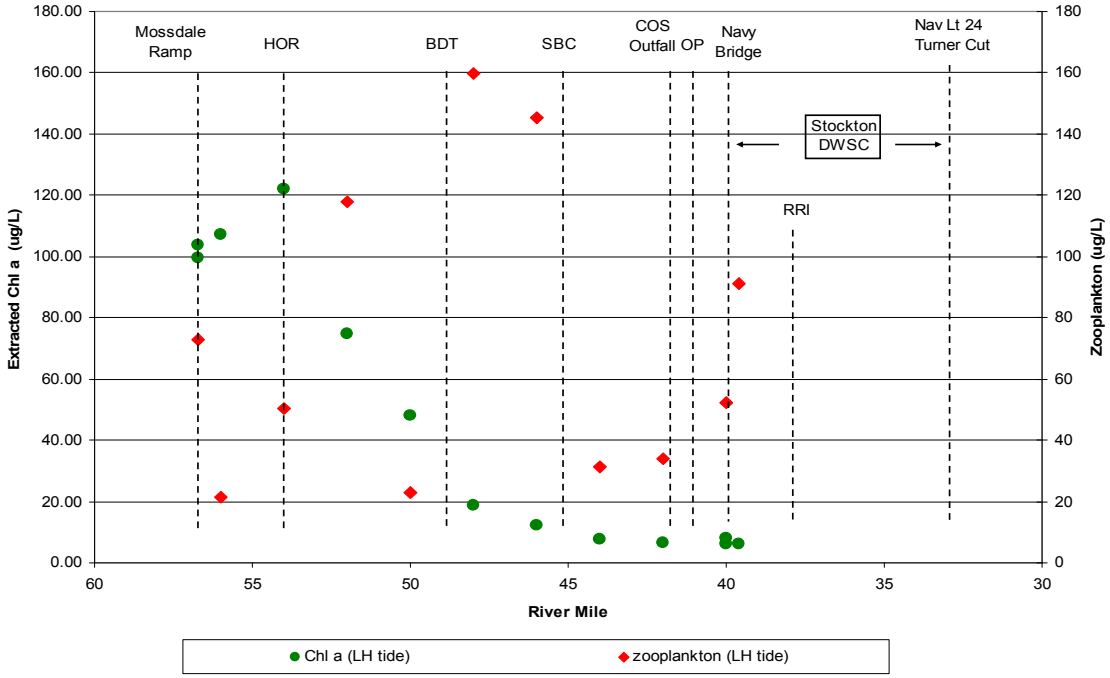

Figure 34: Longitudinal profiles of zooplankton and extracted chlorophyll a concentrations in the San Joaquin River above the DWSC at low-low slack tide on August 23, 2007.

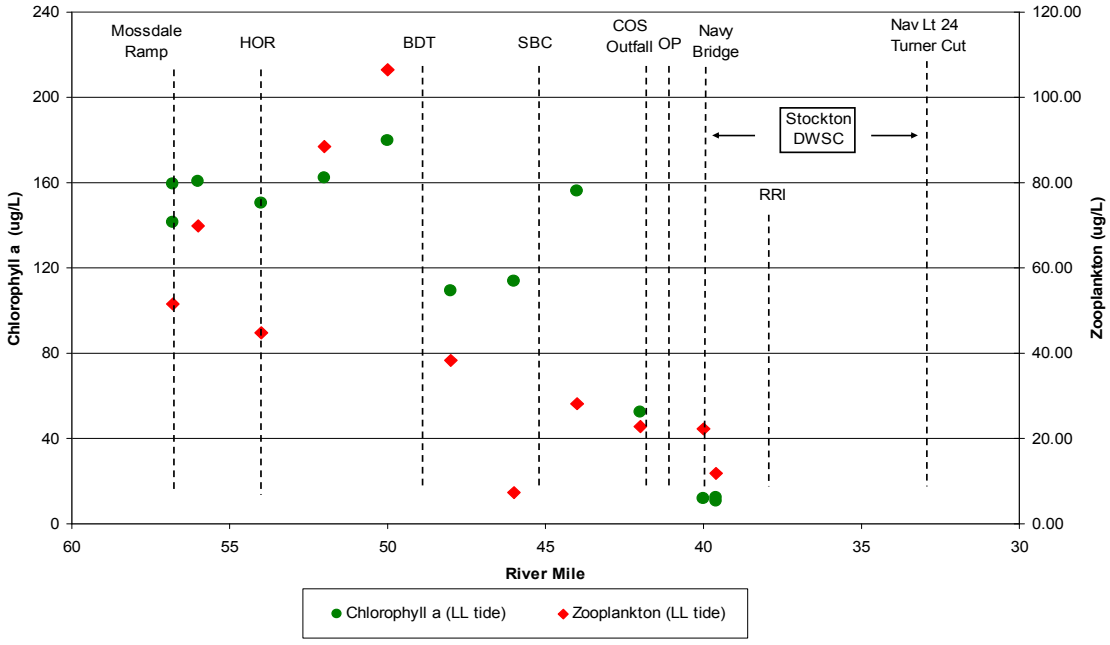

Figure 35: Longitudinal profiles of zooplankton and extracted chlorophyll a concentrations in the San Joaquin River from the DWSC to Mossdale at low-low slack tide on September 6, 2007.

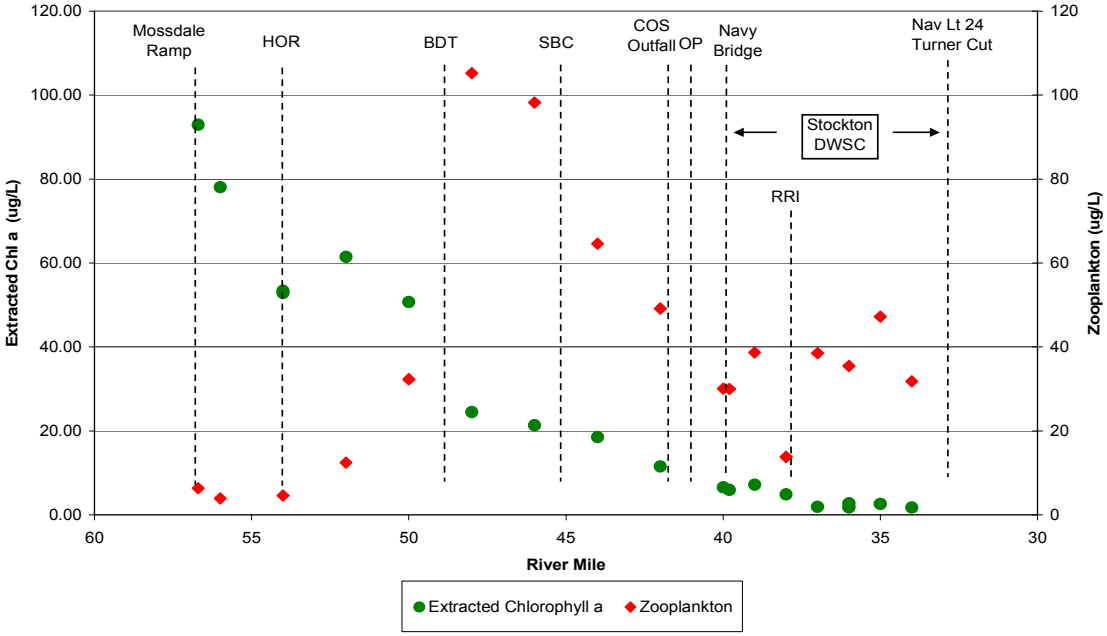

Figure 36: Longitudinal profiles of zooplankton and extracted chlorophyll a concentrations in the San Joaquin River from the DWSC to Mossdale near a high-high slack tide on September 21, 2007.

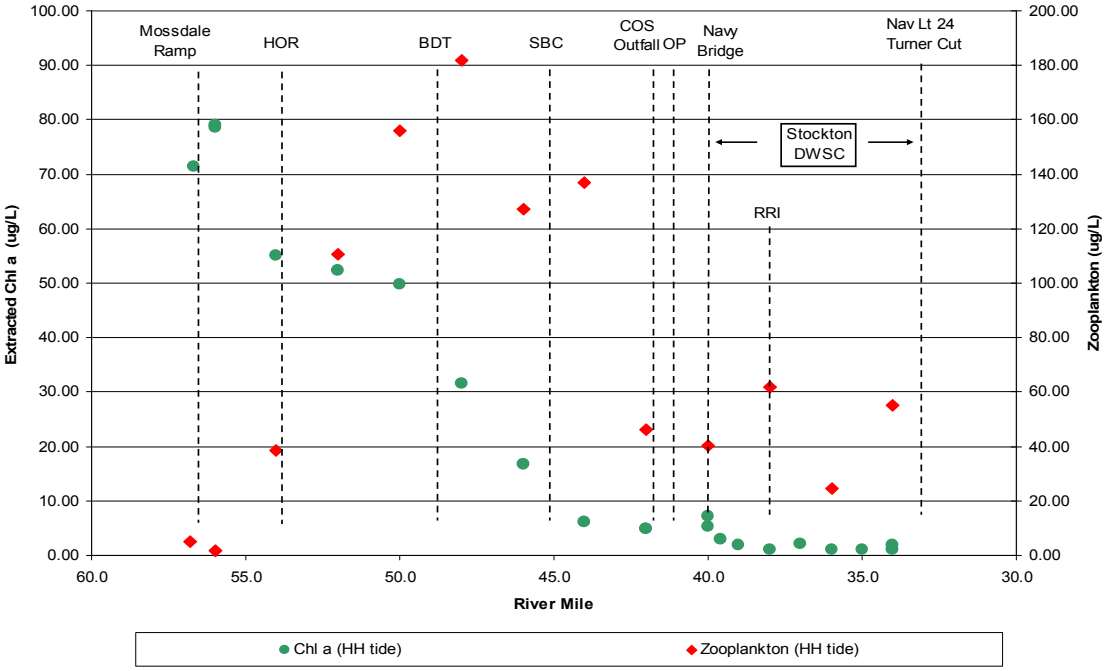

Figure 37: Zooplankton grazing for increasing initial concentrations of Zooplankton after 4.5 hours in the photic zone (approximately 2 ft depth) on September 27, 2007.

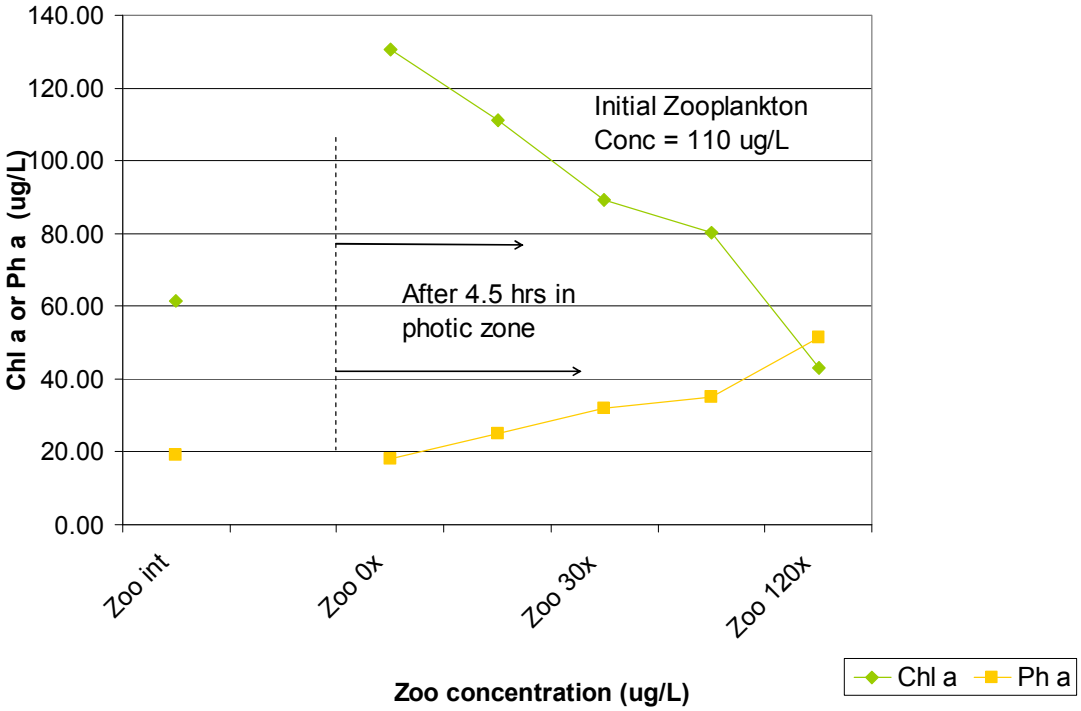

Figure 38: The response of chlorophyll a and pheophytin a in microcosms with and without concentrated zooplankton measured on October 3, 2007.

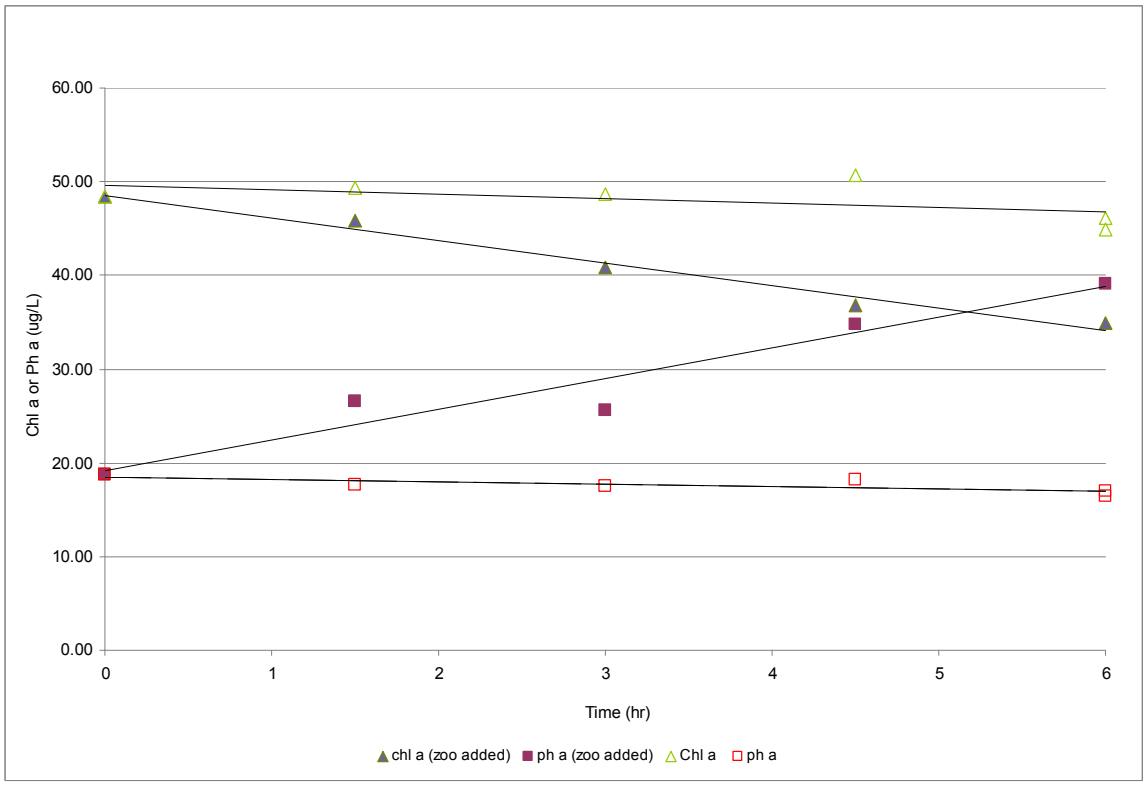

Figure 39: Chlorophyll decay experiment results for water collected at Mossdale (rm56.7) on August 1, 2007 and monitored in the lab for two weeks.

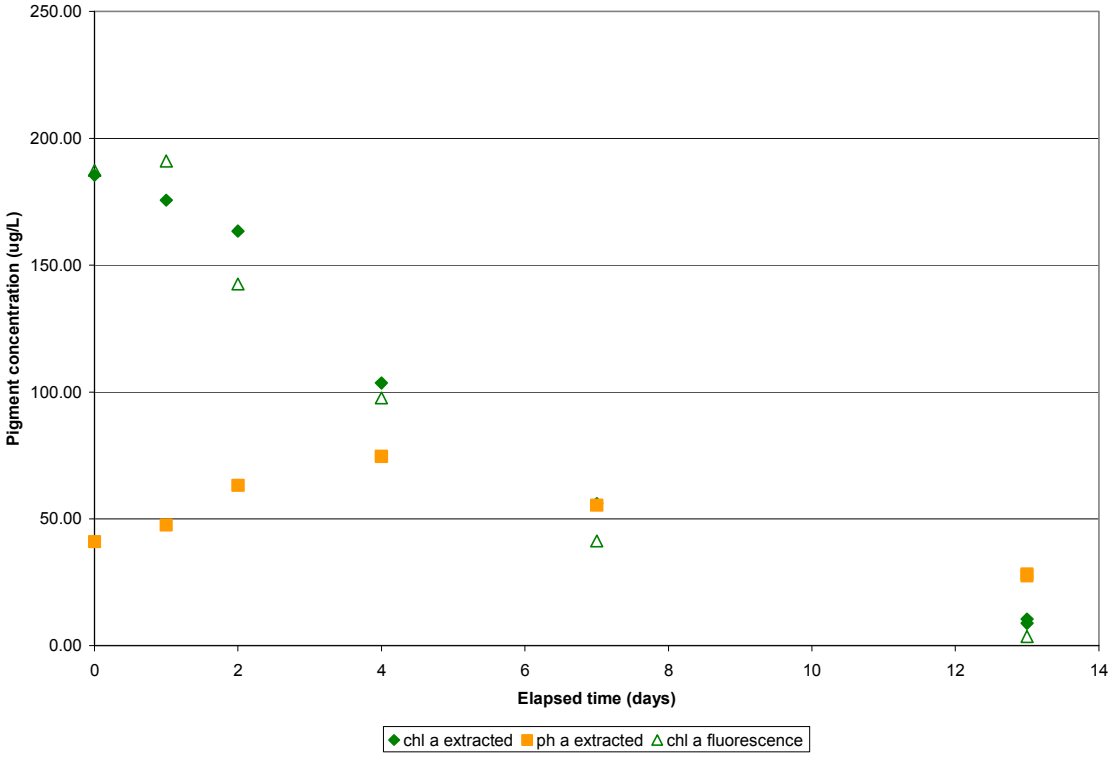

Figure 40: Chlorophyll decay experiment results for water collected at the Brandt Bridge Station (rm48) on August 1, 2007 and monitored in the lab for two weeks.

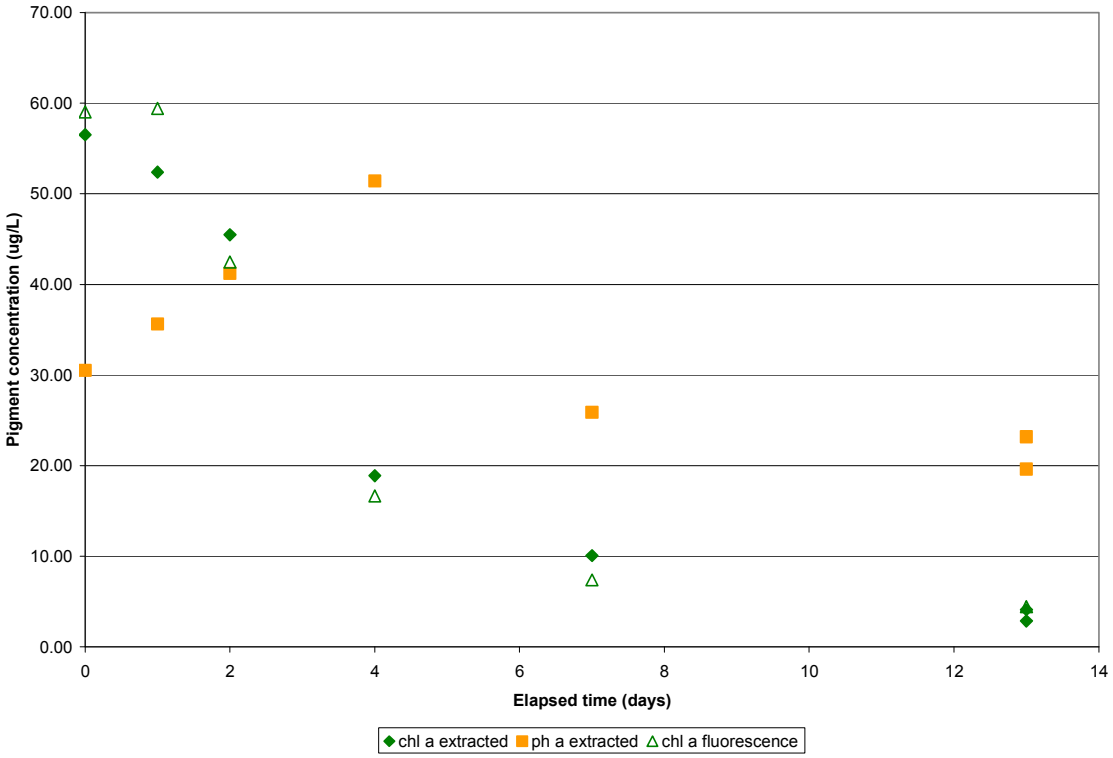

Figure 41: Chlorophyll decay experiment results for water collected at the Stockton Brick Company (SBC) Station (rm45) on August 1, 2007 and monitored in the lab for two weeks.

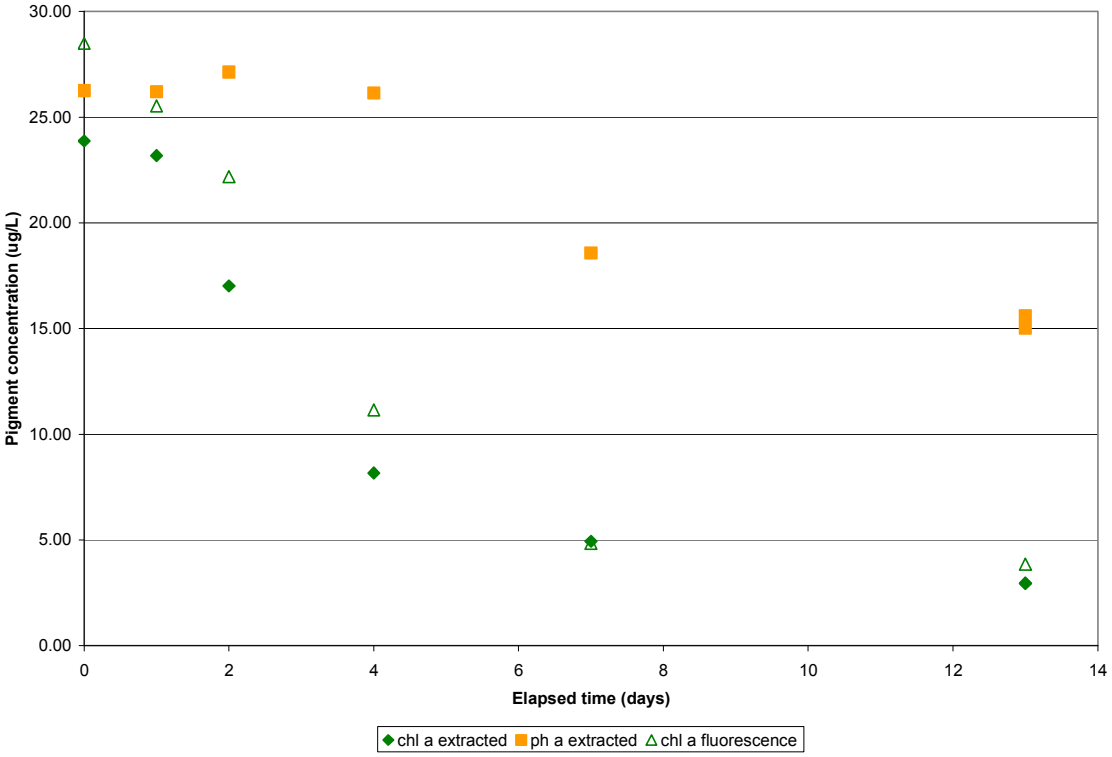

Figure 42: Chlorophyll decay experiment results for water collected at the Outfall Pier (OP) Station (rm41) on August 1, 2007 and monitored in the lab for two weeks.

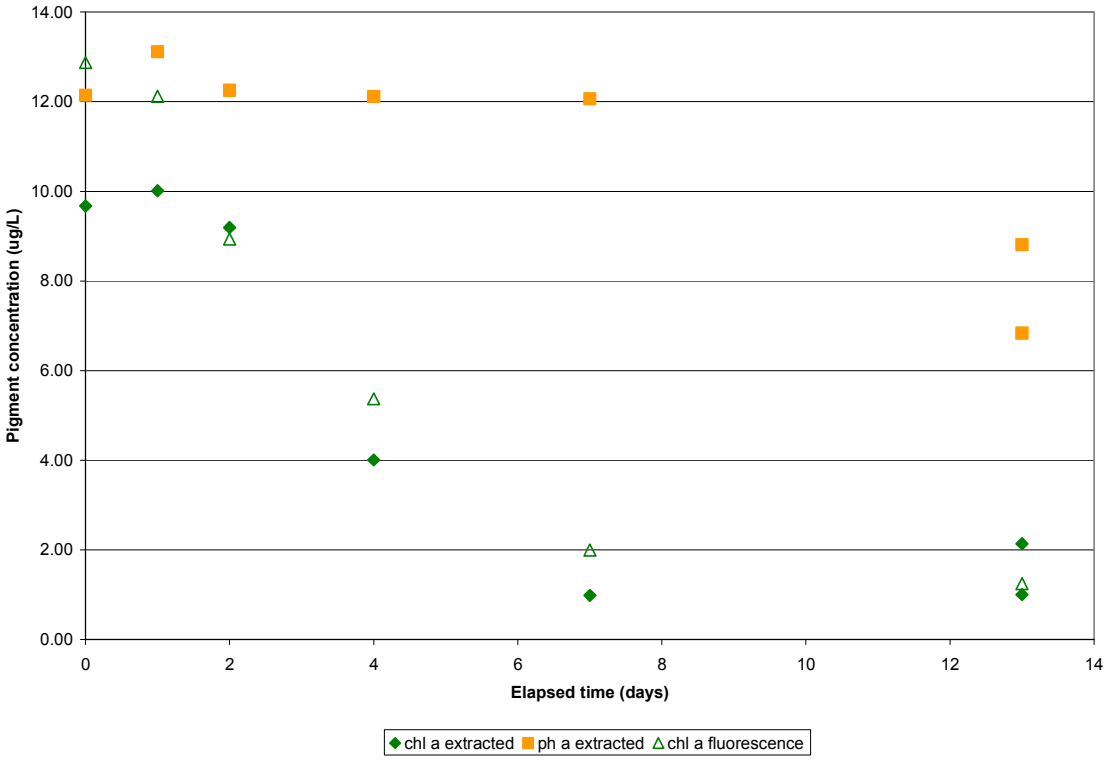

Figure 43: BOD, CBOD and NBOD measured for San Joaquin River water collected at SJR 3, July, 2005.

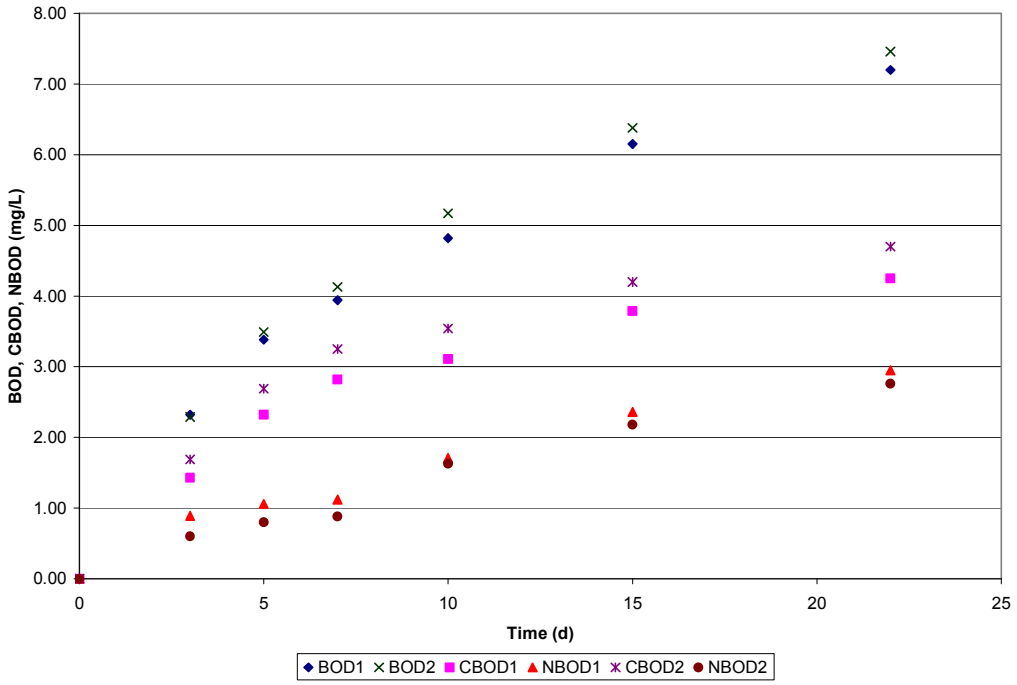

Figure 44: Correlation of BOD_{10} to BOD_{ult} for San Joaquin River samples collected in 2007.

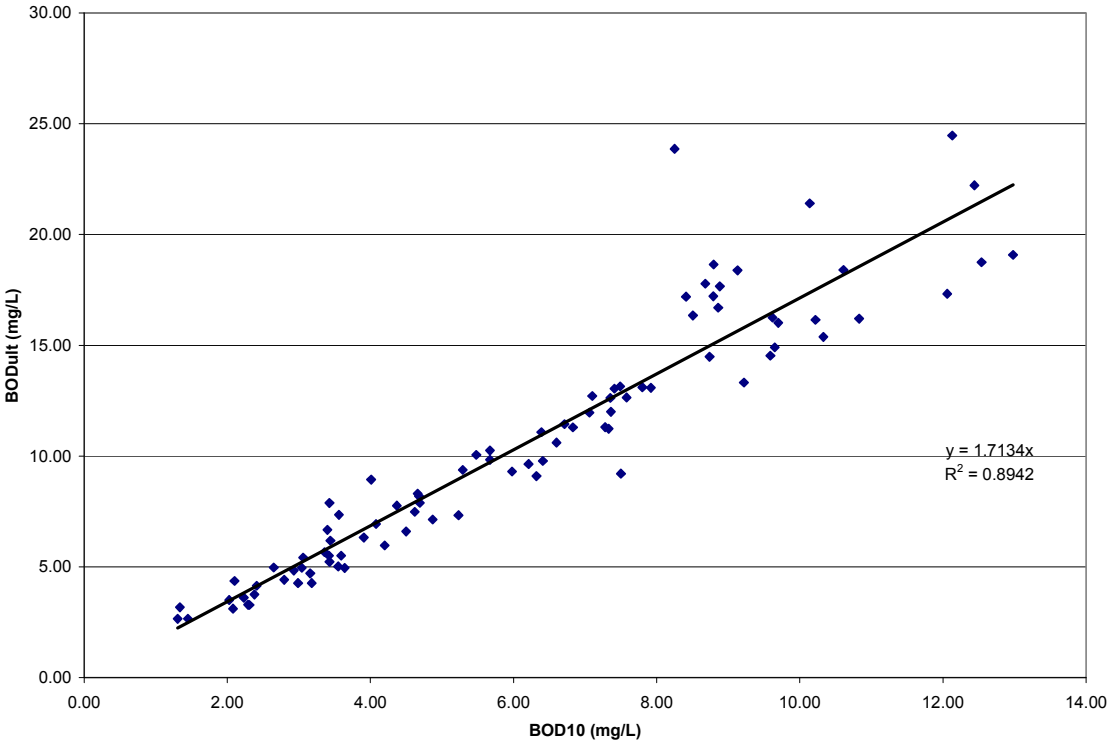

Figure 45: 20-day BOD concentrations for 2005 and 2006 monitoring.

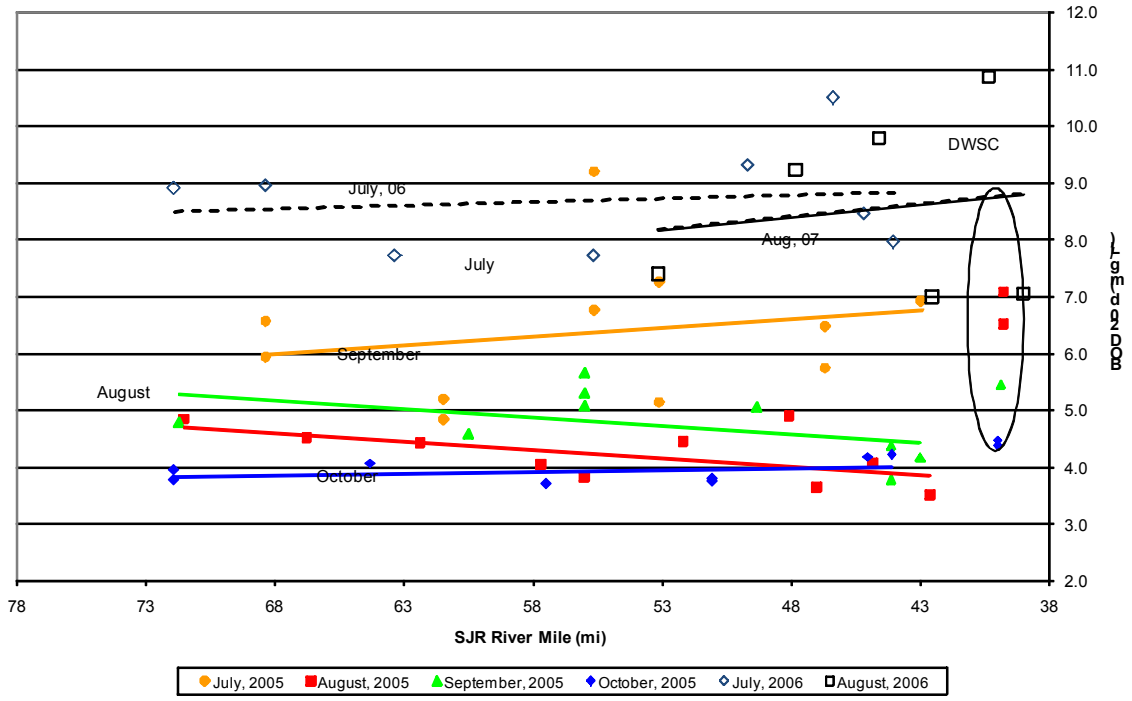

Figure 46: Longitudinal ultimate biochemical oxygen demands, ultimate carbonaceous BOD, and ultimate nitrogenous BOD for June 12-15, 2007 tracking.

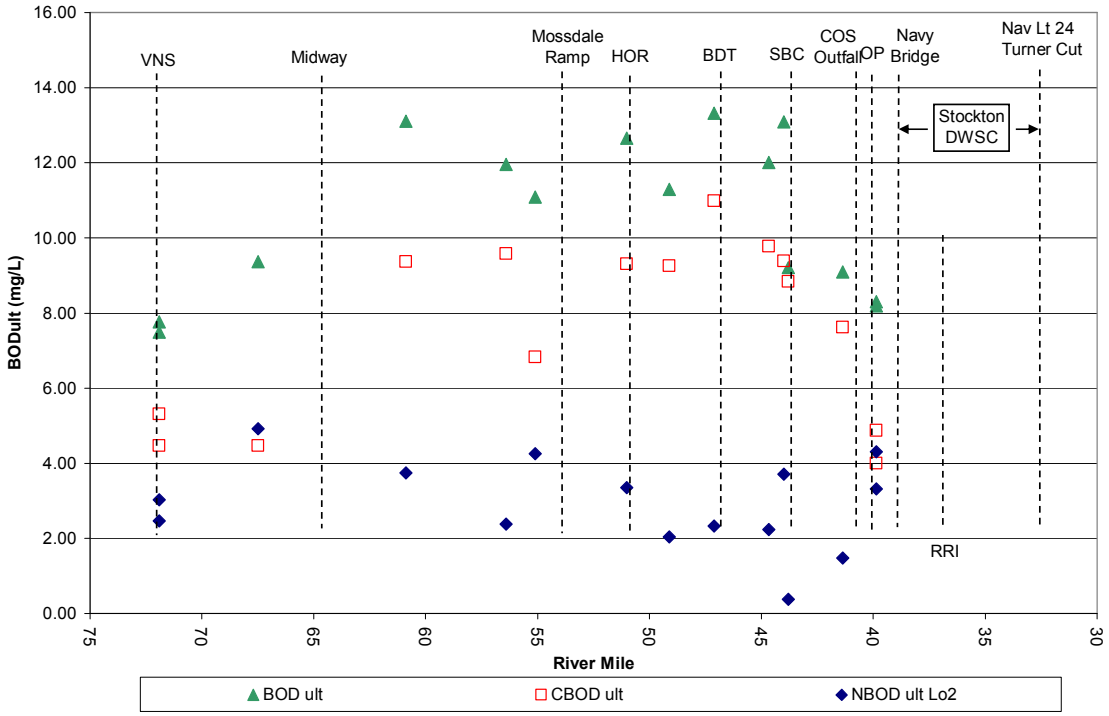

Figure 47: Dissolved oxygen production for measured light intensity at depths of 1, 2, and 3 feet.

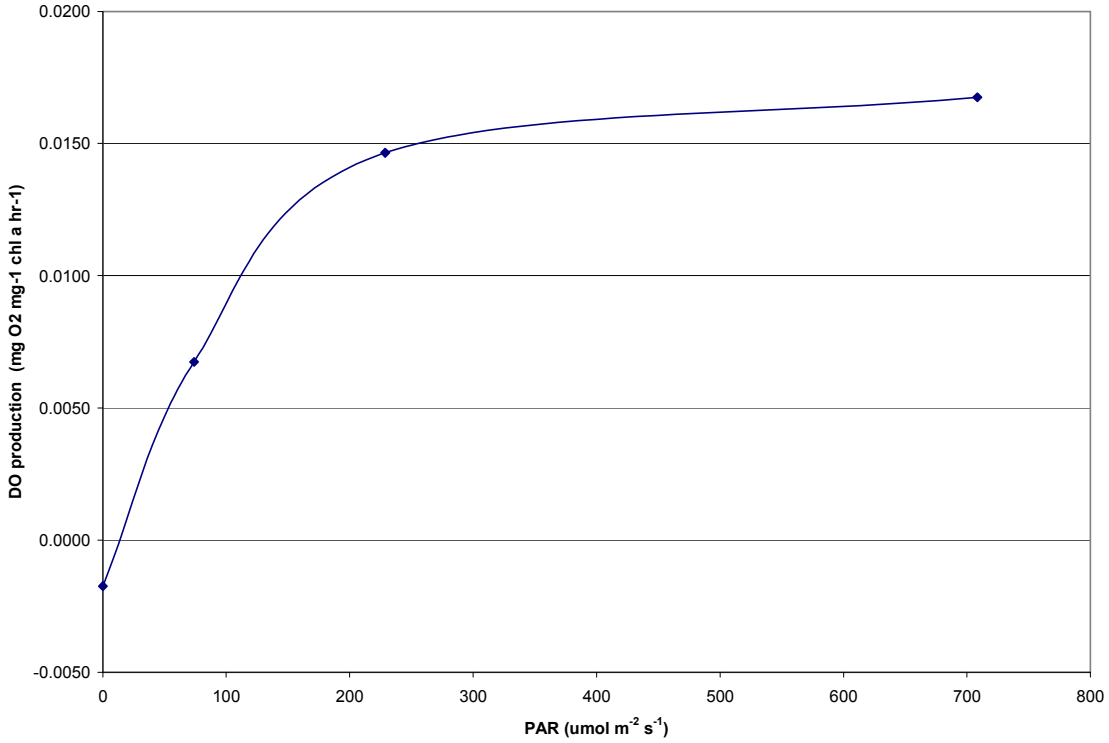

Figure 48: Measured and calculated chlorophyll a production in light-dark bottles deployed below Vernalis (River Mile 72 to 69).

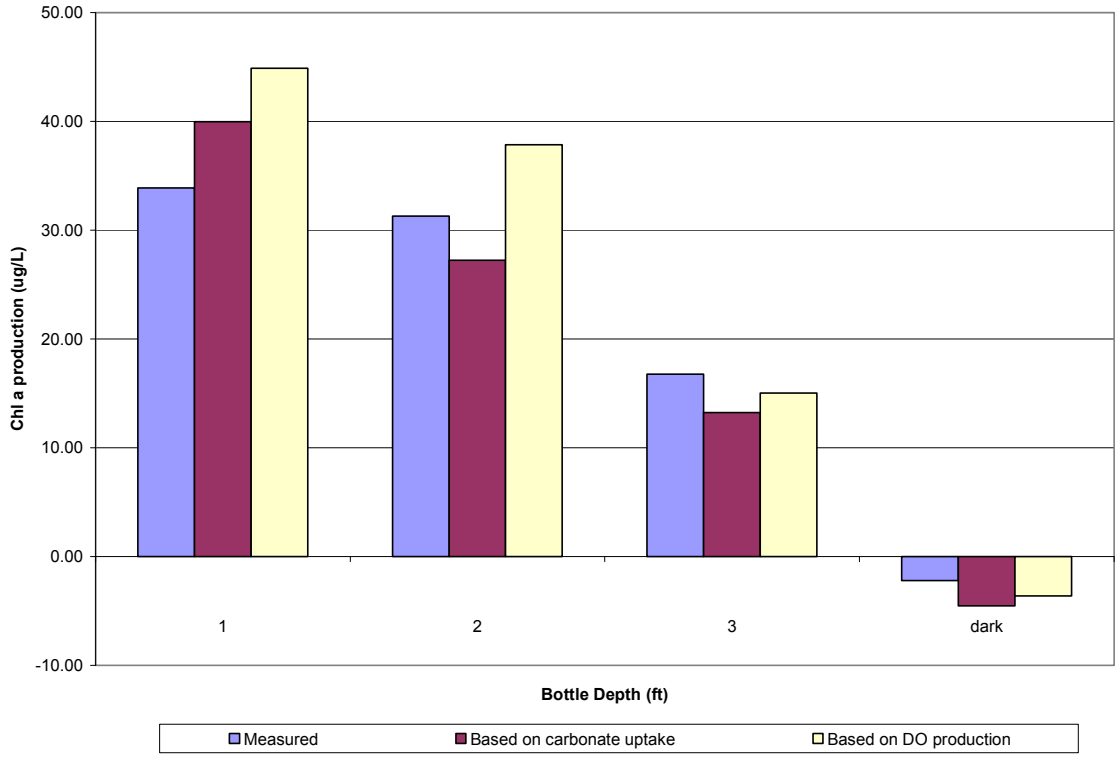

Figure 49: San Joaquin River bathymetry measured during the Lagrangian monitoring.

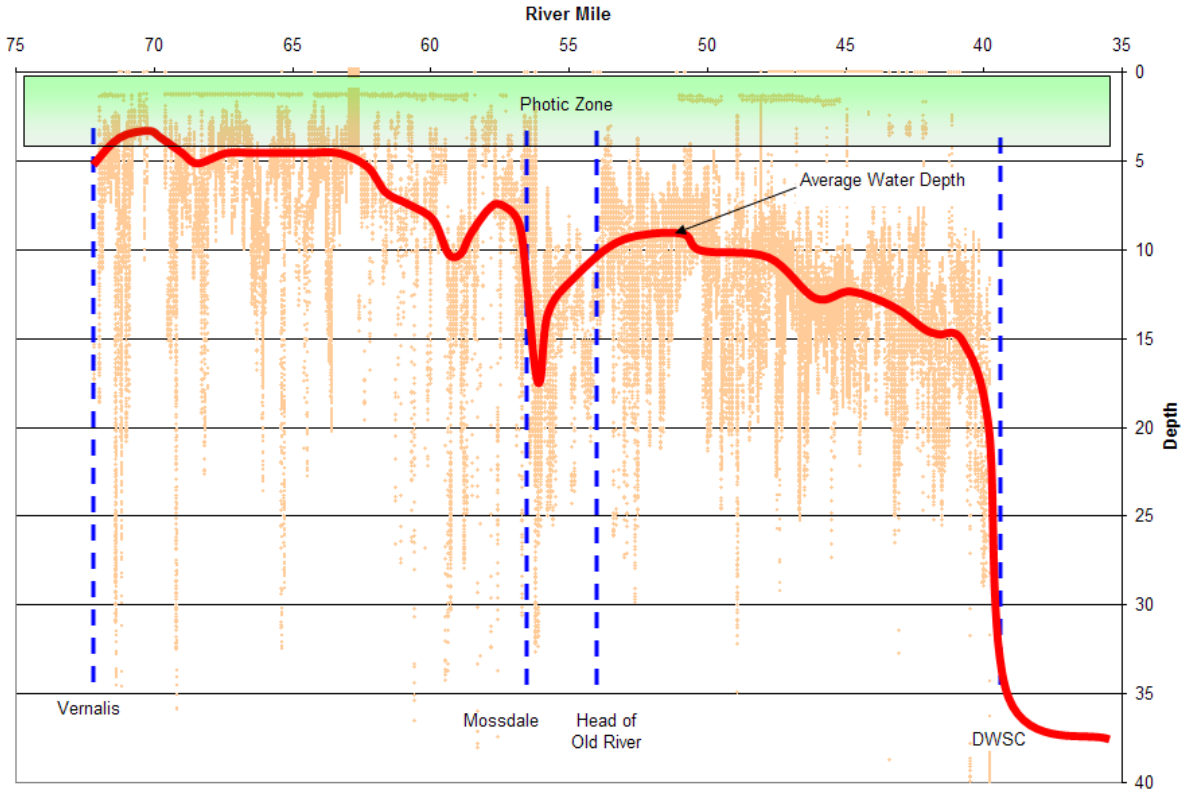

Figure 50: Attenuation fraction of the algal growth rate constant at water depths from 0 to 40 ft in the San Joaquin River. The example was generated with a Secchi-disk depth of 2 ft and optimal light intensity of 1300 umol/L and 2200 umol/L at the air-water interface.

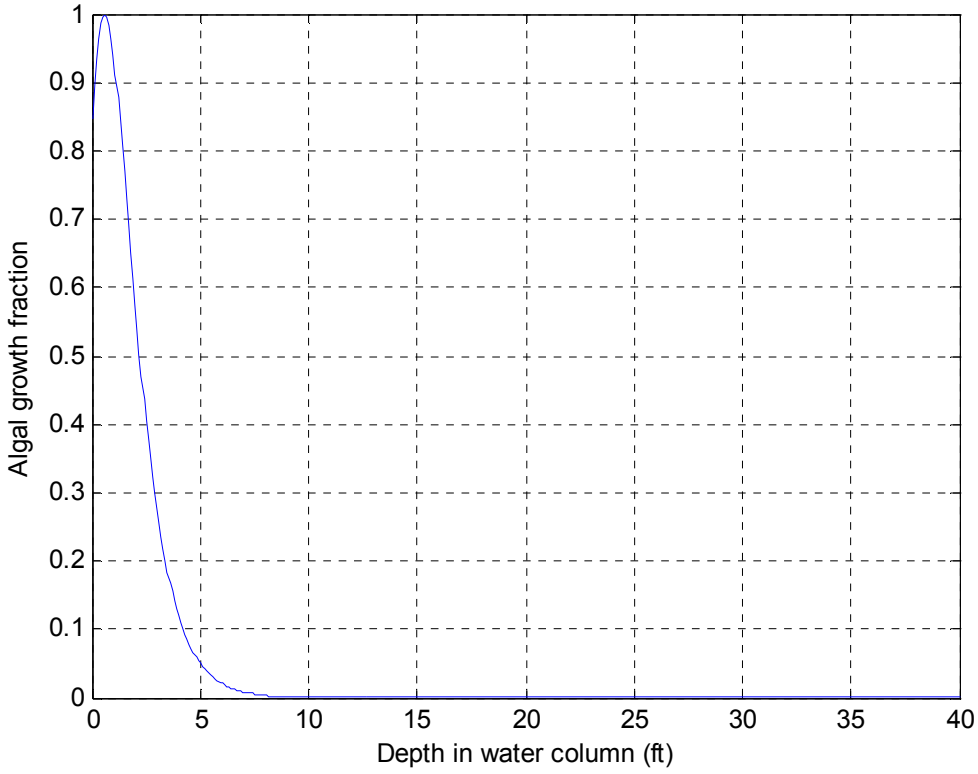

Figure 51: Response of the growth rate attenuation factor to the total water depth for the San Joaquin River. The example was generated with a Secchi-disk depth of 2 ft and optimal light intensity of 1300 umol/L and 2200 umol/L at the air-water interface.

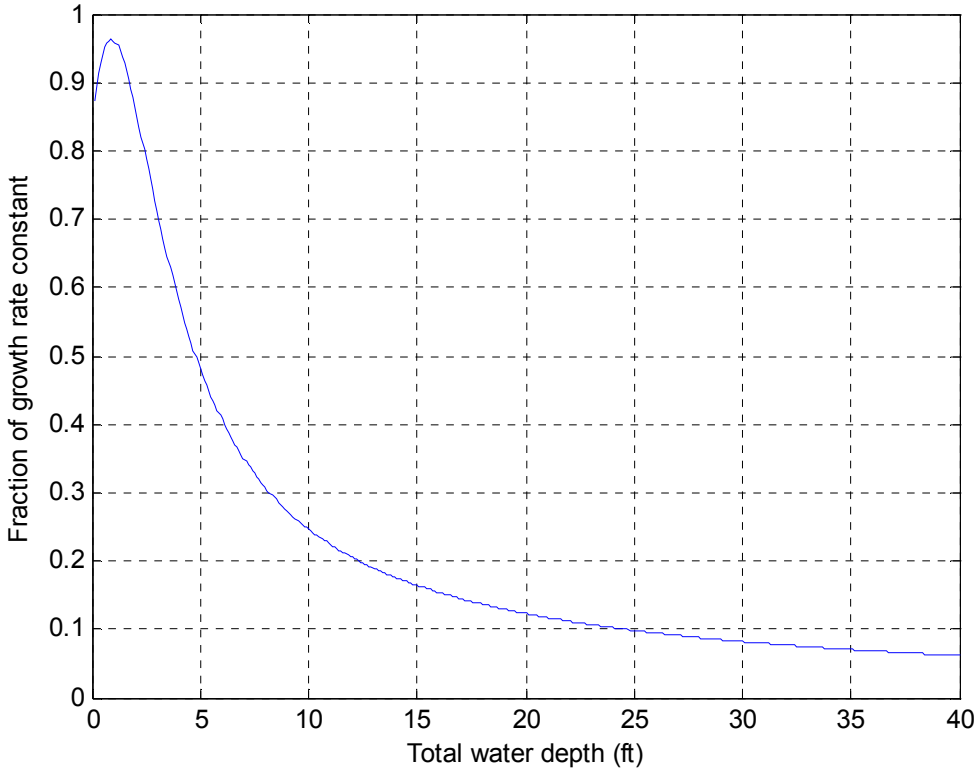

Figure 52: Half-sinusoid approximation of the normalized light intensity using a Fourier series (n=20). The fraction of daylight during the 24-day was 0.6. Time was set to 0 at sunrise.

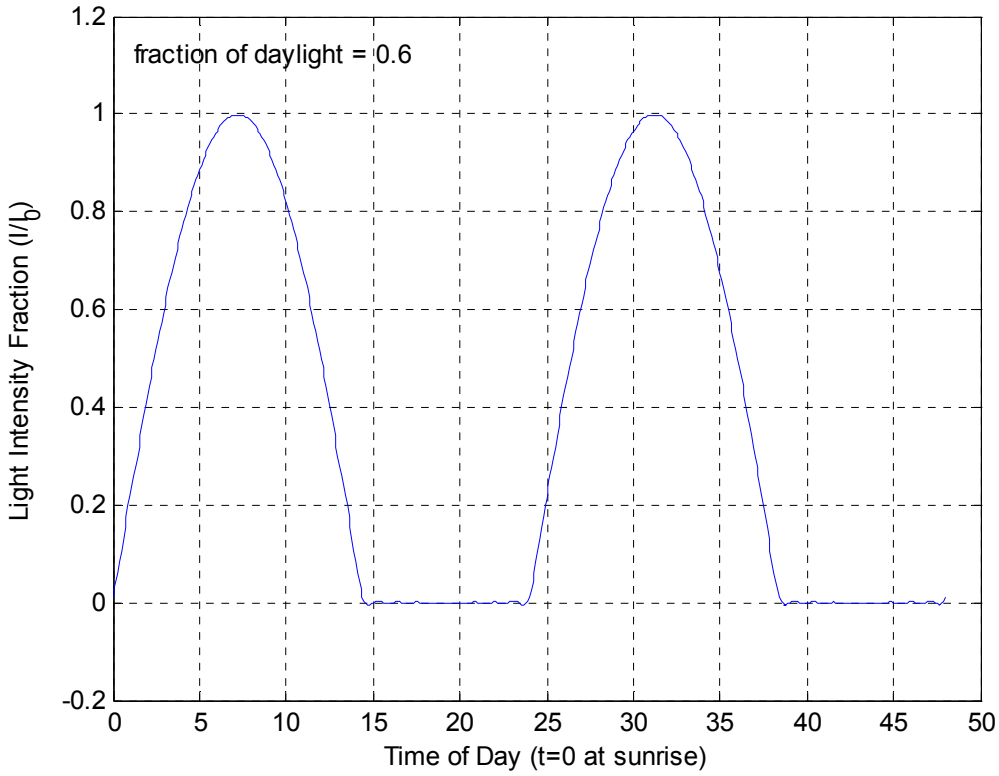

Figure 53: Simulated influence of river depth on chlorophyll *a* from Vernalis to the DWSC for flow conditions of September, 2005. Dye was released at 9:45 AM and tracked for the next 50 hours to the DWSC. The river depth was fixed at 5 feet and 20 feet for two of these simulations, the third line was calculated with the actual measured San Joaquin river depth in this reach. Parameters used in the simulations are presented in Table 3. Night is delineated with the shaded regions.

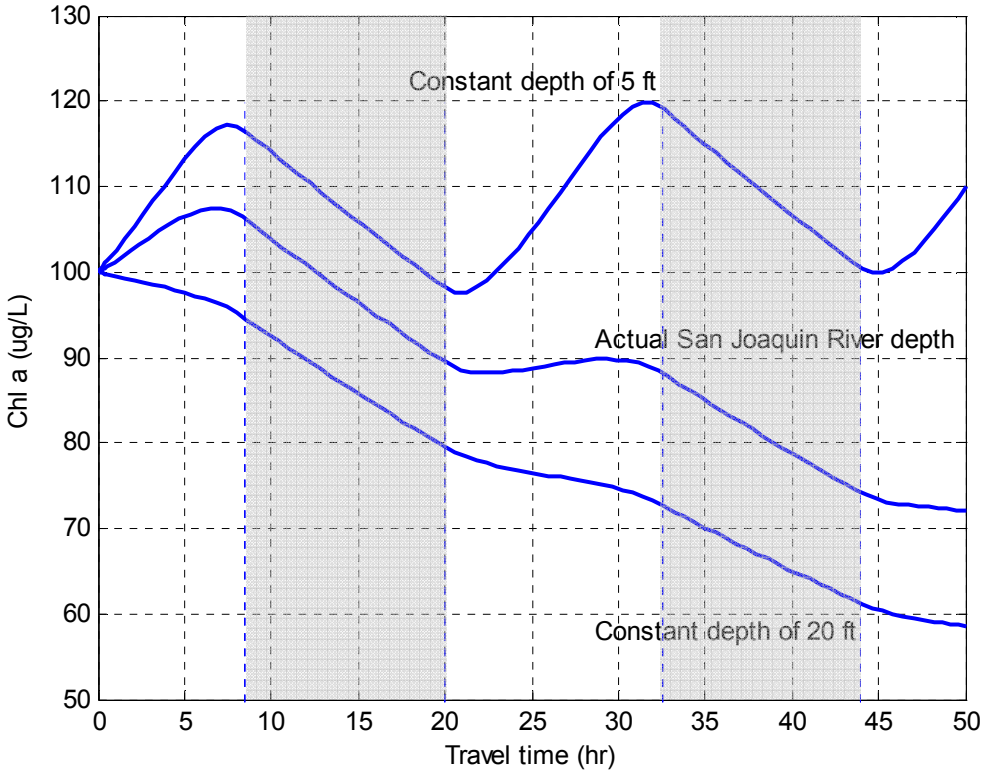

Figure 54: Simulations of chlorophyll a concentrations affected by light attenuation and zooplankton grazing for water traveling from Vernalis to the DWSC. Parameters used in the simulations are presented in Table 3. Night is delineated with the shaded regions.

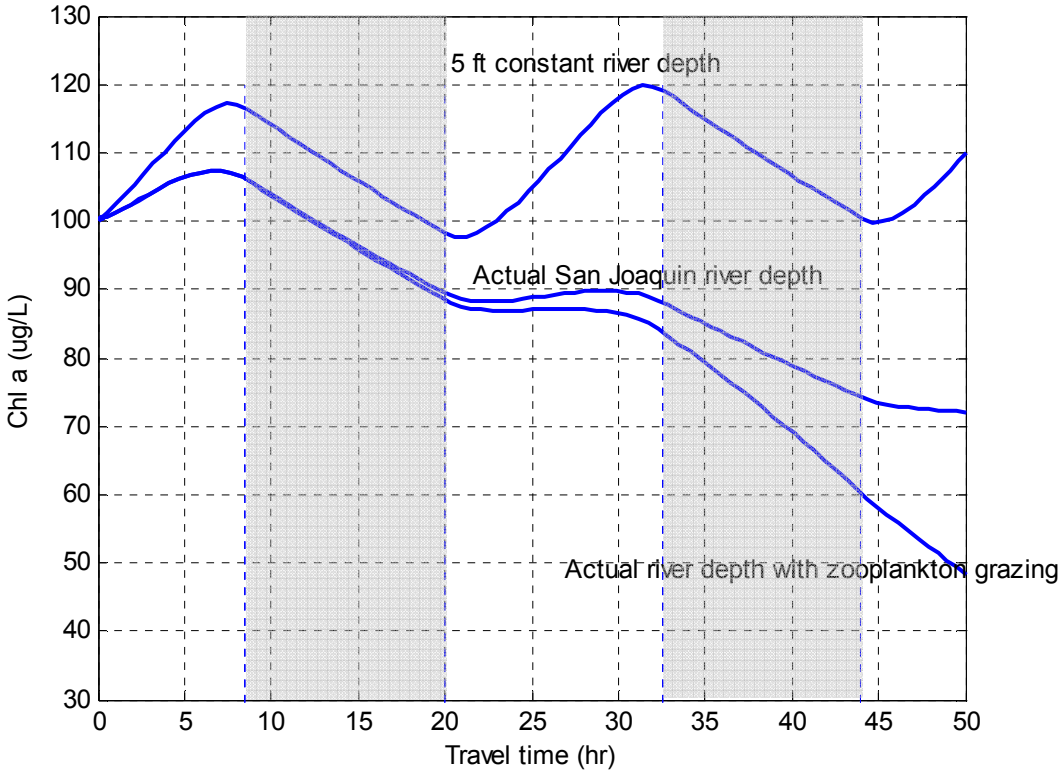

Figure 55: Simulations of the carbon concentrations associated with viable algae, decaying algae, and zooplankton for water flowing from Vernalis to the DWSC in 50 hours. Parameters used in the simulations are presented in Table 3. Night is delineated with the shaded regions.

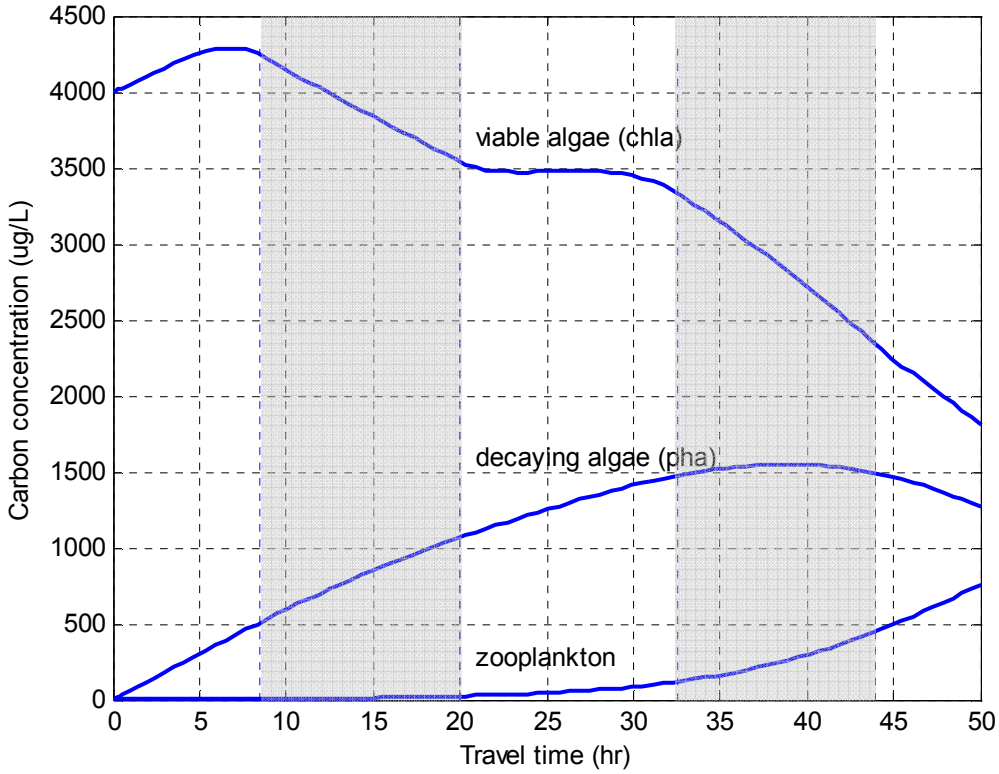

Figure 56: Comparison of observed and simulated chlorophyll a, pheophytin a, and zooplankton concentrations for the August, 2005 lagrangian monitoring.

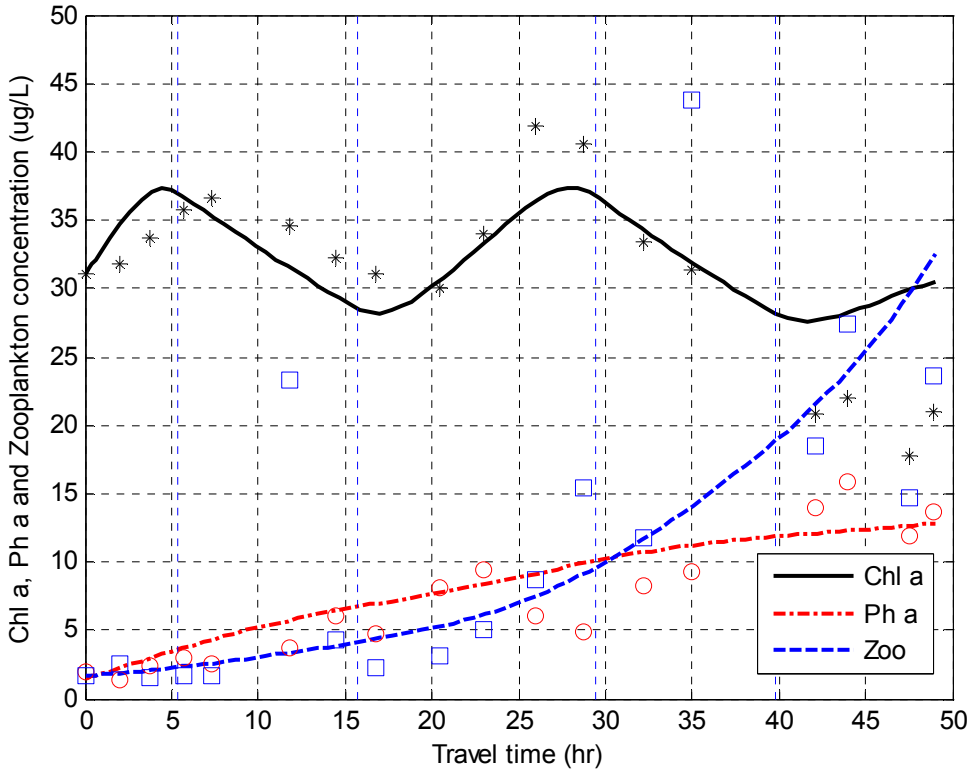

Figure 57: Comparison of observed and simulated chlorophyll a, pheophytin a, and zooplankton concentrations for the June, 2007 Lagrangian monitoring.

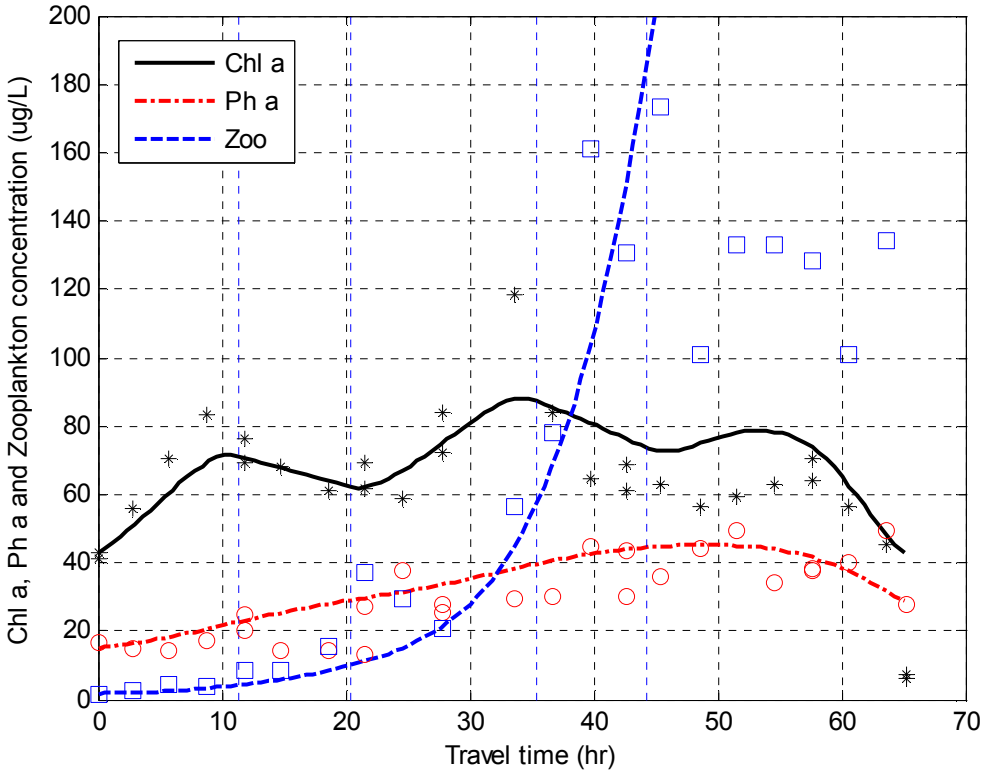

Description of Appendices

Appendix A Ultimate BOD data and figures

Tabular and graphical BOD and CBOD data and figures are contained in this Appendix.

Appendix B 2-D dye simulation text and figures

Development of a two-dimensional model for simulating conservative tracer transport in the San Joaquin River from Vernalis to the DWSC.

Electronic Appendices

Provision data sets have been made available in Excel format. All final data will be made available at the end of the project contract.

1. Fixed sonde data from fixed instruments deployed during the Lagrangian tracking events.
2. Lagrangian montoring data captured *insitu* or measured in the laboratory.
3. Algal productivity and zooplankton grazing microcosm experimental results.

Appendix A Ultimate BOD data and figures

Tabular and graphical BOD and CBOD data and figures are contained in this Appendix.

Table A-1: Summary of BOD for July 2005 Trial

Station	BOD						CBOD						NBOD						
	5 day	10 day	20 day	L_o	k	R^2	5 day	10 day	20 day	L_o	k	R^2	5 day	10 day	20 day	L_0^2	L_0^1	k	R^2
SJR 1	3.0	4.7	6.5	6.9	0.11	0.980	2.3	3.3	4.0	4.4	0.14	0.987	0.7	1.4	2.6	2.5	3.6	0.05	0.195
SJR 1 dup	2.8	3.9	5.9	6.5	0.10	0.955	2.2	2.9	3.8	3.9	0.15	0.974	0.6	1.1	2.1	2.5	-7.0	-0.01	0.200
SJR 3	3.4	3.9	4.8	7.2	0.12	0.967	2.3	2.8	3.1	4.4	0.14	0.973	1.1	1.1	1.7	2.7	2.8	0.10	0.621
SJR 3 dup	3.5	4.1	5.2	7.8	0.12	0.987	2.7	3.3	3.5	4.8	0.15	0.980	0.8	0.9	1.6	3.0	5.2	0.03	0.211
SJR 5	4.7	7.1	9.2	12.7	0.08	0.868	2.8	3.8	4.7	4.9	0.16	0.991	1.8	3.4	4.5	7.8	-12.7	-0.02	0.062
SJR 5 dup	3.3	4.9	6.7	7.2	0.12	0.983	2.8	3.6	4.6	4.8	0.16	0.987	0.6	1.4	2.1	2.4	6.9	0.02	0.064
SJR 6	3.6	5.2	7.2	7.7	0.12	0.976	2.8	4.0	5.0	5.4	0.14	0.991	0.8	1.3	2.3	2.3	2.5	0.08	0.508
SJR 6 dup	3.4	4.0	5.1	7.9	0.11	0.989	2.6	3.0	3.4	4.6	0.15	0.986	0.8	1.0	1.8	3.3	10.5	0.02	0.178
SJR 9	2.6	3.6	5.7	6.5	0.09	0.903	2.4	3.2	4.3	4.6	0.14	0.968	0.2	0.5	1.5	1.9	-0.2	-0.12	0.792
SJR 9 dup	3.0	4.4	6.4	7.0	0.11	0.948	2.3	2.9	4.1	4.4	0.13	0.948	0.8	1.4	2.3	2.6	2.9	0.07	0.643
SJR 11	3.3	5.2	6.9	7.5	0.12	0.980	2.7	3.3	4.5	4.7	0.15	0.945	0.7	1.9	2.4	2.8	3.6	0.18	0.180
SJR 11 dup	2.7	5.2	6.9	8.8	0.08	0.694	2.7	3.6	4.6	4.9	0.14	0.986	0.0	1.6	2.3	3.8			

L_0^1: Determined from differences of individual BOD and CBOD data

L_0^2: Difference of BOD and CBOD Lo values

Table A-2: Summary of BOD for August 2005 Trial

Station	BOD						CBOD						NBOD						
	5 day	10 day	20 day	L_o	k	R^2	5 day	10 day	20 day	L_o	k	R^2	5 day	10 day	20 day	L_0^2	L_0^1	k	R^2
SJR 1	2.7	3.8	4.9	5.9	0.11	0.979	2.2	2.9	3.4	4.2	4.18	0.936	0.50	0.94	1.45	1.7	1.9	0.07	0.750
SJR 3	2.2	3.6	4.5	5.5	0.10	0.993	2.3	3.1	3.7	4.3	4.34	0.954	-0.12	0.47	0.85	1.1	0.1	-0.69	0.540
SJR 5	2.0	3.1	4.4	5.6	0.09	0.995	2.1	2.9	3.5	4.3	0.11	0.951	-0.08	0.24	0.87	1.3	0.1	-0.68	0.469
SJR 6	1.8	3.0	4.0	5.1	0.09	0.997	1.7	2.4	3.0	3.9	0.10	0.905	0.09	0.63	1.00	1.2	-1.4	-0.02	0.025
SJR 8	1.8	2.9	3.8	4.8	0.09	0.991	1.7	2.5	3.2	4.2	0.09	0.915	0.05	0.38	0.61	0.7	-12.6	0.00	0.000
SJR 10	2.1	3.3	4.4	5.6	0.09	0.993	2.0	2.7	3.4	4.1	0.12	0.950	0.03	0.53	1.04	1.5	-0.1	-0.13	0.394
SJR 12	2.3	3.3	4.9	6.3	0.08	0.951	2.5	3.3	4.1	4.9	0.12	0.950	-0.14	-0.06	0.77	1.3	0.0	-0.41	0.629
SJR 14	1.9	3.6	4.1	5.0	0.09	0.863	2.0	2.6	3.2	3.8	0.12	0.947	-0.12	0.98	0.89	1.2	0.1	-0.75	0.463
SJR 15	1.5	2.1	3.6	5.0	0.06	0.825	1.6	2.2	2.9	3.6	0.10	0.930	-0.09	-0.07	0.68	1.4	0.0	-0.43	0.573
SJR 17	1.5	2.2	3.5	4.9	0.07	0.922	1.6	2.2	2.5	3.4	0.11	0.850	-0.12	-0.02	1.02	1.5	0.0	-0.39	0.542
SJR 18	2.9	5.0	6.5	8.1	0.09	0.994	1.6	2.4	2.8	3.6	0.11	0.918	1.32	2.61	3.74	4.5	4.7	0.08	0.909
SJR 18 Dup	3.6	2.4	7.1	10.0	-0.35	0.133	1.9	2.7	3.3	4.1	0.11	0.951	1.70	-0.36	3.76	5.9	0.3	-0.35	0.133

L_0^1: Determined from differences of individual BOD and CBOD data

L_0^2: Difference of BOD and CBOD Lo values

Table A-3: Summary of BOD for September 2005 Trial

Station	BOD						CBOD						NBOD						
	5 day	10 day	20 day	L_o	k	R^2	5 day	10 day	20 day	L_o	k	R^2	5 day	10 day	20 day	L_0^2	L_0^1	k	R^2
SJR 1	4.4	3.2	2.5	3.3	0.08	0.971	8.9	4.9	4.1	5.0	0.11	0.969	-4.4	-1.7	-1.6	-1.8	-1.9	0.16	0.969
SJR 1 Dup	9.3	5.9	4.8	5.8	0.10	0.988	10.6	5.1	4.6	5.5	0.12	0.965	-1.3	0.8	0.2	0.3	20.4	7.67	0.240
SJR 4	8.2	5.7	4.6	5.6	0.09	0.996	8.6	5.0	4.0	4.9	0.12	0.983	-0.4	0.7	0.5	0.8	0.2	-0.79	0.425
SJR 7	10.8	7.0	5.6	6.6	0.11	1.000	9.1	4.9	4.2	5.0	0.12	0.978	1.7	2.2	1.5	1.6	1.6	0.08	0.709
SJR 10	9.6	6.2	5.1	6.1	0.10	0.995	9.7	5.1	6.7	6.2	0.10	0.715	-0.1	1.1	-1.6	-0.1	0.0	-0.40	0.256
SJR 10 Dup	10.1	6.3	5.3	6.4	0.10	0.995	8.7	4.5	4.1	4.9	0.11	0.978	1.4	1.8	1.2	1.5	1.8	0.05	0.698
SJR 12	9.8	6.2	5.0	6.1	0.10	0.991	7.3	5.5	4.2	5.2	0.09	0.996	2.4	0.7	0.9	1.0	1.0	0.14	0.910
SJR 14	7.3	5.5	4.2	5.2	0.09	0.996	8.6	4.5	3.9	4.7	0.12	0.974	-1.2	1.0	0.3	0.5	0.2	-1.12	0.549
SJR 21	7.3	4.7	3.8	4.6	0.10	0.992	6.8	3.6	3.1	3.9	0.11	0.965	0.5	1.1	0.6	0.7	1.0	0.04	0.211
SJR 21 Dup	8.0	5.4	4.4	5.4	0.10	0.994	7.5	4.2	3.5	4.2	0.12	0.979	0.5	1.2	0.9	1.2	-1.6	-0.02	0.088
SJR 23	11.5	7.0	5.5	6.5	0.12	0.978	5.5	3.5	2.9	3.7	0.09	0.978	6.0	3.5	2.5	2.8	2.9	0.15	0.966

L_0^1: Determined from differences of individual BOD and CBOD data

L_0^2: Difference of BOD and CBOD Lo values

Table A-4: Summary of BOD for October 2005 Trial

Station	BOD						CBOD						NBOD						
	5 day	10 day	20 day	L_o	k	R^2	5 day	10 day	20 day	L_o	k	R^2	5 day	10 day	20 day	L_0^2	L_0^1	k	R^2
SJR 1	3.8	4.4	3.9	4.4	0.13	0.941	3.5	3.7	3.5	3.9	0.15	0.948	0.3	0.7	0.4	0.5	0.5	-1.36	0.323
SJR 1 Dup	3.6	4.2	3.8	4.2	0.12	0.941	3.0	3.6	3.5	3.8	0.16	0.926	0.6	0.6	0.3	0.4	26.2	7.52	0.248
SJR 3	4.0	4.5	4.1	4.5	0.13	0.946	3.8	4.3	4.0	4.4	0.17	0.951	0.2	0.2	0.1	0.1	0.0	-0.42	0.467
SJR 5	3.7	4.1	3.7	4.1	0.12	0.945	2.8	3.7	3.4	3.8	0.17	0.926	0.9	0.4	0.3	0.3	0.0	-0.44	0.471
SJR 7	3.7	4.3	3.8	4.2	0.14	0.949	3.1	3.7	3.4	3.8	0.17	0.945	0.6	0.6	0.4	0.4	2.7	-2.68	0.339
SJR 7 Dup	3.3	4.3	3.7	4.2	0.14	0.928	2.5	3.3	3.3	3.6	0.16	0.899	0.8	1.1	0.4	0.6	0.0	-0.60	0.537
SJR 9	3.1	4.8	4.2	4.6	0.14	0.898	4.0	4.9	4.2	4.7	0.13	0.939	-0.9	-0.1	0.0	-0.1	0.0	-1.16	0.763
SJR 11	4.0	4.9	4.2	4.7	0.13	0.939	3.2	3.8	3.5	4.0	0.17	0.940	0.7	1.1	0.7	0.7	0.2	-0.82	0.456
SJR 12	5.1	4.9	4.5	5.0	0.12	0.974	3.5	4.0	3.6	4.1	0.17	0.953	1.5	0.9	0.8	1.0	0.3	-0.94	0.515
SJR 12 Dup	5.3	4.8	4.4	4.9	0.13	0.981	3.1	3.6	3.4	3.8	0.17	0.944	2.2	1.2	1.0	1.1	0.1	-0.71	0.558

L_0^1: Determined from differences of individual BOD and CBOD data

L_0^2: Difference of BOD and CBOD Lo values

Table A-5: Summary of BOD for July 2006 Trial

Station	BOD						CBOD						NBOD						
	5 day	10 day	20 day	L_o	k	R^2	5 day	10 day	20 day	L_o	k	R^2	5 day	10 day	20 day	L_0^2	L_0^1	k	R^2
SJR 1	4.4	7.3	8.9	10.1	0.13	0.999	3.5	5.2	6.1	6.7	0.16	0.998	0.9	2.1	2.8	3.4	4.5	0.05	0.746
SJR 1 Dup	4.5	7.3	8.9	10.1	0.13	0.999	4.3	6.1	7.2	7.9	0.16	0.991	0.2	1.2	1.7	2.2	-0.8	-0.07	0.292
SJR 3	3.9	6.4	7.7	8.7	0.13	0.999	3.0	4.1	5.5	6.0	0.14	0.974	0.9	2.2	2.3	2.7	2.7	0.11	0.758
SJR 5	3.9	6.5	7.7	8.7	0.13	0.997	2.8	4.2	5.0	5.5	0.15	0.997	1.1	2.3	2.8	3.2	3.5	0.09	0.885
SJR 7	4.5	7.4	9.3	10.7	0.12	0.999	4.1	5.9	6.9	7.0	0.19	0.903	0.4	1.5	2.4	3.7	-1.0	-0.07	0.323
SJR 9	5.1	8.4	10.5	12.1	0.12	0.999	4.2	6.1	7.3	7.9	0.16	0.987	0.9	2.3	3.2	4.2	15.6	0.01	0.055
SJR 11	4.1	7.0	8.5	9.6	0.13	0.996	4.2	6.7	8.0	8.8	0.14	0.997	-0.1	0.3	0.5	0.8	0.0	-0.60	0.578
SJR 13	4.2	6.7	8.0	8.8	0.14	0.997	3.5	4.9	5.9	6.4	0.16	0.990	0.8	1.8	2.1	2.4	2.8	0.08	0.717
DWSC	3.2	4.8	5.9	6.5	0.14	0.996	2.6	3.8	4.3	4.7	0.17	0.996	0.7	1.0	1.6	1.8	2.2	0.07	0.925

L_0^1: Determined from differences of individual BOD and CBOD data

L_0^2: Difference of BOD and CBOD Lo values

Table A-6: Summary of BOD for August 2006 Trial

Station	BOD						CBOD						NBOD						
	5 day	10 day	20 day	L_o	k	R^2	5 day	10 day	20 day	L_o	k	R^2	5 day	10 day	20 day	L_0^2	L_0^1	k	R^2
SJR 1	3.9	6.1	7.4	8.5	0.13	0.999	3.6	4.9	5.8	6.5	0.16	0.993	0.29	1.23	1.58	2.0	-3.3	-0.02	0.056
SJR 3	4.9	7.5	9.2	10.5	0.13	1.000	4.5	6.3	7.5	8.4	0.15	0.996	0.40	1.16	1.72	2.1	2	0.07	0.925
SJR 6	5.2	8.2	9.8	11.2	0.13	0.998	4.8	6.7	8.1	9.1	0.14	0.994	0.40	1.48	1.65	2.1	7.3	0.02	0.025
SJR 9	5.4	8.6	10.8	12.6	0.11	0.999	4.2	5.8	6.9	7.7	0.15	0.993	1.18	2.85	3.94	4.9	8.4	0.03	0.450
SJR 11	4.4	6.1	7.0	7.8	0.16	0.996	3.8	5.6	6.6	7.4	0.14	0.996	0.58	0.48	0.37	0.4	0.6	0.46	0.986
DWSC	4.3	5.8	7.0	7.9	0.15	0.993	4.4	6.1	7.4	8.3	0.15	0.992	-0.17	-0.28	-0.38	-0.4	-0.4	0.10	0.806

L_0^1: Determined from differences of individual BOD and CBOD data

L_0^2: Difference of BOD and CBOD Lo values

Table A-7: Summary of BOD for June 12, 2007 Trial

Station	River Mile	BOD						CBOD					
		5	10	20	Lo	k	R^2	5	10	20	Lo	k	R^2
SJR 1	71.90	2.77	4.62	6.59	7.49	0.11	0.97	1.99	3.32	4.00	4.46	0.15	1.00
SJR 1 dup	71.90	2.51	4.37	6.52	7.76	0.09	0.97	2.01	3.07	4.74	5.30	0.11	0.91
SJR 2	67.50	3.03	5.29	7.88	9.37	0.09	0.97	1.99	3.32	4.00	4.46	0.15	1.00
SJR 4	60.88	4.48	7.80	11.20	13.11	0.10	0.98	3.26	5.53	8.13	9.37	0.10	0.97
SJR 6	56.40	4.08	7.06	10.28	11.96	0.10	0.97	3.08	5.47	8.00	9.58	0.09	0.98
SJR 8	55.10	3.52	6.39	9.08	11.08	0.09	0.98	2.47	4.18	6.06	6.83	0.11	0.96
SJR 10	51.00	4.21	7.58	10.68	12.65	0.10	0.99	2.89	5.25	7.73	9.30	0.09	0.98
SJR 12	47.10	5.54	9.22	11.85	13.32	0.13	0.99	4.13	7.18	9.78	10.99	0.11	0.99
SJR 14	44.67	4.26	7.36	10.33	12.00	0.11	0.98	2.73	5.02	7.70	9.77	0.08	0.97
SJR 16	49.10	4.33	6.83	10.04	11.30	0.11	0.94	2.57	4.74	7.32	9.26	0.08	0.97
SJR 18	44.00	3.75	7.92	10.39	13.09	0.09	0.98	2.84	5.38	7.69	9.38	0.09	1.00
SJR 20	43.80	6.16	7.50	7.74	9.21	0.27	0.98	5.91	7.19	7.42	8.83	0.27	0.98
SJR 22	41.36	3.20	6.32	7.80	9.09	0.11	0.99	2.41	4.45	6.35	7.62	0.09	0.99
SJR 23	39.86	1.74	4.66	5.73	8.30	0.07	0.75	1.33	2.51	3.41	3.99	0.10	1.00
SJR 23 dup	39.86	1.76	4.68	5.75	8.19	0.07	0.76	1.89	3.29	4.35	4.87	0.12	0.99

Table A-8: Summary of BOD for July 17, 2007 Trial

Station	River Mile	BOD						CBOD					
		5	10	20	Lo	k	R^2	5	10	20	Lo	k	R^2
Lt 48	39.50	1.73	3.44	4.87	6.18	0.08	1.00	1.63	2.68	3.18	3.53	0.15	0.99
SJR RM 40	40.00	1.69	3.04	4.22	4.96	0.10	0.99	1.57	2.42	3.20	3.58	0.14	0.97
SJR RM 44	44.00	1.68	3.56	5.25	7.35	0.07	0.99	1.51	2.30	3.14	3.47	0.13	0.96
SJR RM 48	48.00	3.95	8.86	12.17	16.70	0.07	0.95	2.90	5.01	6.76	7.72	0.11	0.99
SJR RM 52	52.00	4.33	8.68	12.99	17.79	0.07	0.97	3.60	6.17	8.35	9.49	0.11	0.98
SJR RM 54	54.00	5.52	10.61	14.84	18.40	0.09	0.99	4.68	7.41	9.93	11.04	0.13	0.97
Lt 48	39.50	2.02	4.01	6.28	8.94	0.06	0.98	1.71	2.77	3.60	4.03	0.13	0.99
SJR RM 40	40.00	2.36	4.69	6.41	7.89	0.09	1.00	2.00	3.13	4.03	4.48	0.14	0.98
SJR RM 44	44.00	4.03	8.41	12.40	17.20	0.07	0.99	3.81	6.67	8.86	10.09	0.12	0.99
SJR RM 48	48.00	5.18	10.14	15.64	21.41	0.07	0.98	4.88	8.21	10.71	12.01	0.13	0.99
SJR RM 52	52.00	6.06	12.44	17.42	22.22	0.08	1.00	5.44	8.99	12.03	13.51	0.12	0.98
SJR RM 54	54.00	6.40	12.13	18.75	24.47	0.07	0.97	5.88	9.64	13.14	14.74	0.12	0.97

Table A-9: Summary of BOD for July 20, 2007 Trial

Station	River Mile	BOD						CBOD					
		5	10	20	Lo	k	R^2	5	10	20	Lo	k	R^2
SJR 1	71.90	3.43	7.41	10.11	13.05	0.08	0.99	2.83	5.06	6.60	7.57	0.11	0.99
SJR 1 dup	71.90	3.38	7.10	9.89	12.71	0.08	0.99	2.68	4.83	6.44	7.45	0.11	0.99
SJR 3	64.00	5.61	10.83	13.95	16.20	0.11	0.96	4.72	8.70	11.97	14.12	0.10	0.98
SJR 5	61.00	5.22	10.33	13.19	15.38	0.10	0.95	4.39	7.68	10.57	12.22	0.11	0.98
SJR 7	58.00	4.55	9.59	12.15	14.53	0.10	0.95	3.67	6.57	8.75	10.09	0.11	0.99
SJR 8	56.70	4.29	9.65	12.12	14.91	0.09	0.93	n/a	n/a	n/a	n/a	n/a	n/a

Table A-10: Summary of BOD for July 24, 2007 Trial

Station	River Mile	BOD					
		5	10	20	Lo	k	R^2
Lt 48	39.60	1.96	3.40	5.38	6.67	0.08	0.99
SJR RM 40	40.00	2.03	3.43	5.91	7.88	0.07	0.97
SJR RM 44	44.00	4.00	8.25	14.53	23.87	0.05	0.92
SJR RM 48	48.00	5.14	8.51	14.18	16.35	0.09	0.89
SJR RM 52	52.00	4.98	8.88	14.84	17.66	0.08	0.84
SJR RM 54	54.00	5.32	9.13	15.34	18.38	0.08	0.90
Mossdale	56.70	4.98	8.79	14.24	17.21	0.08	0.95
Mossdale dup	56.70	4.93	8.80	14.89	18.65	0.07	0.91

Table A-11: Summary of BOD for August 15, 2007 Trial

Station	River Mile	BOD						CBOD					
		5	10	20	Lo	k	R^2	5	10	20	Lo	k	R^2
Lt 48	39.60	1.02	2.23	2.87	3.61	0.09	0.97	1.12	1.72	2.04	2.31	0.16	0.99
Lt 48 dup	39.60	1.32	2.38	3.22	3.75	0.11	0.99	1.23	1.88	2.26	2.56	0.16	0.98
SJR RM 40	40.00	1.26	2.41	3.40	4.15	0.09	1.00	1.39	2.05	2.41	2.72	0.18	0.98
SJR RM 42	42.00	1.03	2.10	3.14	4.37	0.07	0.99	1.02	1.70	2.33	2.70	0.11	0.97
SJR RM 46	46.00	1.48	3.06	4.24	5.42	0.08	1.00	1.06	1.74	2.33	2.68	0.12	0.97
SJR RM 50	50.00	2.18	4.08	5.73	6.93	0.09	0.99	2.23	3.30	4.07	4.51	0.16	0.98
SJR RM 54	54.00	4.92	8.74	12.30	14.49	0.10	0.99	4.78	7.68	9.82	10.80	0.14	0.99
Mossdale	56.70	5.65	9.62	14.01	16.25	0.10	0.97	4.78	7.68	9.82	10.80	0.14	0.99
Mossdale dup	56.70	5.33	9.70	13.59	16.02	0.10	0.99	4.78	7.64	9.84	10.79	0.14	0.98
Lt 48	39.60	2.01	3.55	4.44	5.02	0.13	1.00	1.93	2.68	3.22	3.59	0.18	0.98
SJR RM 40	40.00	1.90	3.42	4.68	5.50	0.10	0.99	1.50	2.35	3.06	3.44	0.14	0.97
SJR RM 40 dup	40.00	2.04	3.59	4.79	5.50	0.11	0.99	1.78	2.71	3.32	3.72	0.16	0.98
SJR RM 42	42.00	1.72	3.43	4.39	5.23	0.10	1.00	1.14	1.94	2.49	2.85	0.13	0.99
SJR RM 46	46.00	2.60	4.87	6.19	7.14	0.12	1.00	2.10	3.35	4.04	4.49	0.16	0.99
SJR RM 50	50.00	5.34	10.22	13.53	16.15	0.10	1.00	4.85	7.75	9.80	10.74	0.15	0.99
SJR RM 54	54.00	6.36	12.06	14.95	17.33	0.12	1.00	5.69	9.36	11.75	12.94	0.14	0.99
Mossdale	56.70	6.78	12.54	16.27	18.75	0.11	1.00	5.69	9.36	11.75	12.94	0.14	0.99
Mossdale dup	56.70	6.88	12.98	16.49	19.08	0.11	1.00	5.80	9.41	11.74	12.88	0.15	0.99

Figure Set A-1: Plots of BOD, CBOD, and NBOD vs. Time for the July 2005 Trial

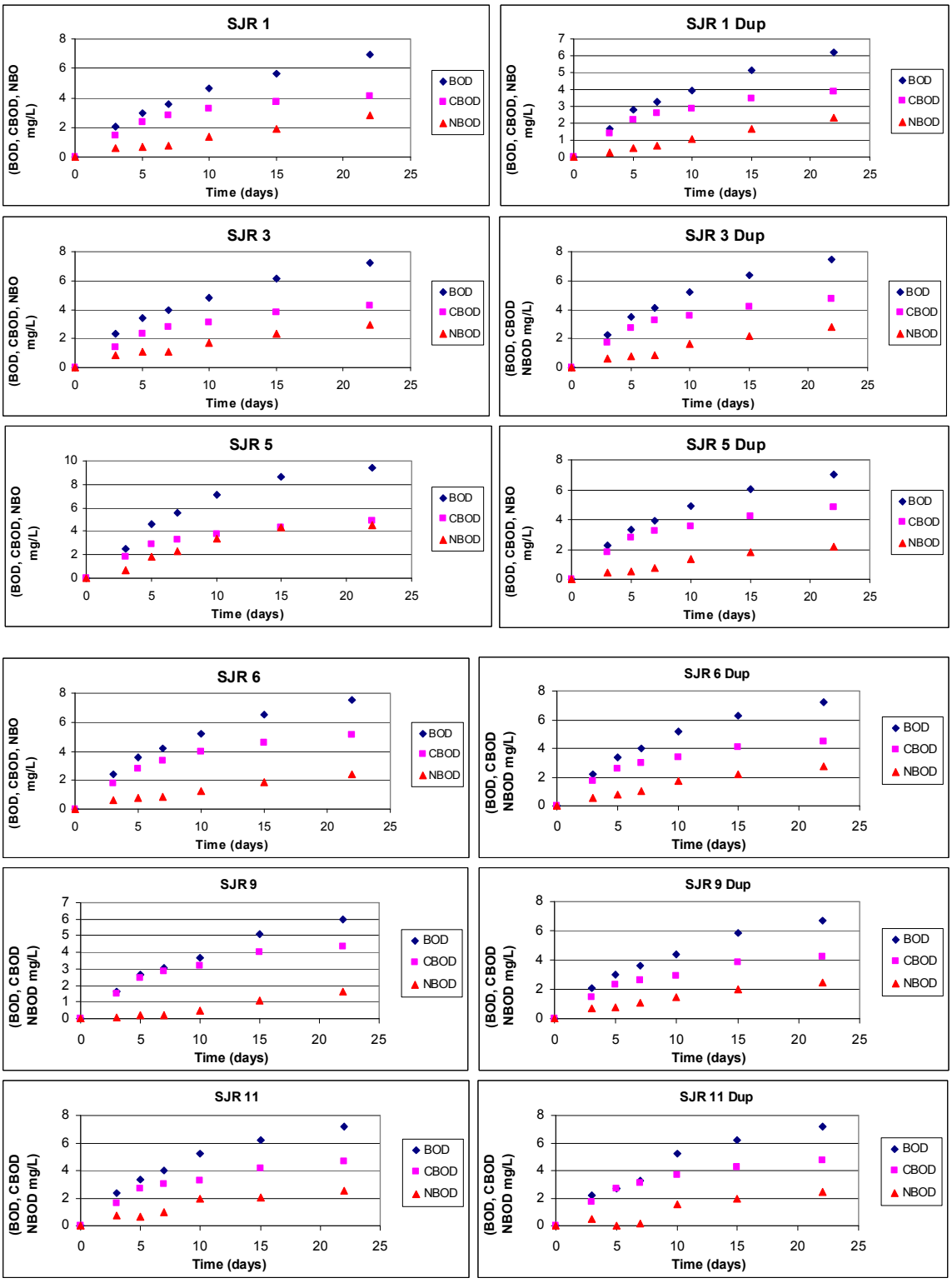

Figure Set A-2: Plots of BOD, CBOD, and NBOD vs. Time for the August 2005 Trial

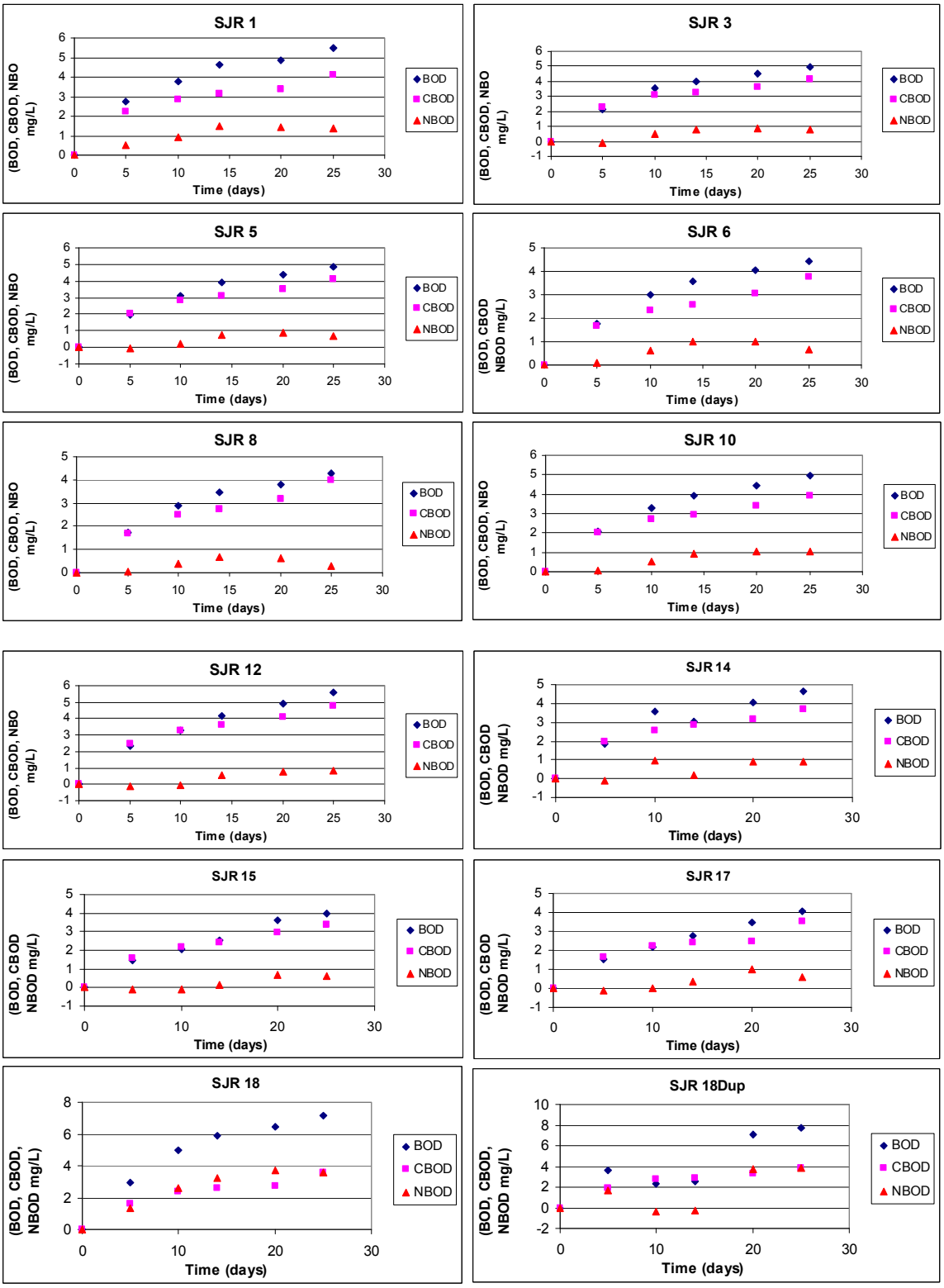

Figure Set A-3: Plots of BOD, CBOD, and NBOD vs. Time for the September 2005 Trial

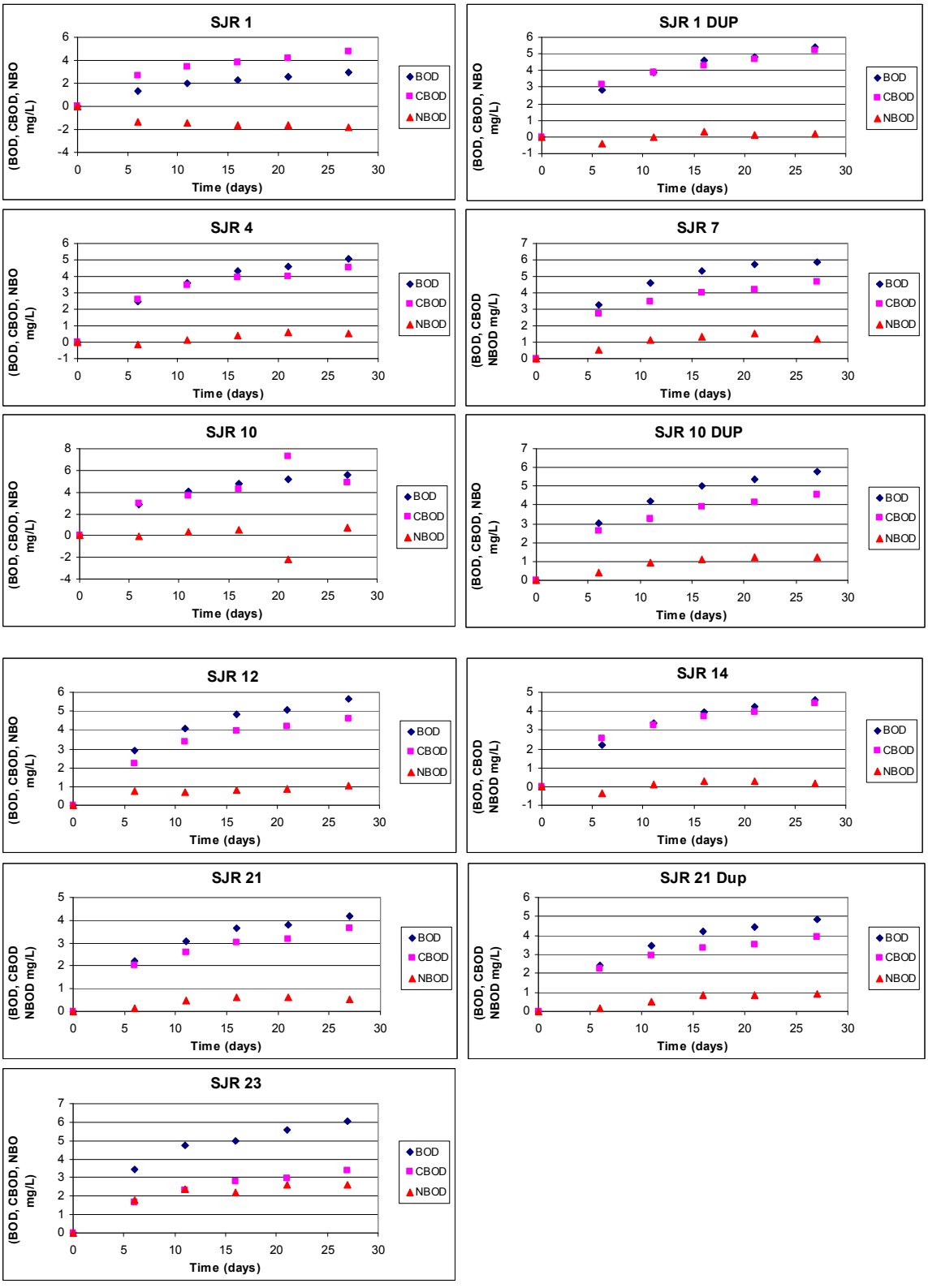

Figure Set A-4: Plots of BOD, CBOD, and NBOD vs. Time for the October 2005 Trial

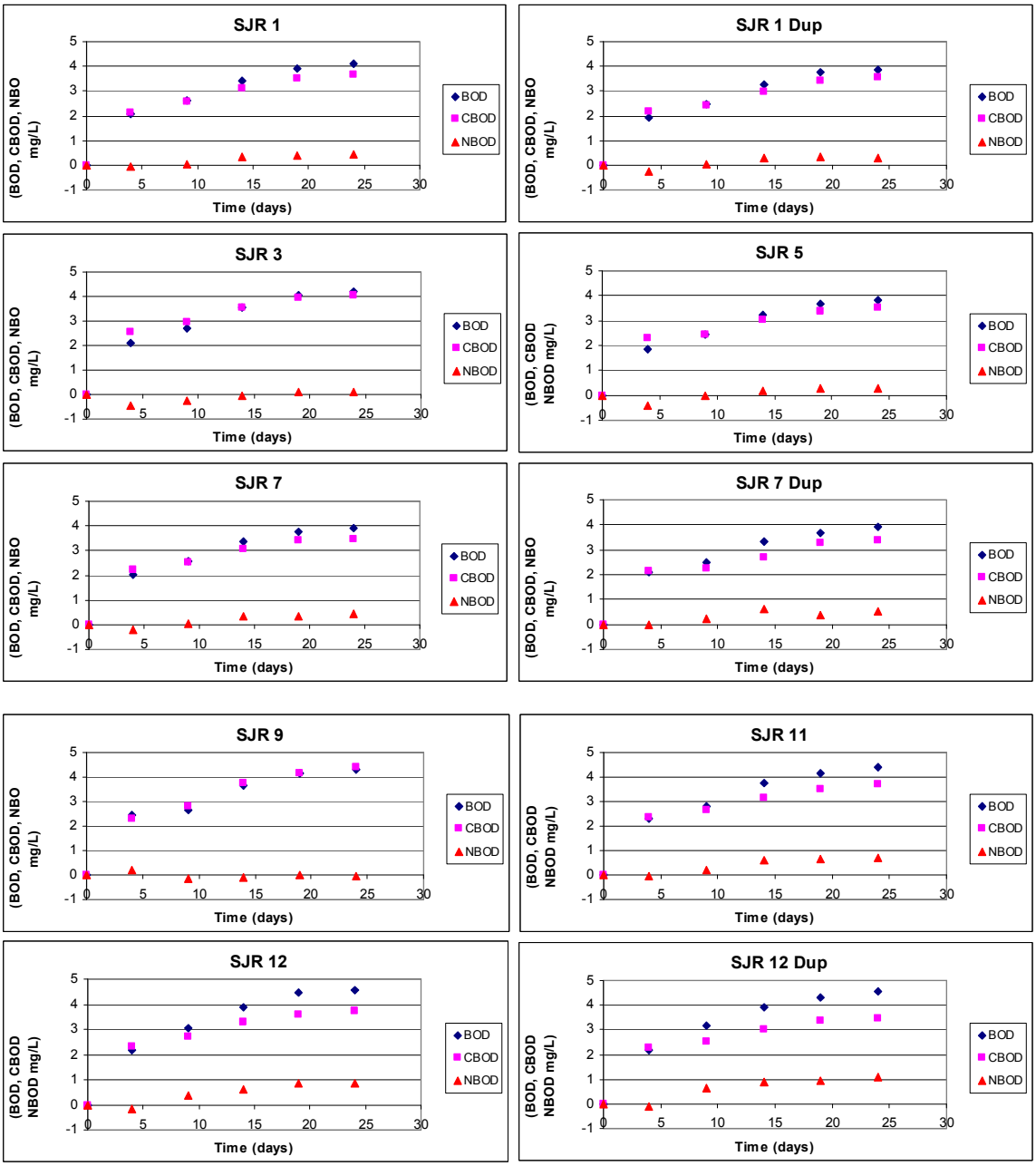

Figure Set A-5: Plots of BOD, CBOD, and NBOD vs. Time for the July 2006 Trial

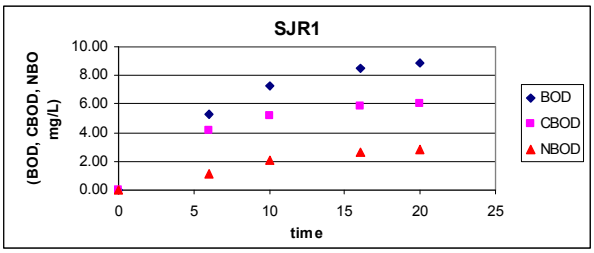

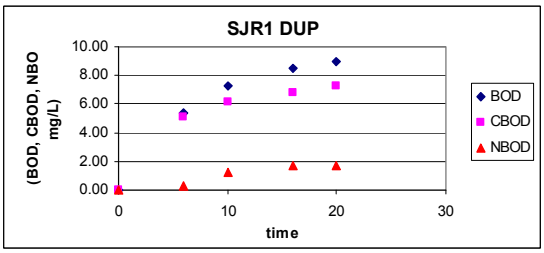

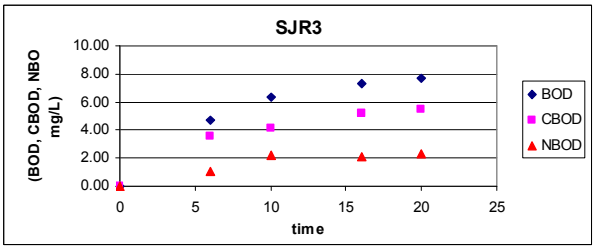

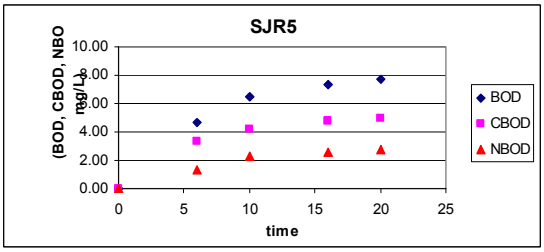

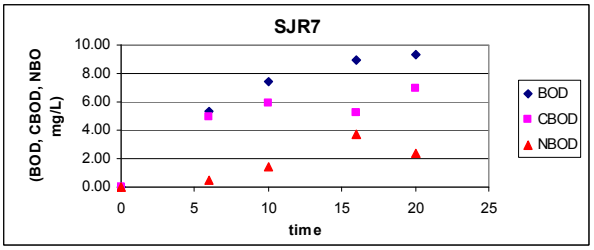

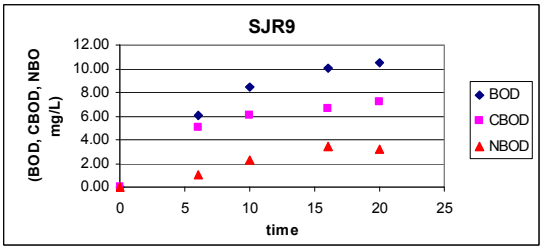

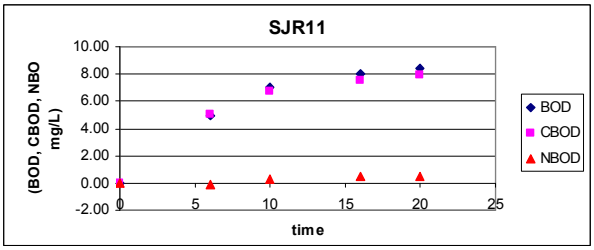

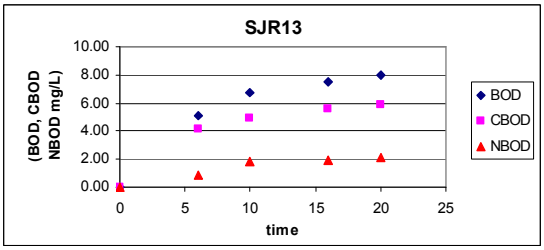

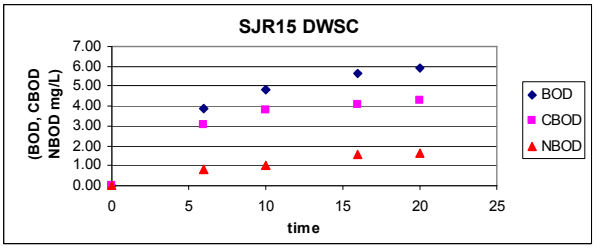

Figure Set A-6: Plots of BOD, CBOD, and NBOD vs. Time for the August 2006 Trial

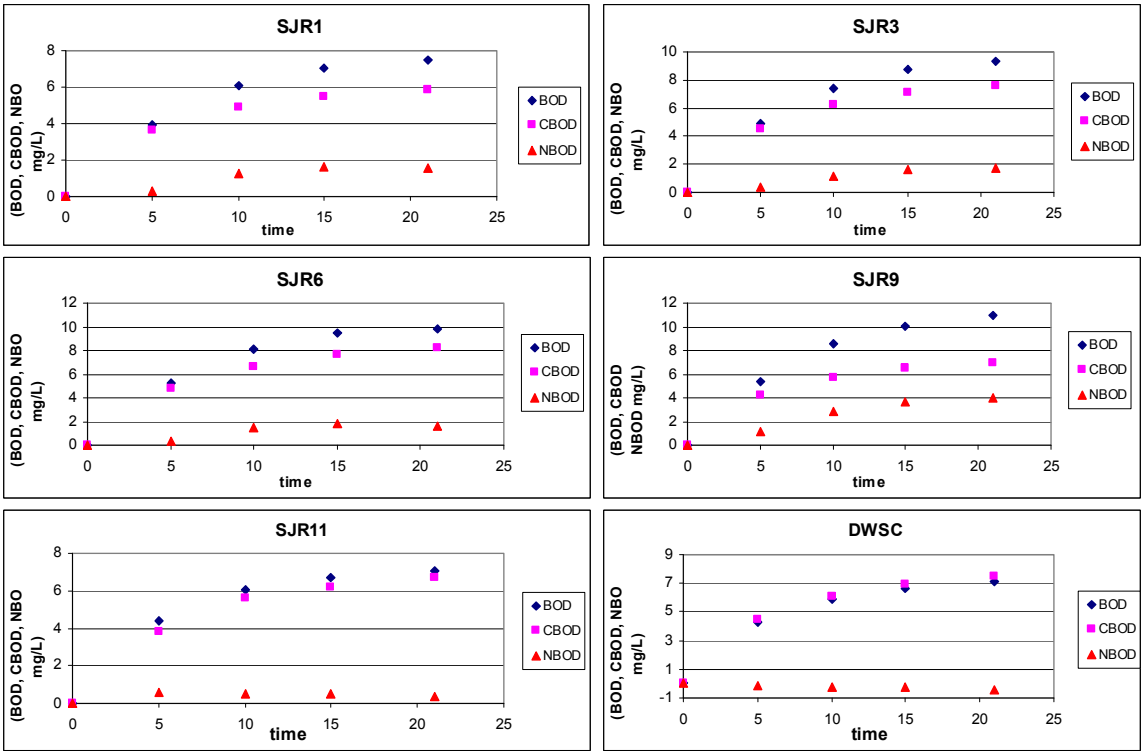

Figure Set A-7: Plots of BOD vs. River Mile for June 2007 Trial

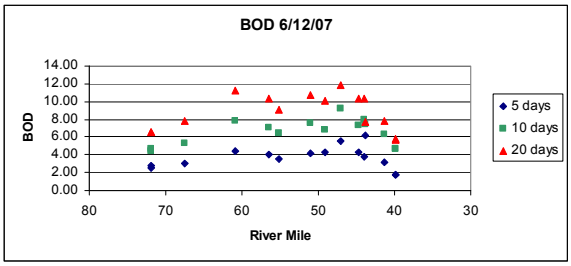

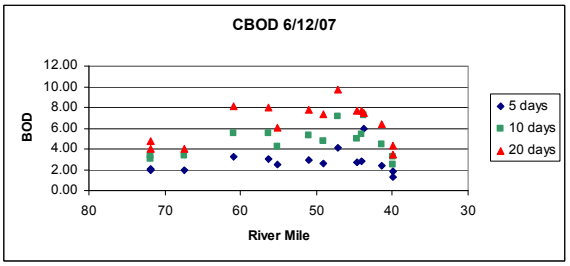

Figure Set A-8: Plots of BOD vs. River Mile for July 2007 Trial

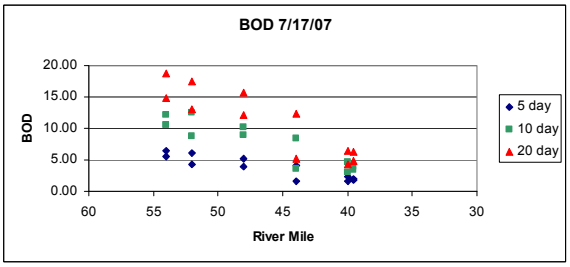

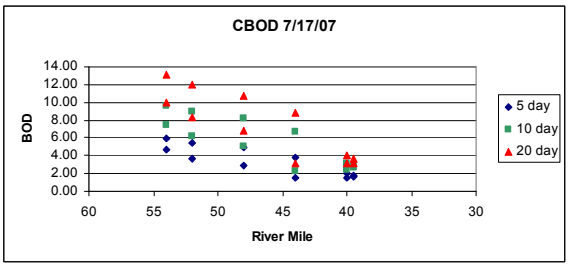

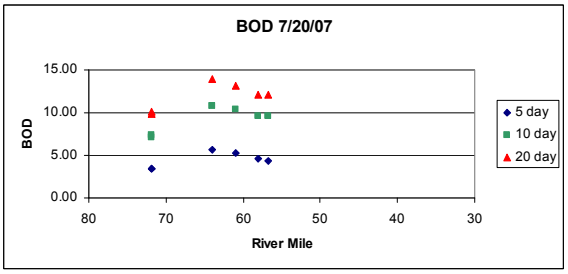

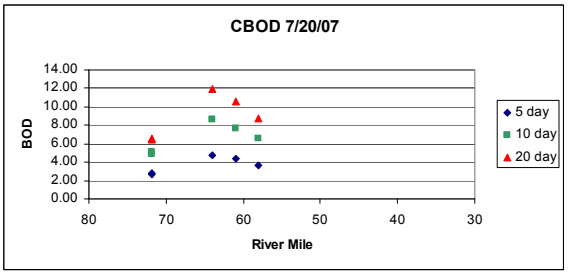

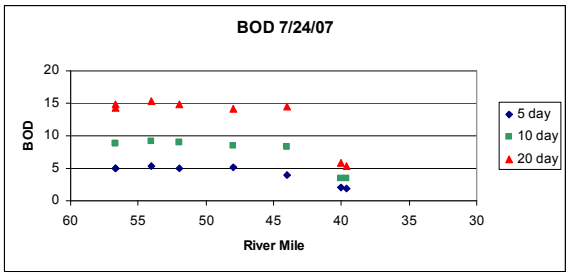

Appendix B 2-D dye simulation text and figures

Development of a two-dimensional model for simulating conservative tracer transport in the San Joaquin River from Vernalis to the DWSC.

Task 8-supplemental

DO TMDL Project
Draft Final Report 2008

2-D MODEL OF ALGAE FATE AND TRANSPORT BASED ON DYE TRACER STUDIES IN THE SAN JOAQUIN RIVER

Nigel W.T. Quinn, PhD, P.E.
Berkeley National Laboratory
1 Cyclotron Road, Bld 70A-3317H
Berkeley, CA 94720

Thomas Heinzer and Diane Williams
MPGIS, US Bureau of Reclamation/
Michael-Thomas Group
2800 Cottage Way
Sacramento, CA 95825

Søren Tjerry
DHI Water & Environment
319 SW Washington Street, Suite 614
Portland, OR 97204

Gary M. Litton, PhD, P.E.
School of Engineering
University of the Pacific
3601 Pacific Avenue
Stockton, CA 95211

Mark S. Brunell, PhD
School of Biology
University of the Pacific
3601 Pacific Avenue
Stockton, CA 95211

Abstract

During late summer of 2005 through 2007 dye tracer studies were conducted in conjunction with a Lagrangian algal fate study to improve understanding of algal dynamics between Vernalis and the Deep Water Ship Channel. Previous studies had shown a reduction in algal bimass in this reach of the river which was not explained by the flow bifurcation at Old River or by riparian diversions from the river at Banta Carbona Irrigation District or the private pumping stations along the river serving delta agriculture. The dye study was conducted in both Lagrangian and Eulerian modes – the Lagrangian study followed the peak dye concentration as it moved downstream in a moving boat that was fitted with instruments capable of simultaneous GPS positioning and real-time dye measurement – the Eulerian study was conducted from a boat moored at a fixed location that measured the dye pulse as it swept past. A hand-held instrument capable of simultaneously recording dye concentration and GPS coordinates was used to analyze the dye pulse as it was carried past the boat downstream. Dye trace profiles were plotted and qualitative descriptions of the longitudinal dispersion of the dye trace were obtained. In order to improve the simulation of algae dynamics in the reach between Vernalis and the Deep Water Ship Channel (especially the transition zone in the vicinity of Mossdale where the river becomes influenced by tidal dynamics and algae experience flow reversal accompanied by periods of quiescence as the flood tide transitions into an ebb tide) a more detailed dynamic model of the river reach was sought. A simple plug flow model was developed in MATLAB by Gary Litton, which was able to simulate the celerity of the dye pulse reasonably well. However to develop and understanding of the influence of river morphology on conservative dye transport and retardation - a two dimensional hydrodynamic flow model has been developed to account for such phenomena as eddying, which is caused by river sinuosity and that is a primary causal factor in longitudinal dispersion of both dye and algae in the River. After reviewing several candidate models – the new curvilinear version of the Danish Hydrologic Institute's Mike 21c code was chosen to perform the model simulations. This computer code has been used by many years by restoration scientists and engineers, has good user interfaces and contains a powerful visualization tool box that allows effective communication of results. This final report describes the development of the model, use of GIS to visualize the river bathymetry and the simulation experiments performed to date.

Introduction

Algal dynamics in a riverine system are complex, especially in a river such as the San Joaquin where the river transitions from a levee-constrained flow regime, in its middle reaches, to a tidally-dominated river as it enters the Delta (Lee and Lee; 2000, Chen and Tsai, 2002). The transition point location is dynamic and is affected primarily by flow volumes in the San Joaquin River and the amplitude of the ocean tides expressed at the Golden Gate Bridge. Flow volumes is the San Joaquin River are also highly dynamic – river diversions made by local water districts and unincorporated riparian diverters can change instream flow quite dramatically, especially in dry and critically dry years where River flow at Vernalis can be substantially below 1000 cfs and the largest four riparian diverters (including Banta Carbona Irrigation District located downstream of Vernalis)

have the capability of removing flows in excess of 700 cfs from the River. (Kratzer et al., 1987). Irrigation return flows, rainfall runoff and wastewater treatment plant discharges that flow into the River are also dynamic but do not typically account for flow variations that are as dramatic as the stopping and starting of pumped diversions. Simulation of water quality in the San Joaquin River system is even more complicated given the large number of discharge points along the river and the highly variable water quality discharged at each of these locations (Kratzer et al, 1987; Kratzer et al., 2004; Pate, 2001; Wilde, 2005). Each of these point source discharges as drainage collectors for large diverse watersheds. The salinity, nutrient and sediment content of these discharges is influenced by local soil conservation and water management practices (Kratzer et al., 2004). Since the modeling of algal dynamics is at the core of this study and many of the other upstream studies – it is clear than any realistic algae growth and decay model will first need to provide a realistic simulation of flow and water quality (Brown and Huber, 2004; Herr and Chen, 2006). The reach of the San Joaquin River between Vernalis and the Stockton Deep Water Ship Channel differs from the reaches upstream in that, with the exception of Banta Carbona Irrigation District, water returned to the river is derived from water diverted from the same source. Banta Carbona Irrigation District receives a portion of the annual water supply from the Delta Mendota Canal. The reach also passes through heavily urbanized areas – return flows from urban areas have a much different chemical signature than those return flows from irrigated lands. The reach between Vernalis and the Stockton Deep Water Ship Channel has significant sinuosity – tracking algal biomass between these points requires an understanding of how river morphology affects longitudinal dispersion. The Rhodamine dye trace studies conducted by the study team during 2005, 2006 and 2007 provide data on hydrodynamic longitudinal dispersion during the 3-5 day duration of each experiment. These data are used to evaluate the validity and future potential of a simulation model of flow and mass transport.

Hydrodynamic transport

Hydrodynamic turbulent mixing in rivers and streams has been studied for more than a century – the fundamental theory derives from Fourier's law of heat flow (1822) and Fick's (1855) concepts of molecular diffusion in fluids. These conceptual models relate the mass flux of a solute with the concentration gradient. Classical texts such as Carslaw and Jaeger (1959) provide solutions to many classical heat flow problems that involve molecular diffusion that are direct analogs of turbulent mixing in rivers. Under certain conditions "Fickian" turbulent mixing theory can be used to describe the mixing phenomena in rivers. Taylor (1953, 1954) developed the theory relating the spread of dissolved contaminants in laminar and turbulent flows to velocity gradients in the flow domain. He referred to flows where velocity gradients were present as "shear flows" and the mechanism of induced mixing and the "shear effect". The theory of shear flow dispersion is the most helpful in understanding the mechanics of longitudinal dispersion in rivers. Fischer et al. (1979) introduced the concept of "scales of turbulence" as a means of explaining how the velocity of a moving fluid varies in both space and time as a result of strong non-linearities in fluid motion – especially at large Reynold's numbers (the Reynolds number is a ratio of the inertial to the viscous forces in a fluid which is either laminar or turbulent). The effect of these non-linearities is to "spread the kinetic

energy of the fluid motion over a range of eddy sizes through the interaction of the large and smaller scales of motion" (Fisher et al, 1979).

Fischer et al (1979) found it useful to describe turbulent mixing mathematically using the diffusion equation together with a turbulent mixing coefficient in place of the molecular diffusion coefficient typical of Fickian mixing. Under ideal conditions of a straight channel of constant depth and large width (sufficient to minimize the shear induced by sidewalls) a cloud of tracer would grow until it filled the depth of the channel and then would continue to grow in volume in the directions of both length and breadth. The phenomenon of turbulent mixing can be described mathematically as a product of the Lagrangian length scale (a measurement of the distance a particle must travel before it forgets its initial velocity) and the intensity of the turbulence according to the following expression (Fischer et al., 1979):

$$\varepsilon_x = l_L [< U^2 >]^{½} \qquad [1]$$

Where : e_x = turbulent mixing coefficient
l_L = depth of flow
U = velocity of a particle

Experiments conducted by Laufer (1950) and other researchers have suggested that turbulence intensity on any flow contained by channel boundary (walls) is directly proportional to the shear stress imposed on the channel walls. Shear velocity is related to shear stress and fluid density by the relationship :

$$u^* = [\tau_o/\rho]^{1/2} \qquad [2]$$

Where : u^* = shear velocity
τ_o = shear stress
ρ = density of the fluid

For uniform open channels shear stress is calculated by a force balance according to the equation:

$$u^* = [gdS]^{½} \qquad [3]$$

Where : u^* = shear velocity
g = acceleration due to gravity
d = channel depth
S = channel bed slope

Channel mixing

Empirical studies of open channel flow by a number of investigators including Elder (1959), Jobson and Sayre (1970) and Csanady (1973) suggest developing separate mixing coefficients for vertical, transverse and longitudinal mixing. Breaking down these

components of mixing can help develop generic functions that can be applied to rivers of various configurations.

Vertical mixing coefficients can be derived from the theoretical velocity profiles for the channel.. Theoretical velocity profiles show increased velocity with height above the bed – the boundary layer next to the bed being the zone of greatest shear stress. Elder (1959) obtained the following equation for the vertical mixing coefficient ε_v based on an arithmetic law velocity profile :

$$\varepsilon_v = \kappa d u^*(z/d)[1 - (z/d)]$$

Where :
ε_v = vertical mixing coefficient
u^* = shear velocity
d = channel depth
z = vertical depth increment
κ = coefficient

Since there is no direct analog of the vertical mixing profile for transverse mixing – transverse mixing coefficients must be derived empirically. There is a large literature of transverse mixing experiments being conducted in regular irrigation canals and channels. Fischer et al. (1979) reviewed experiments by Lau and Krishnappan (1977) and Okoye (1970) which suggested a wide range of empirical values that could be approximated by the general expression :

$$\varepsilon_t \sim= 0.15\, d u^*$$

Where :
ε_t = transverse mixing coefficient
u^* = shear velocity
d = channel depth

Longitudinal mixing is considered by Fischer et al. (1979) to occur at about the same rate as transverse mixing in cases, where boundaries do not artificially restrict spreading. However some researchers, such as Sayre and Chang (1968), found that longitudinal mixing and spreading of polystyrene particles was as high as three times that of transverse spreading. Fischer et al. (1979), Aris (1956) and Elder (1959) discount the impact of turbulent eddies in causing longitudinal mixing and considers the shear flow dispersion coefficient caused by the velocity gradient to be much larger in value than the mixing coefficient due to turbulence. Elder (1959) suggested that the dispersion coefficient in a logarithmic velocity profile could be described as follows :

$$K = 5.93\, d u^*$$

Where :
K = dispersion coefficient
u^* = shear velocity
d = channel depth

The value of K in this relationship is approximately 40 times the expected magnitude of the turbulent mixing coefficient. Aris (1956) maintained that turbulent and shear mixing effects were additive and they dominating any effects due to longitudinal turbulent mixing alone. Fischer et al (1979) acknowledged that it is difficult to separate the mixing effects due to longitudinal turbulence and those due to shear forces alone in river dye experiments.

Channel curvature

Natural channels are rarely regular in cross section and in rivers such as the San Joaquin – channels are characterized by sharp bends, large sidewall irregularities such as groins and irregular depth profiles. Channel irregularities typically do not have much effect on vertical mixing – this has been verified empirically in flume experiments. However transverse and longitudinal mixing, are strongly affected by bends and sidewall irregularities. In general the greater the scale of the sidewall irregularity the faster the rate of transverse mixing. River studies by Holley and Abraham (1973), Jackman and Yotsukura (1977) and Mackay (1970), that were reviewed by Fisher et al. (1979), show values of $\varepsilon_t / d u^*$ in the range of 0.4 to 0.8 – when flow rounds a bend. In this case, the centrifugal forces induced by the flow tend to direct the flow towards the outside bank at the river surface – this is compensated by a reverse flow near the bottom of the river channel which induces transverse mixing to occur.

Although Elder's empirical analysis was found to work for transverse dispersion in real streams it was found to underpredict the rate of longitudinal dispersion (Fischer et al.,1979). Godfrey and Frederick (1970) and Yotsukura et al. (1970), whose work was summarized by Fischer et al. (1979), found values of $K / d u^*$ that ranged from 140 to over 7500 (in the instance of Yotsukura et al.'s study) – these are consistently higher than the values obtained by Elder (1959). Fischer et al.'s (1990) explanation for the wide range of values is that Elder didn't fully appreciate the fact that velocity varies across a typical stream – the profile used in Elder's analysis extended only over the depth of flow (d). Fischer et al. (1979) suggested that since the longitudinal dispersion coefficient is typically proportional to the square of the distance over which the shear flow profile extends. Given the typical cross-sectional topology of the San Joaquin River it follows that longitudinal dispersion is dominated (two orders of magnitude) by transverse mixing than by vertical mixing. The width to depth ratios of the San Joaquin River is generally greater than 10.

In the San Joaquin River, deep holes in the river channel up to 40 ft in depth, which typically occur immediately downstream of regions of constricted flow, can cause significant retardation of the dye and contribute to longitudinal dispersion. These deep holes in the River bed are sufficiently large to induce localized eddies as the River passes over the top of them. Although the vertical mixing may not be as important in causing dye retardation – having the dye trapped within a large eddy could induce greater shear flow than might otherwise occur – resulting in much more significant dye retardation than due to vertical mixing alone. Two dimensional modeling of the San Joaquin River is justified based on the fact that it has the ability to simulate the occurrence of shearing forces that appear to affect dye mixing and hence the degree of longitudinal dispersion.

Although, modeling the River in three dimensions would provide even more information, this approach is computationally intense and beyond the scope of the current study.

Modeling Objectives

A number of candidate one-dimensional and two dimensional numerical model codes were considered for simulating dye dispersion within the San Joaquin River between the stations at Vernalis and Channel Point. The goal of the modeling effort is to improve the understanding of algae biomass fate and transport between the Vernalis monitoring station (the most downstream station not subject to tidal influence) and the Stockton Deep Water Ship Channel. Previous monitoring studies provided evidence of a reduction in algal biomass within this reach of the San Joaquin River that could not be explained by River hydrology. The series of dye tracer experiments conducted by Gary Litton (team leader), Nigel Quinn and Mark Brunell over the three years of the project between 2005 and 2008 were designed to monitor the fate of a unit volume of water containing algae biomass (represented by the peak dye concentration) as it was conveyed along the River and into the Deep Water Ship Channel. A two dimensional hydrodynamic simulation model has been developed using Mike 21c, a state-of-the-art, curvilinear version of the Danish Hydrologic Institute's Mike 21 code, to simulate transport of the Rhodamine dye tracer. The rationale for this modeling approach is that accurate simulation of the transport of a conservative substance such as Rhodamine would provide greater assurance that the model was capable of simulating algae fate and transport. Without this proof of concept it is possible that algae losses in the system could be ascribed to the coefficients chosen for algae growth and decay. The Mike 21-c curvilinear model mesh allows the alignment of the computational model finite difference cells (elements) with the tortuosity of the river. This is a major advantage in the numerical simulation of dye dispersion and is more computationally stable than more traditional finite difference approaches that apply a regular grid mesh to the region containing the river.

Developing a computationally efficient and accurate curvilinear grid is difficult - the quality of the grid generation affects the performance of the model. Model accuracy is reduced when grid cells are not orthogonal or when the difference in cell sizes of adjacent cells is too great – accuracy is also compromised when grid cells are not aligned sufficiently closely to river bed contours to accurately describe river bathymetry. Bifurcations, branches, confluences and major diversion points have to be simulated as separate grids which are finally merged into the master model grid using a stepwise fitting algorithm that is included in the Mike 21c software. The tolerance between grid points at the merging boundary can be specified in the software. There is also a grid update option which applies smoothing algorithms to the model mesh – improving model orthogonality up to the point where it starts over-smoothing and distorting the mesh. This process is as much art as science.

The first phase of the project concentrated on developing an accurate and computationally efficient model mesh for the San Joaquin River between monitoring stations at Vernalis and at Rough and Ready Island (east of Burns Cut). Initial grid development required that the bounds of the model be defined prior to invoking the Mike 21c curvilinear grid generator. Digital imagery of the San Joaquin River between

Vernalis and the Deep Water Ship Canal at Rough and Ready island was imported into ESRI's ArcMap software. The San Joaquin River cross-sectional profile was defined using the River levees – the slope break point along each levee, where the top of the levee and the levee banks join (on the river-side of each levee) determined the left and right banks. Defining the river boundaries required creating a photo-mosaic of almost 30 scenes – GIS line boundaries had to be edge patched to ensure that the final model domain was a closed polygon.

The second step was to determine a suitable mesh interval for the River cross-section. Having grid cells that are too widely spaced defining the River cross-section may fail to accurately simulate the River cross-sectional area along its length. Grid cells that are too small can significantly increase computation time and cause numerical dispersion errors if the width to length ratio is too small. Another potential problem that needed resolution was the presence of sand bars in the certain reaches of the flow domain. Truncation of a flow line due to an obstruction such as a sand bar can lead to numeric instabilities. However confining the River streamlines just to the inundated area would be very limiting – especially if flows decreased further, exposing more sand bars.

This approach would also be ill-advised since the river bed is dynamic and continually in motion – the bed configuration using the existing cross-section and bathymetry data may be drastically changed as a result of a large flood. The approach taken was to allow the streamlines to pass around islands and objects in the River that were never inundated and to treat sand bars that were commonly inundated during high flows as part of the River.

San Joaquin River model bathymetry data

After the conceptual model and mesh configuration was completed the next step involved developing the dataset containing River bathymetry and cross-sectional profiles. The most comprehensive dataset produced for the model study reach is that produced by the US Army Corps of Engineers for the Sacramento and San Joaquin River Basins Comprehensive Study ((1997 – 2003).

River bathymetry and morphology is dynamic and it is unlikely that the survey data collected for this study depicts current conditions exactly given the lapse in time since these surveys were made. However, given the fact that the River is contained between levees along the entire model study reach, the Comprehensive Study data is considered to represent a reasonable "average" condition of River morphology.

Obtaining access to the US Corps of Engineers dataset was difficult and took more than six months to accomplish because of national security concerns that needed to be resolved. Final resolution was achieved through the intervention of the US Bureau of Reclamation which was able to obtain the data through a cooperative agreement of data sharing with the Department of Water Resources. Even after the data was rendered readable – considerable effort was required to process this large dataset so that it could be read into a geo-database. The geo-database used was Arc-Info GIS. Figure 2 shows the data points that were provided by the USCOE survey. The survey data extends beyond the River levees into the flood plain. For the purposes of the current study the cross-

sectional profiles were clipped to the model domain defined by the levee slope break points.

The San Joaquin River bifurcation at the head of Old River is shown in Figure 3 together with a 3-dimensional image of the survey points used to obtain the River cross section and bathymetry. The morphology of the junction dictates channel hydraulics which in turn affects the flow volume split between Old River and the main San Joaquin River channel. In the Mike 21c model the boundary condition at the Old River flow monitoring station is simulated as a dynamic head boundary that rises and falls with the tidal flux through the Delta.

Development of 3-D bed surface profiles

Although the purpose of this study is to improve the conceptual understanding of dye transport in the San Joaquin River reach between the monitoring stations at Vernalis and the Deep Water Ship Channel the model was developed and implemented within Mike 21c to serve future studies

of algae fate and transport and the transport of other non-conservative constituents of concern. A model mesh configuration that would serve future simulations of algal biomass in the San Joaquin River would need to include the diversion at Banta Carbona Irrigation District, the flow split at Old River, the confluence at French Camp Slough and smaller confluences from minor east-side sloughs (which have been shown to contribute significantly to River algae biomass during each ebb tide). The development of this configuration that allows the hydrodynamic impacts of these features to be represented requires that separate model meshes first be created within a GIS – these are then merged into the main model mesh using custom procedures within the Mike 21c software.

The initial dye studies using rhodamine dye as a conservative tracer, which are reported upon in this chapter, use the three primary boundary conditions i.e Vernalis, Old River and the Deep Water Ship Channel. This was done to speed up the initial model calibration process and deliver more timely output.

Figure 5 shows the bathymetry of the San Joaquin River as it empties into the much deeper Stockton Deep Water Ship Channel. During a typical tidal cycle San Joaquin River can flow into the Deep Water Ship Channel only to be pushed back into the River channel during the following flood tide. The potential transformations in water quality while the water is resident in the Ship Channel include decreases in turbidity, algal biomass concentration, temperature and dissolved oxygen – these should be simulated in order to fully understand the dynamics of water quality in this transition zone. Under normal, positive flow downstream conditions, the tidal excursion in the San Joaquin River can be up to several miles in extent, depending on the flow conditions and the strength of the tidal pulse – this is usually sufficient to prevent the River discharge into the Ship Channel from re-entering the River channel more than once.

Figure 6 shows the bifurcation of the San Joaquin River at the head of Old River. A separate model mesh of the short reach of the Old River between the mouth and the monitoring station at Head is conjoined with the mesh of the San Joaquin River main channel using procedures contained within the Mike 21c software. Inspection of the

transitional mesh shows that orthogonality has been maintained which should help to avoid numerical instability and lead to realistic simulation of the flow split.

Steady-state hydrodynamic model

Technical modeling staff at the Danish Hydrologic Institute suggested developing a steady-state model using a simple mesh configuration with only the major boundary conditions included to simplify the initial calibration process and to provide initial conditions for the simulation experiments. Complex hydrodynamic models typically require an initial "warm-up period" during which the model resolves numerical instabilities. The closer the initial river elevations specified in the model are to the measured data the more quickly the model will resolve the momentum and conservation equations that simulate the river hydrodynamics.

To develop the steady-state model the boundary conditions specified were the flux boundary at Vernalis (upper boundary of the model), an intermediate tidal head boundary at the Old River bifurcation and a lower tidal head boundary condition within the Deep Water Ship Channel at Rough and Ready Island. Figure 2 is an output plot from Mike 21c showing the head distribution along the entire San Joaquin River model reach.

Preparation of dye simulation data files

Dye release experiments were conducted every month between July and October during 2004, 2005, 2006 and 2007. In each of these experiments 50 lbs of concentrated Rhodamine WT dye was dispersed in the River adjacent to the Vernalis monitoring station using the Litton research vessel to apply the dye across the River cross-section and making use of the propeller wake from both the research vessel and the smaller 14 ft Jon boat to mix the dye within the water column. Figure 8 shows the dye being pumped from the research vessel using an on-board peristaltic pump. Manual pouring was used during later dye experiments to achieve a faster rate of initial mixing. The research vessel is equipped with a continuously recording Rhodamine dye sonde, an accurate GPS recorder and a MatLab software interface that permitted the real-time dye concentration to be plotted, together the outputs from other sensors, with the vessel's exact location (Litton et al., 2007). This software program allowed the boat operator to find the dye peak concentration within the dye plume and stay within this dye prism as it was swept downstream.

A second 50 lb container of dye was added to the existing dye peak, just below the Old River bifurcation, within the tidal reach of the River. This was necessary owing to the reduced dye concentration as the effects of longitudinal dispersion, adsorption to organic matter and degradation in sunlight combined to diluted the dye signal. The mean celerity of the River declines within the tidal reach and the average water depth increases. Even with the added dye the peak dye concentration can be difficult to ascertain because of tidal dispersion.

Dye concentration measurements were made in both Langrangian (boat travels with the dye peak) and Eulerian (collected by a stationary boat and the dye passes downstream) experiments. Figure 9 is a typical set of Eulerian concentration profiles showing the

manner by which the dye tracer disperses longitudinally as it moves downstream from Vernalis, encountering a variety of influences including channel irregularity, channel tortuosity, obstructions, groins, sand bars and other factors that increase dye retardation within the channel reach. Although the shapes of the dye plumes can be described by polynomial expressions the rate of longitudinal dispersion is significantly influenced by mixing and retardation factors which can vary with rate of flow and channel morphology, as previously discussed. Gary Litton (Litton et al., 2007) was able to simulate dye travel time reasonably well using a simple Matlab plug-flow model (Figure 10). However this model does not simulate the mechanisms of longitudinal dispersion, nor is it likely to be valid for all flow conditions in the River, especially within the reaches subject to tidal excursions. Simulation of the mechanisms of dye (and by inference algal biomass) can only be achieved with a more detailed numerical model of the River reach between the Vernalis and Rough and Ready monitoring stations such as the MIKE 21c model previously described.

Figure 11 is a Rhodamine dye trace obtained by trawling upstream during slack tide (tidal reversal during which time advective flow is zero). In this instance the transition is from an ebb tide to a flood tide. The sharp dye front is pushed back through the lower concentration dye cloud which essentially destroys the shape of the dye pulse, especially during low flow hydrologic conditions where tidal excursions are greater owing to the smaller volume of water opposing the flood tide. It is expected that eddying and secondary flows would be more prevalent under low flow hydrologic conditions resulting in increased longitudinal dispersion of dye.

Preliminary results of Mike 21c simulations

Two numerical simulations of the dye experiments were selected to represent both high and low River hydrology and to fully test the stability of the MIKE 21c code. The first experiment conducted in March 2005, although outside the typical period of low dissolved oxygen conditions in the San Joaquin River which occur in late summer and early fall, provided a number of useful dye traces against which to compare the numerical model. Flows recorded at Vernalis during March 2005 were above 5,000 cfs and produced a dye transport flow regime which was strongly advective. This created more of a plug-flow regime in the non-tidal River reach below Vernalis and resulted in a minimal number of tidal excursions in the tidal reach, before the dye passed into the Ship Channel.

The second dye experiment chosen was started on September 20, 2007 and lasted approximately 6 days. During the latter part of 2007 the San Joaquin River experienced hydrology similar to that in 2004, with extremely low flows at Vernalis and conditions that produced very little advection through the tidal reaches of the River between Mossdale and the Deep Water Ship Channel. Under these conditions eddies and secondary flows become more dominant in their tendency to disperse dye and the number of tidal excursions is large before the dye finally passes into the Stockton Deep Water Ship Channel.

Model simulation experiments

Numerical simulations with MIKE 21c require the development of an input data deck which provides initial and boundary conditions and initial values for parameters such as bed cohesion, eddy viscosity and bed roughness that affect dispersion. The simulations are performed in three steps. The first step requires that the model be supplied with realistic heads at each grid cell since stage measurements are available at a small number of gauging stations along the River. This is achieved most efficiently by running the model iteratively until it reaches a steady-state condition, as previously described. The stage values at the steady-state condition are used as initial conditions for a transient run of the model. For the March 2005 dye experiment – the MIKE 21c model took 59 hours on a 3.0 GHz Dell computer with a dual Xeon processor to achieve a steady-state condition. A parallelized beta version of the MIKE 21c code was provided by DHI Inc. – once this was properly functional it reduced the computation time to one quarter of the time. The parallelized code performs approximately 1.2 million computational points/sec – whereas the non-parallelized code runs at 300,000 computational points/sec.

A transient run is then made using the "hot start" initial condition files using a time step that is as large as possible that still allows the model to run to completion. This is a trial and error procedure – the larger the model time step the quicker the model runs to completion. For the highly advective, March 2005 flow condition, a 15 second time step was found to be desirable. However the August 2007 model run – which spawns more eddies and secondary flows owing to the smaller flow volumes – the time step had to be reduced to 1 second.

After a successful flow simulation was achieved the simulation was re-run to simulate transport of Rhodamine dye. MIKE 21c does not contain a water quality module that can be used to simulate dye transport – rather we were advised by DHI to use the sediment transport capability of MIKE 21c and to simulate dye transport as sediment with properties of zero settling velocity (neutral density) and with zero bed cohesion. The simulation was started approximately 5 days in advance of the dye (sediment) injection to allow the model to stabilize and was continued for another 15 days after the initial dye injection to allow all of the dye to be pushed out of the River. The strongly advective March 2005 simulation ran efficiently without any major problems – however the weakly advective case was inherently unstable and did not run to completion with the parameter values initially selected.

On the advice of Søren Tjerry the alluvial resistance model, which is contained within the MIKE 21c River Morphology module, was run to address the tendency for the flow to concentrate on River point bars. This phenomenon occurs naturally because the flow path is shorter over the bars than in the outer bend scours. To make the flow more sensitive to the depth, the algorithm causes the flow to deflect away from shallow areas into deeper areas. Using a Manning coefficient of M=32 for all water depths the flow tends to concentrate on point bars, looks un-natural and is prone to instabilities. Using the applied alluvial resistance model - Manning's M is set to a value of 32 for deep water, while for shallow regions (depth of 1m or less) M is set equal to 10. A higher bed resistance is always stabilizing for low flow cases. Smoothing the bathymetry, and lowering the time-step to 1 second, raising the eddy viscosity to 2 m^2/s and using an alluvial resistance where $M = 10 * h^{0.5}$ were steps taken to get the model to run to completion.

Model Scenario run – Vernalis high flow > 5000 cfs : March 23, 2005

The first dye release experiment was conducted on March 23, 2005 with Vernalis as the dye release point. Figure 13 shows the longitudinal dispersion of the dye plume as the dye is transported downstream. The first dye concentration profile is obtained by driving the boat downstream through the dye peak – the second is obtained from a stationary boat as the dye moves past the instrument. These plots are primarily in the non-tidal reaches of the San Joaquin River under moderately high flow conditions which minimizes the effect of tidal excursions.

MIKE 21c simulations results are shown in Figure 14. This shows snapshots from an animation of the dye release experiment. The San Joaquin River has been broken into smaller reaches and placed on the viewing screen from right to left to allow the entire simulation to be viewed on a single screen. The color ramped dye concentrations in the animation show the strongly advective dye pulse. The tidal excursion during this experiment was small owing to the large volume of water passing along the San Joaquin River which resists the force of the flood tide.

Model Scenario run – Vernalis low flow < 1000 cfs : September 20, 2007

The second dye release experiment was conducted on September 20, 2007 with downstream of the Head of Old River as the dye release point. Figure 15 shows the longitudinal dispersion of the dye plume as the dye is transported downstream. The dye

concentration profile is recorded at three observation platforms – (1) the Dos Reis campground site – 3 miles downstream from the HOR dye release location; (2) Brant Bridge (BDT) – a little over 6 miles downstream from HOR; and (3) the Outfall Pier – located about 1 mile from the entrance to the Deep Water Ship Channel and about 13 miles downstream from HOR.

Figure 15 shows the series of flood and ebb tidal excursions that continue over the six days after the dye release on 9/20/2007. The first dye peak is very sharp at Dos Reis as would be expected – the second dye peak is somewhat dispersed but still strong as the sensor picks up the second ebb tide almost 23 hours later. It is interesting to observe that the first flood tide (after the initial strong ebb tide) provides a very weak dye signal. This may be caused by the weakness of the tidal excursion which failed to push the center of the dye cloud past the sensor at the Dos Reis dock. The Brandt Bridge station sees the dye peak concentration approximately 8 hours after the dye release. This is a strong signal – probably due to the strength of the ebb tide. Each subsequent flood tide tends to broaden and attenuate the dye peak. The signal disappears after day 5. At the Outfall Pier the first strong Rhodamine dye signal is observed on the ebb tide about 3.5 days after the dye release on September 20. The dye peaks, although attenuated, remain surprisingly distinct even after three tidal reversals. The signal disappears from the system after day 5.

Figures 16-1 through 16-7 show the model simulated dye concentration profiles along the San Joaquin River starting from Old River (model node 1850) down through the Deep Water Ship Channel and the Rough and Ready monitoring Stations (model node 0). At this time the model node numbers have not been mapped to River mile. The dye concentration in g/m^3 is also scaled for each plot – which makes it difficult to make a direct comparison to the data shown in Figure 15. This will be improved after further work. However it is clear that the distinct dye concentration profiles that were observed in the field data also are observed in the model simulations. The model appears to be producing the right amount of longitudinal dispreson from a purely qualitative assessment.

In Figure 16-7 the model simulation shows a reasonably identifiable dye signal 3 days after the release of the dye just downstream from the Head of Old River. The field data picked up the dye signal after about 3.5 days. The model simulation shows a gradual decay through day 6 of the experiment. The decay of the signal was more rapid in the case of the field data. This is likely a result of the assumption being is being made to simulate the dye as non-cohesive, neutrally buoyant sediment. In reality Rhodamine dye concentrations decay because of adsorption to organic matter and sediment and due to a natural decay in the fluorescent property of the dye. This issue can be dealt with through calibration or by introducing a decay term for the Rhodamine dye.

Conclusions

A state-of-the-art numerical simulation model of the lower San Joaquin River between Vernalis and the Rough and Ready Island monitoring station within the Stockton Deep Water Ship Channel has been developed to provide a working tool that captures some of the field observations made by the Litton team during 2005 – 2007. The numerical

modeling approach uses the Danish Hydrologic Institute's MIKE 21c model code which has a new curvilinear mesh feature which allows the model to more accurately simulate the complex dynamics of flow along a highly sinuous River reach with high variable bathymetry. Preliminary model simulations have demonstrated the model's significant potential as a research and decision support tool to further improve the understanding of dye and algal fate and transport in the San Joaquin River. A well-calibrated two-dimensional simulation model of the River can significantly reduce the costs associated with real-time monitoring.

Acknowledgements

This study is an extension of the Task 8 project, led by Dr Gary Litton, entitled "Linking the San Joaquin River to the Stockton Deep Water Ship Channel". We are also grateful to Joseph McGahan and Nettie Drake for their work in administering this grant work and to Will Stringfellow who distilled our collective ideas into a workable proposal that allowed the work to be funded. Also to the California Bay-Delta Authority and the various Project Managers who guided this multi-agency project to a successful conclusion.

References

Brown, R. and A. Huber. 2005: "Initial Simulation of 2000-2003 Flows and Water Quality in San Joaquin River Using DSM2-SJR Model", Jones and Stokes, Sacramento, CA

Carslaw H.S. and J.C. Jaeger, 1959. Conduction of Heat in Solids. 2nd edition. Oxford University Press, London.

Chen C. W. and W. Tsai. 2002. Improvements and Calibrations of Lower San Joaquin River DO Model. Final Report for CALFED Grant 99-B16, and DWR 4600000989, Systech Engineering, Inc., San Ramon, CA 94583.

Csanady G.T. 1973. Turbulent Diffusion in the Environment. Geophysics and Astrophysics Monographs. Volume 3.

Fick A. 1855. On Liquid Diffusion. Philso. Mag. 4(10), 30-39. (referenced in Fischer et al. 1979).

Fischer H.B., E.J. List, R.C.Y. Koh, J. Imberger and N. H. Brooks, 1979. Mixing in Inland and Coastal Waters. Academic Press Inc.

Foe C., M. Gowdy and M. McCarthy. 2002. Strawman Load Allocation of Responsibility Report. Draft, Central Valley Regional Water Quality Control Board, Sacramento, CA. Jones & Stokes. 1998. Potential Solutions for Achieving the San Joaquin Dissolved Oxygen Objectives, Prepared for City of Stockton, Jones & Stokes, Sacramento, CA

Fourier J.B.J. 1922. Theorie Analytique de la Chaleur. Didot, Paris (referenced in Fischer et al. 1979).

Godfrey R.G.and Frederick, B.J. 1970. Dispersion in Natural Streams. US. Geological Survey Professional Paper, 433-B. (referenced in Fischer et al. 1979).

Herr J. and C.W. Chen 2006. Forecasting Procedure Report. Task 6 Report for Upstream San Joaquin River Monitoring and Investigations Project (A CALFED Directed Action Project), Systech Engineering, Inc., San Ramon, CA.

Holley E.R. and G. Abraham. 1973. Laboratory Studies on Transverse Mixing in Rivers. J. Hydraul. Res. 11, 219-253. (referenced in Fischer et al. 1979).

Jackman A.P. and Yotsukura N. 1977. Thermal Loading of Natural Streams. U.S. Geological Survey Professional paper 991. (referenced in Fischer et al. 1979).

Kratzer C.R., P.J. Pickett, E.A. Rashimawi, C.L. Cross, and K.D. Bergerson. 1987. An Input-Output Model of the San Joaquin River from the Lander Avenue Bridge to the Airport Way Bridge : Technical Committee Report No. N.Q. 85-1. California Water Resources Control Board, Sacramento, CA.

Kratzer C.R., P.D. Dileanis, C. Zamora, S. R. Silva, C. Kendall, B.A. Bergamaschi and R. A Dahlgren. 2004. Sources and Transport of Nutrients, Organic Carbon, and Chlorophyll-a in the San Joaquin River Upstream of Vernalis, California, during

Summer and Fall, 2000 and 2001 : Water Resources Investigations Report 03-4127, US Geological Survey, Sacramento, CA.

Lee G.F. and A.J. Lee. 2000. Synopsis of Issues in Developing the San Joaquin River Deep Water Ship Channel DO TMDL : available from http://www.gfredlee.com/SJRsynopsis.pdf. Lehman, P.W., J. Sevier, J. Giulianotti, and M. Johnson. 2004. Sources of Oxygen Demand in the Lower San Joaquin River, California, Estuaries, Vol. 27, No. 3, pp 405-418.

Litton G.M., M. Brunell, N.W.T. Quinn and J.C. Monroe. 2007. Task 8. Linking the San Joaquin River to the Stockton Deep Water Ship Channel. Interim task Report # 3. University of the Pacific, Stockton, CA.

Mackay. J.R. 1970. Lateral Mixing of the Laird and Mackenzie Rivers Downstream from their Confluence. Can. J. Earth Sci. 7, 111-124. (referenced in Fischer et al. 1979).

Pate T. 2001. DSM2 San Joaquin Boundary Extension : in Chapter 5 of Methodology for Flow and Salinity Estimates in the Sacramento-San Joaquin Delta and Suisun Marsh, 22nd Annual Progress Report to the State Water Resources Control Board in Accordance with Water Right Decision 1485, Order 9, Department of Water Resources, Sacramento, CA.

Wilde J. 2005. Using Dye-Injection Study to Revise DSM2-SJR Geometry : in Chapter 2 of Methodology for Flow and Salinity Estimates in the Sacramento-San Joaquin Delta and Suisun Marsh, 26th Annual Progress Report to the State Water Resources Control Board in Accordance with Water Right Decision 1485, Order 9, Department of Water Resources, Sacramento, CA.

Yotsukura, N. H.B. Fischer and W.W. Sayre 1970. Measurement of Mixing Characteristics of the Missouri River between Sioux City, Iowa and Plattsmouth, Nebraska. US Geological Survey Water Supply Paper 1899-G. (referenced in Fischer et al. 1979).

Appendix B Figures

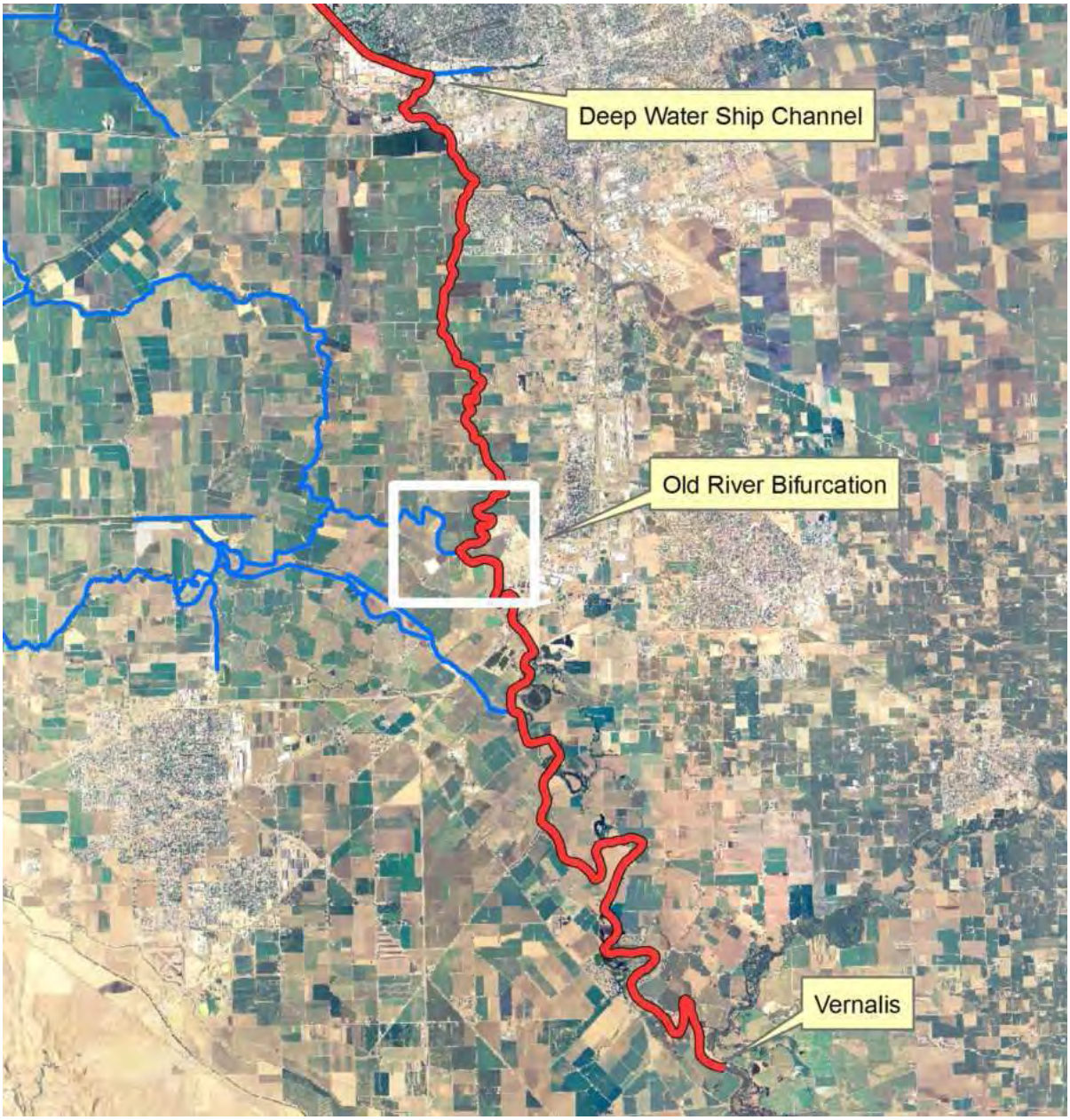

Figure 1. Mike 21c model reach from the Vernalis monitoring station to the monitoring station at Rough and Ready Island showing the confluence between the San Joaquin River and the Deep Water Ship Channel at the top of the image and the bifurcation at Old River.

Figure 2. Model reach showing the US Corps of Engineers channel cross-section and DEM dataset that was made available through a US Bureau of Reclamation – Department of Water Resources cooperative agreement. Data is of sufficient refinement to allow accurate 3-D cross section profiles to be developed for the model study reach between the Vernalis and Rough and Ready Island monitoring stations.

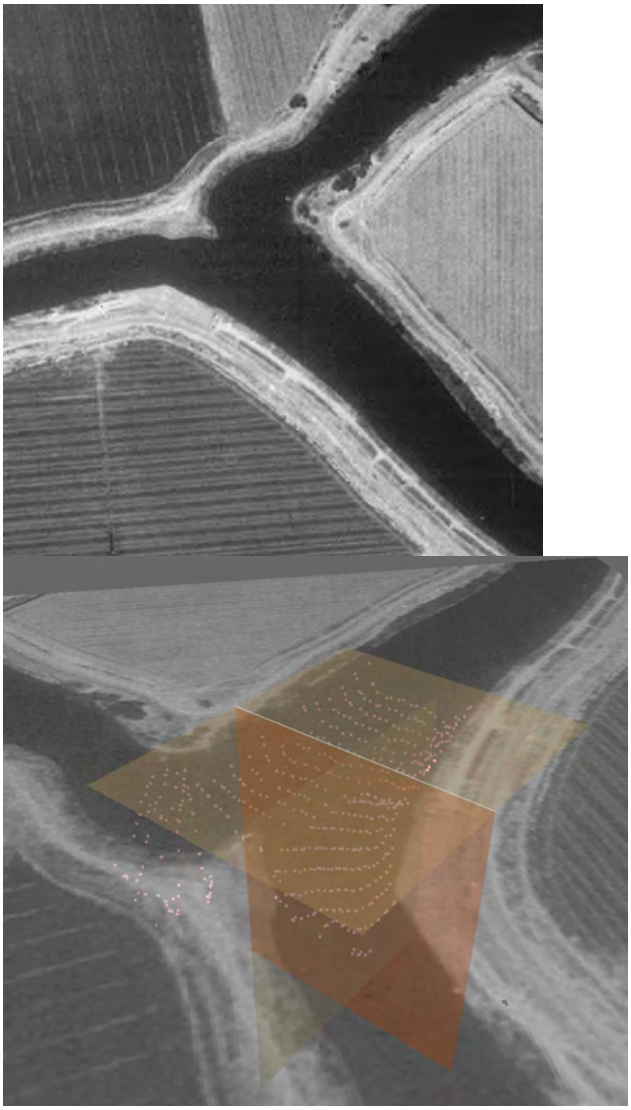

Figure 3. Plan view of the San Joaquin River bifurcation at Old River. USCOE cross section dataset is used to develop a 3-D rendering of the River morphology at this flow split.

Figure 4. Detailed view of the confluence of the shallow (< 20ft) San Joaquin River discharging into the deeper Stockton Deep Water Ship Channel (30 – 40ft).

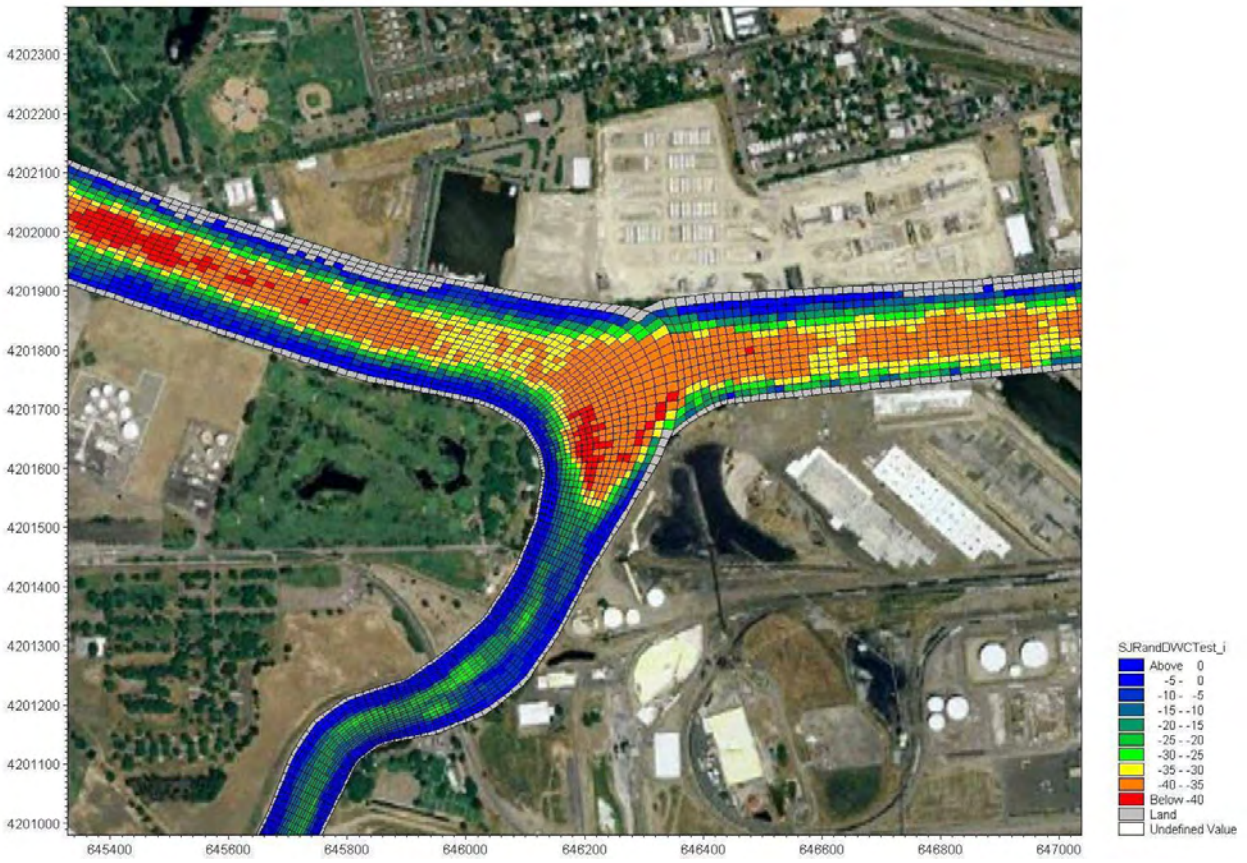

Figure 5. Model channel discretization at the San Joaquin River confluence with the Stockton Deep Water Ship Channel. Image shows the final result of merging a second model mesh (of the turning Basin) with the mesh of the main channel. Depth of channel shown in (negative) feet.

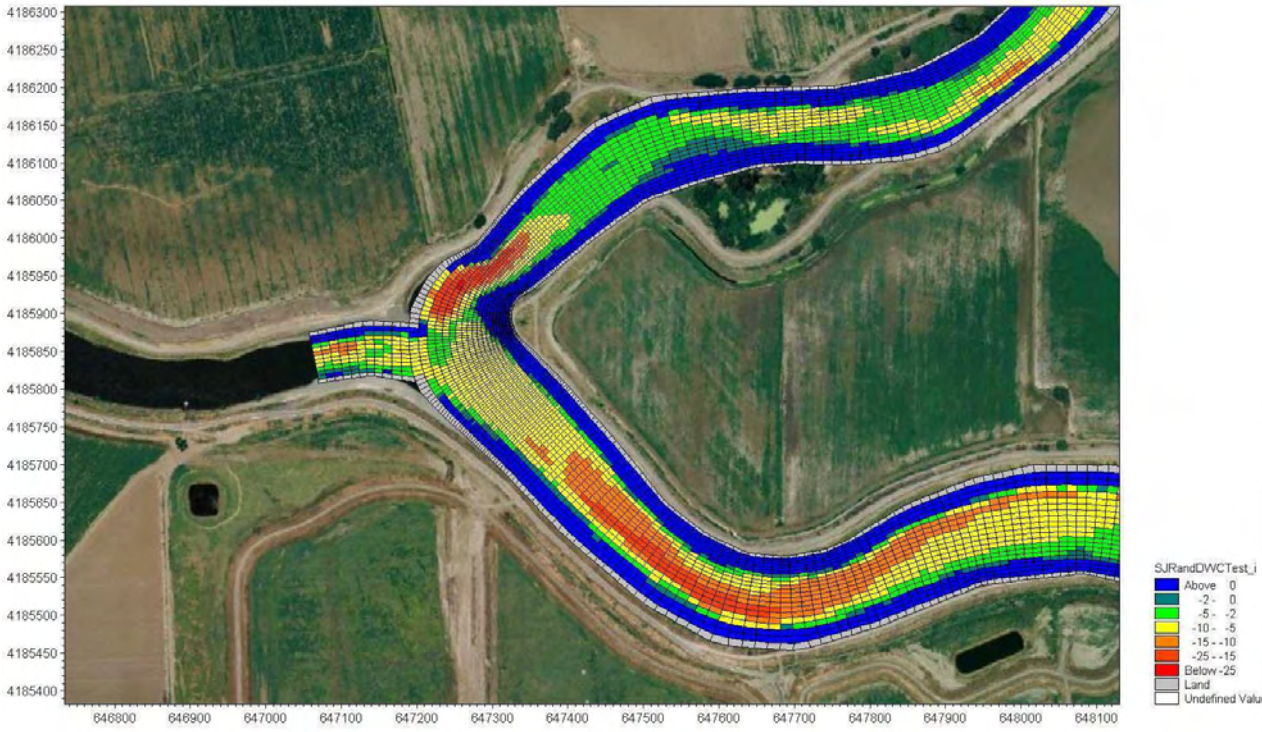

Figure 6. Model channel discretization at the San Joaquin River bifurcation with Old River.. Image shows the final result of merging a second model mesh (of the head of Old River) with the mesh of the main channel. Depth of channel shown in (negative) feet.

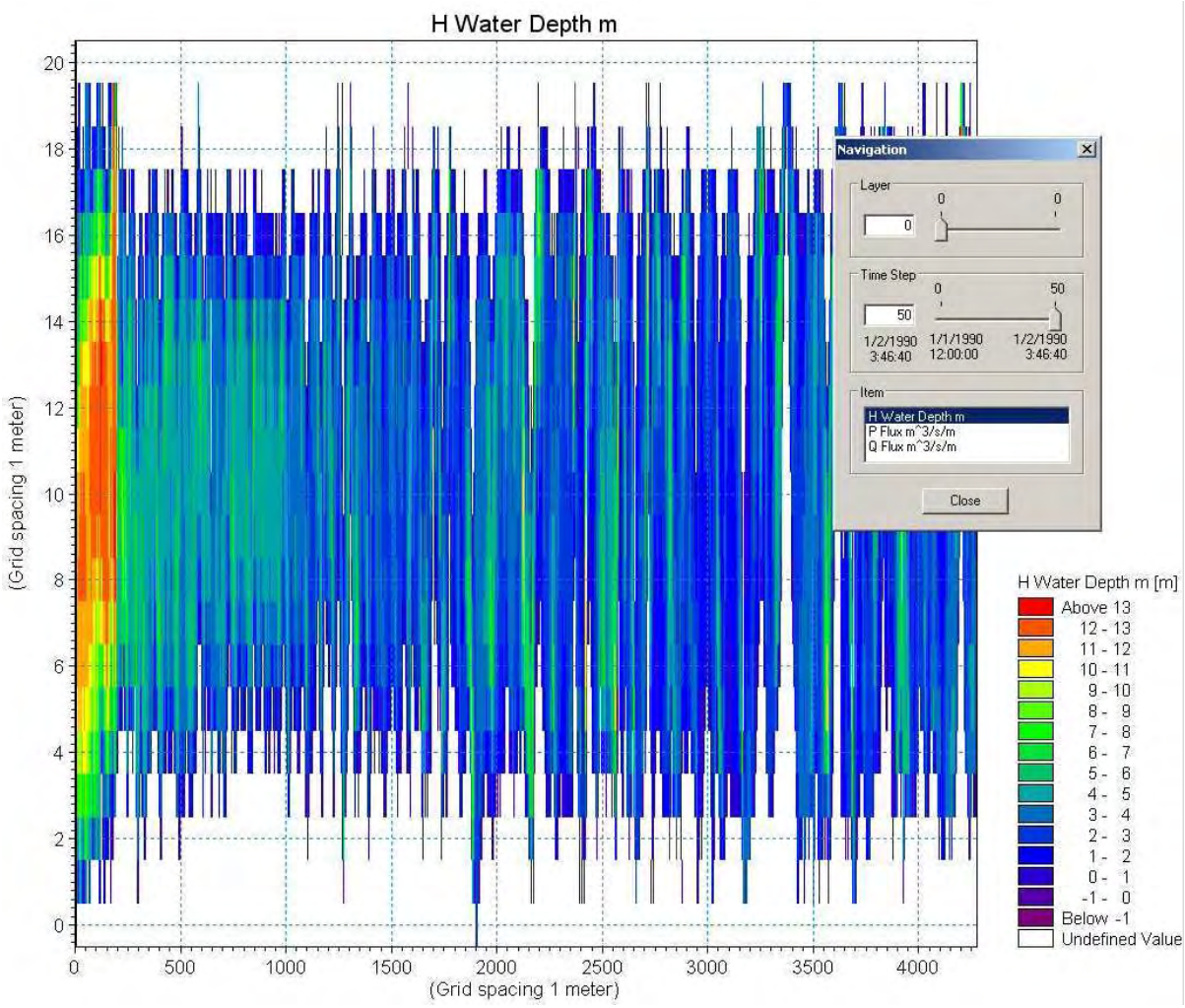

Figure 7. Steady-state water levels within the model finite difference mesh as seen from an orthogonal representation in Mike 21c. After the dynamic runs are complete, the head values are projected from orthogonal space into "real world" coordinates for visualization in a GIS and for use as initial conditions in subsequent runs.

Figure 8. Rhodamine WT dye dispersal from Litton research vessel with Jon boat riding in the wake of the larger boat to assist with vertical mixing of the dye. Uniform mixing within the water column was achieved within 2 – 3 miles downstream. The research vessel then drifted downstream attempting to stay with the dye concentration peak.

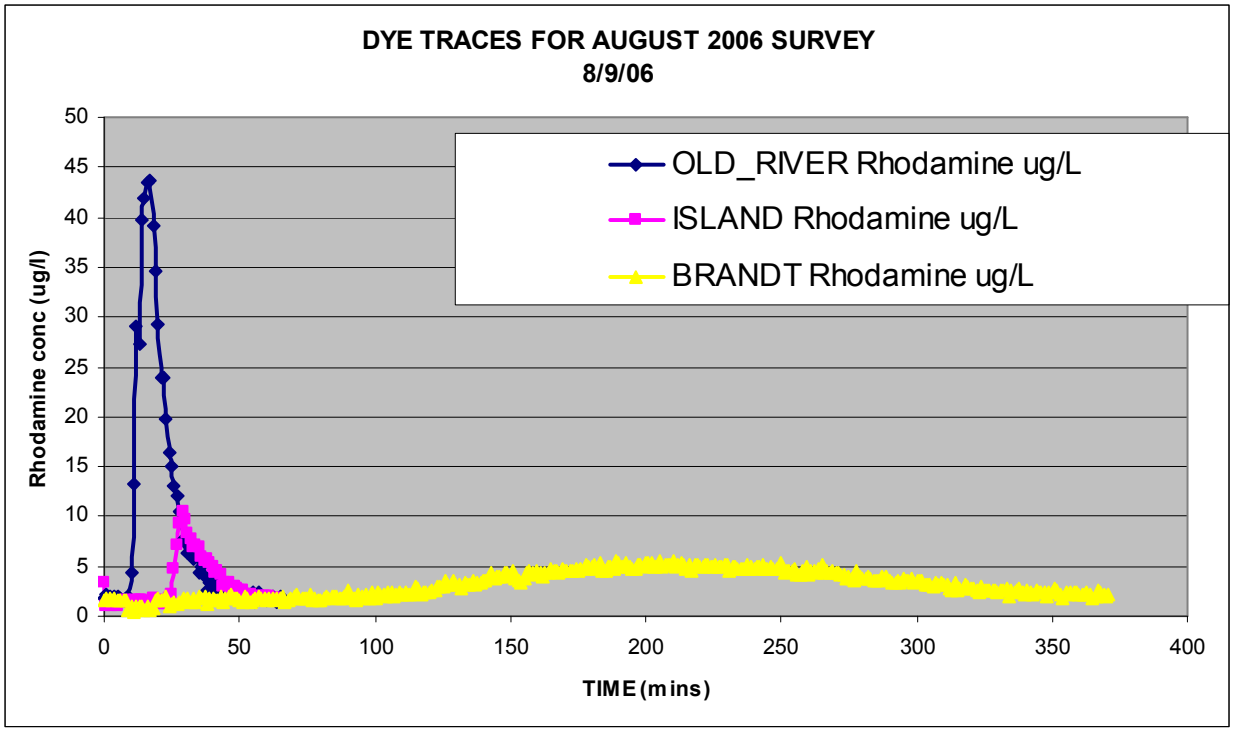

Figure 9. Dye longitudinal dispersion in the reach of the San Joaquin River between the Vernalis monitoring station and Dos Reis campground, located approximately 16 miles downstream.

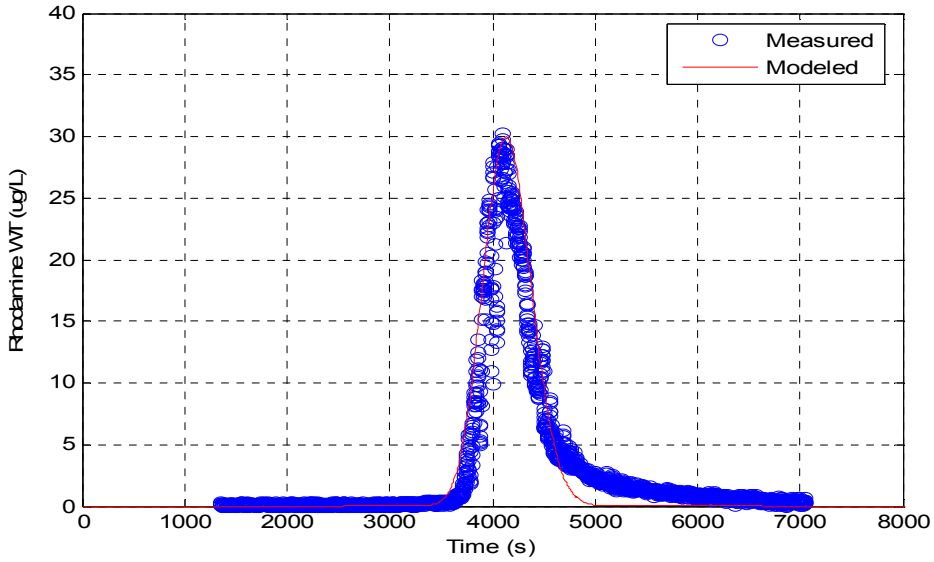

Figure 10. Comparison of measured and modeled Rhodamine WT concentrations in the San Joaquin River (river mile 53.07) using Litton MatLab model. Dye release occurred at river mile 53.7 (just downstream from the Head of Old River) at 2:30 a.m. on July 14, 2005.

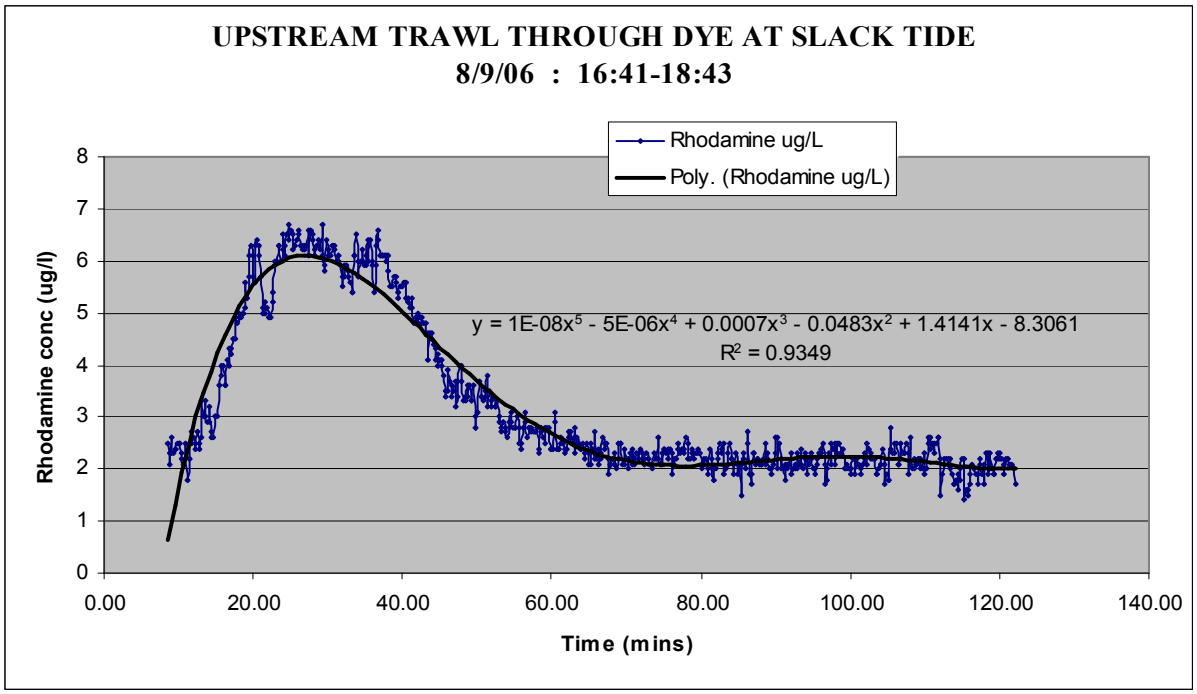

Figure 11. Upstream trawl through the dye starting at the (Brickyard) SBC Stack site (river mile 45.0) starting at 4:41 p.m. on August 8, 2006.

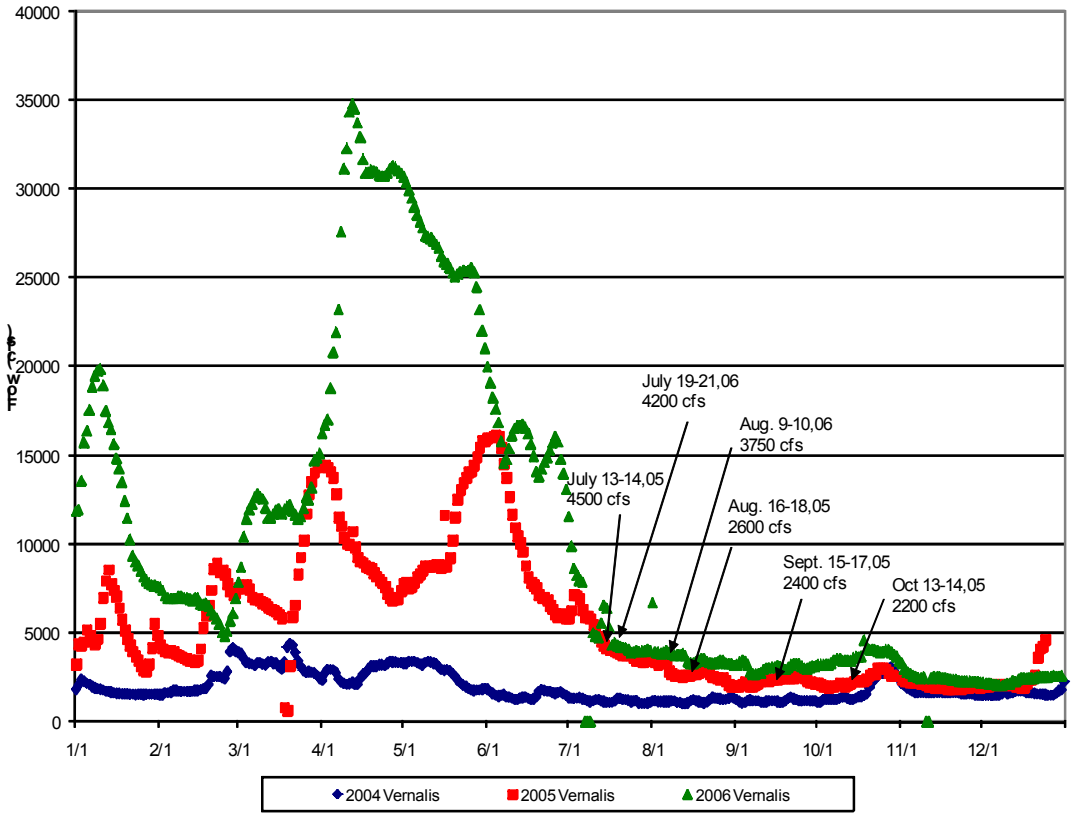

Figure 12. Flows at Vernalis 2004 – 2006 showing dates of dye experiments.

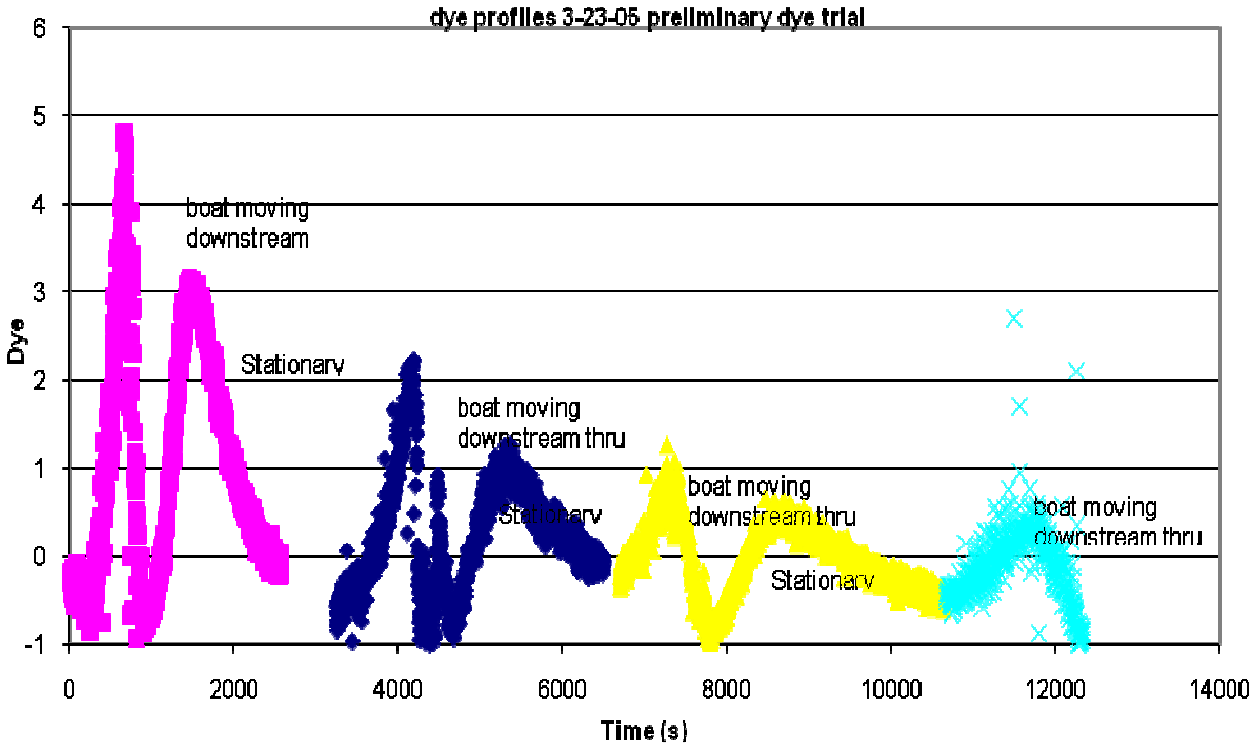

Figure 13. Dye profiles collected for the preliminary dye trail on March 23, 2005. Release point was Vernalis and dye profiles were obtained by alternately driving the boat through the dye cloud and waiting for the dye to pass the stationary boat.

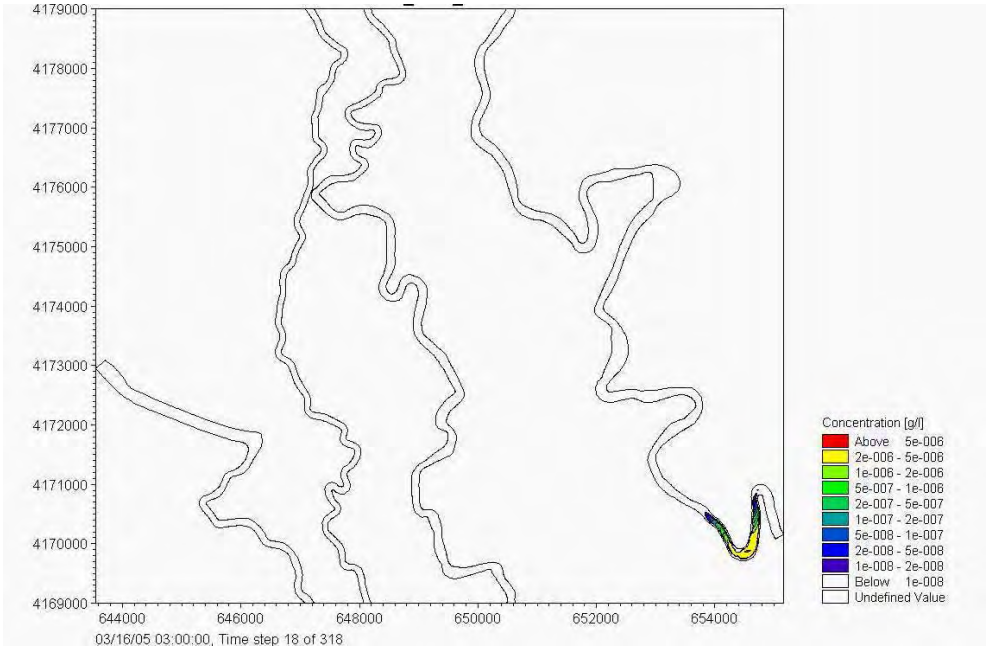

Figure 14-1. Downstream from dye release – 03/16/08 : 03:00:00. Time step 18.

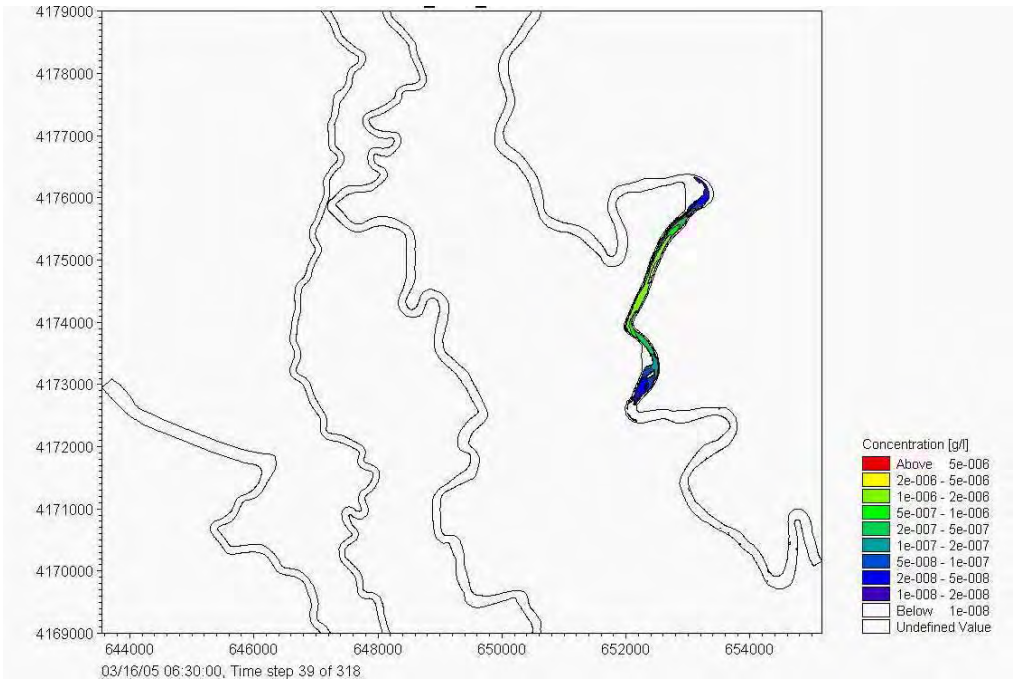

Figure 14-2. Downstream from dye release – 03/16/08 : 06:30:00. Time step 39.

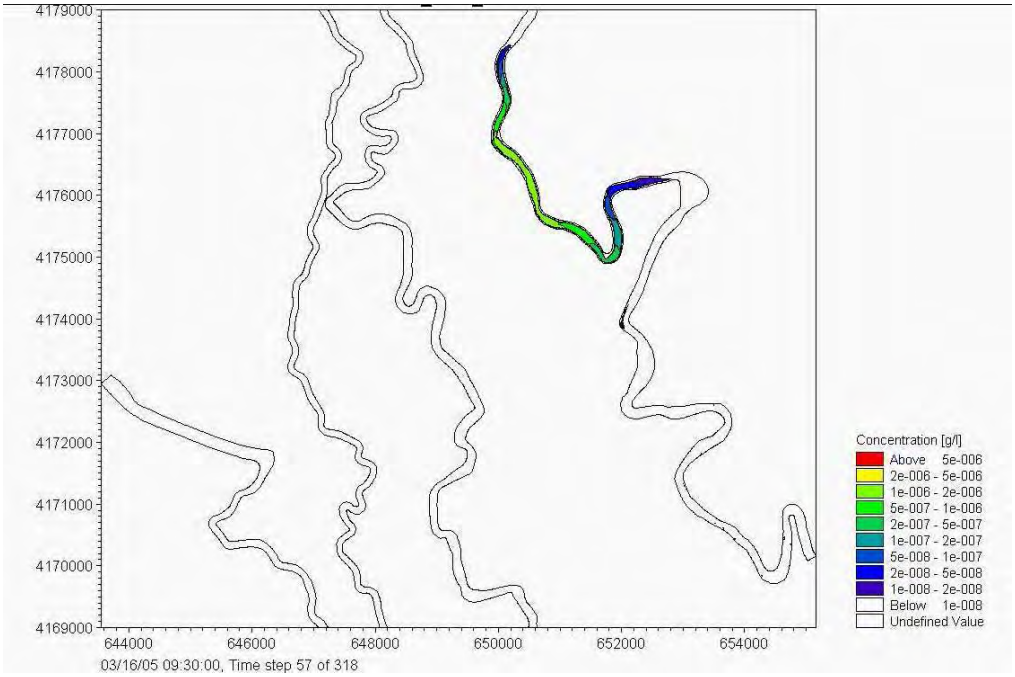

Figure 14-3. Downstream from dye release – 03/16/08 : 09:30:00. Time step 57.

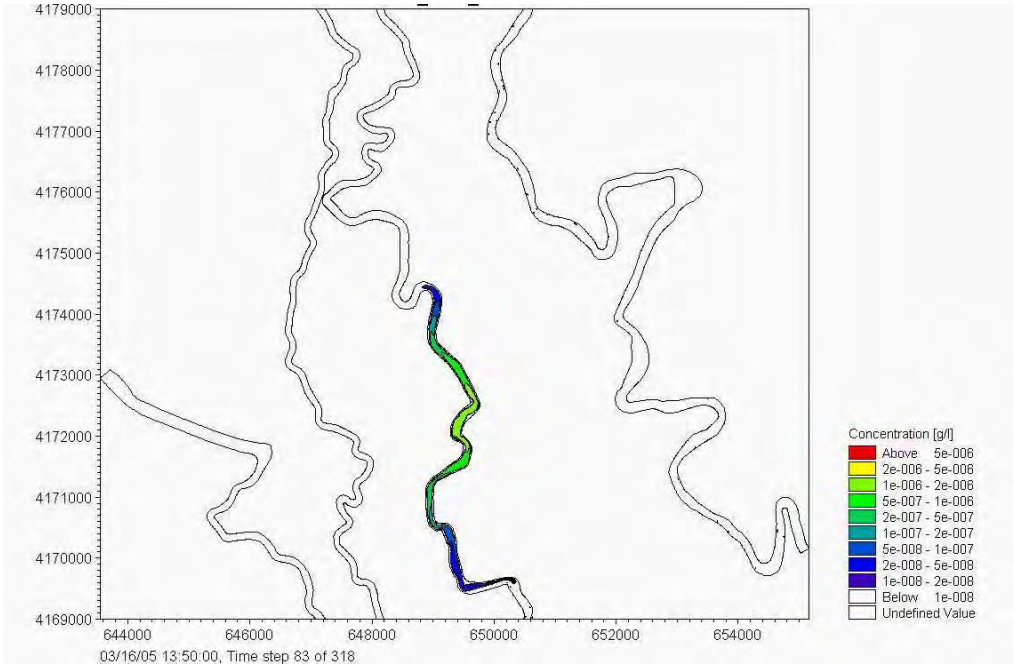

Figure 14-4. Downstream from dye release – 03/16/08 : 13:50:00. Time step 83.

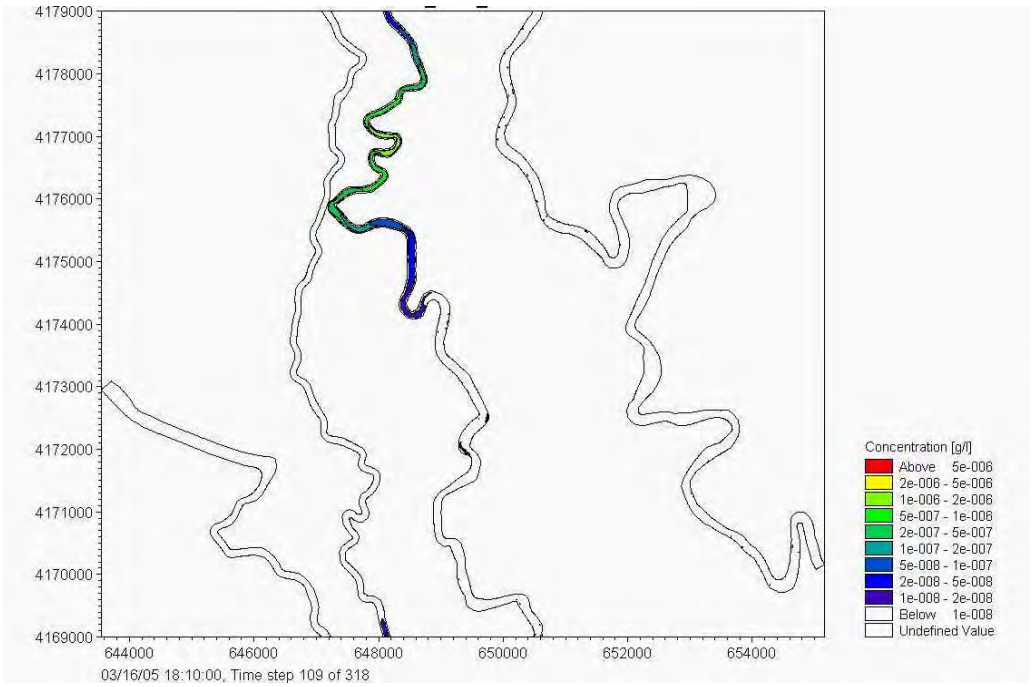

Figure 14-5. Downstream from dye release – 03/16/08 : 18:10:00. Time step 109.

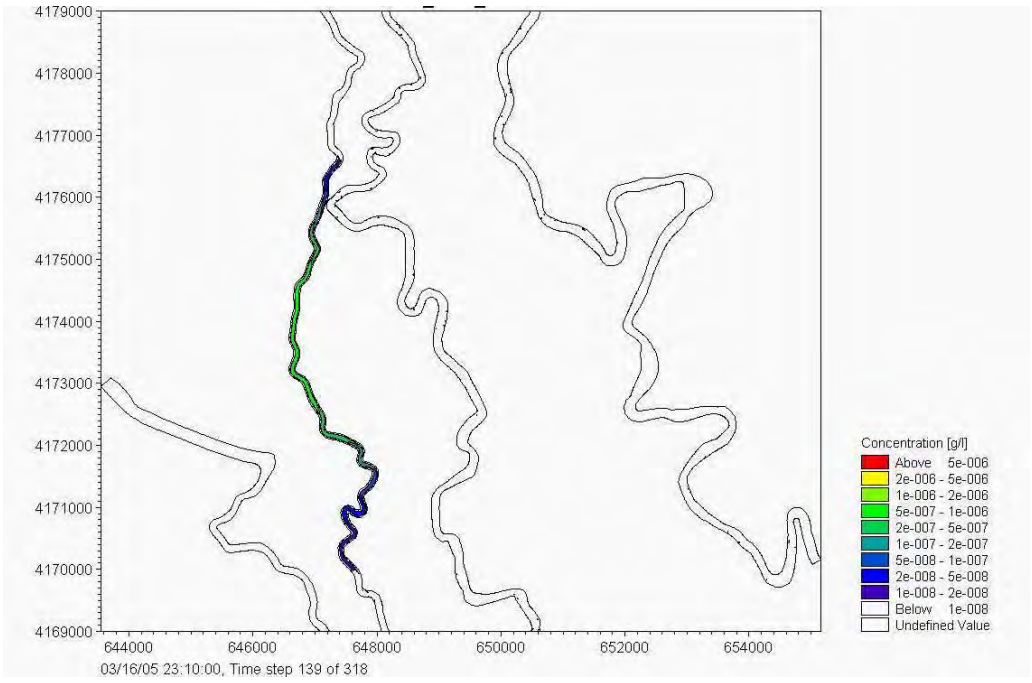

Figure 14-6. Downstream from dye release – 03/16/08 : 23:10:00. Time step 139.
Dye shown in tidally-influenced reach of the San Joaquin River.

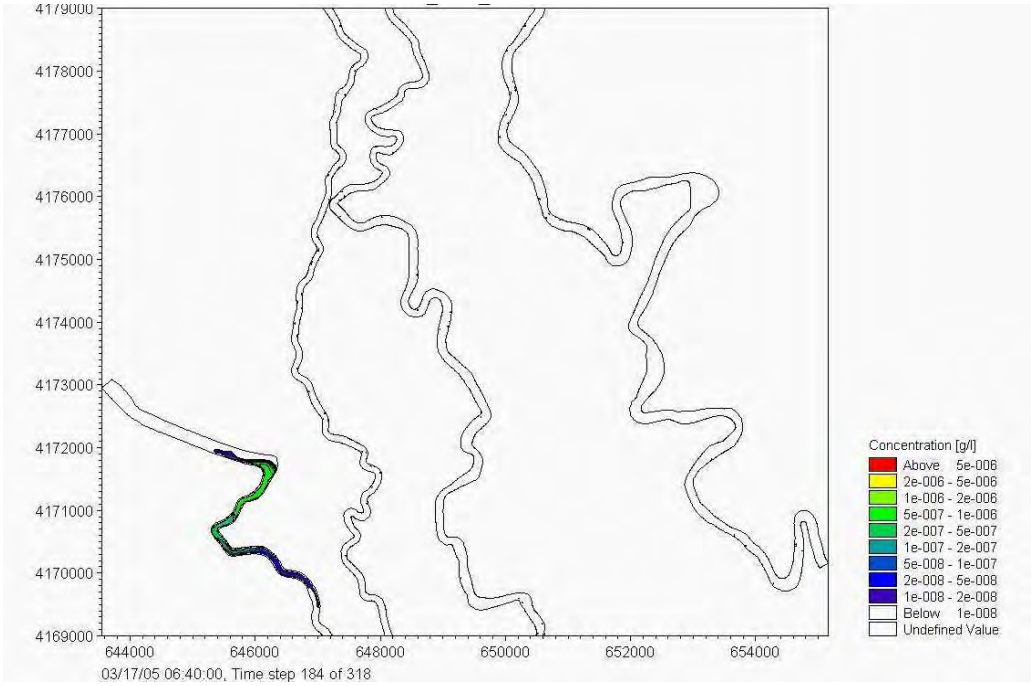

Figure 14-7. Downstream from dye release – 03/17/08 : 06:40:00. Time step 184. Dye shown just entering the Deep Water Ship Channel after 1 tidal excursion.

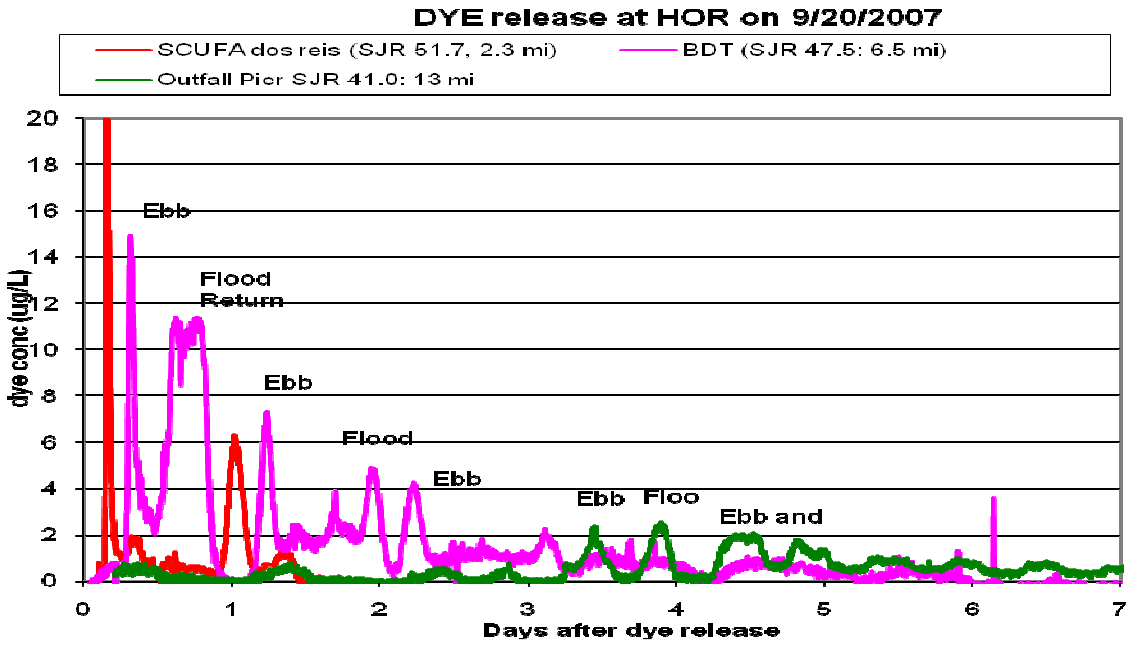

Figure 15. Dye concentration profiles in the tidal reach of the San Joaquin River showing the frequency of tidal excursions against a weak advective outflow.

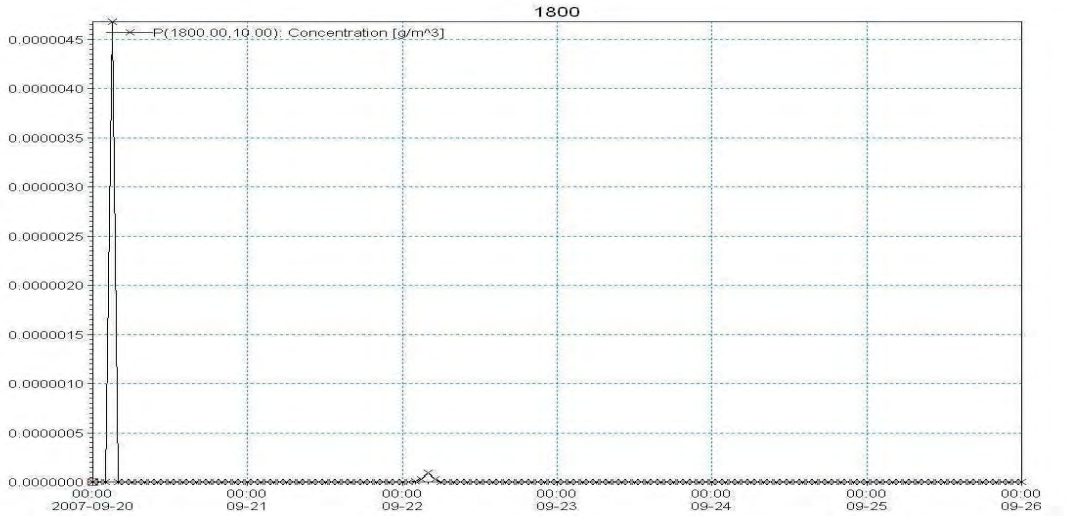

Figure 16-1. Dye concentration profile at model node 1800 immediately downstream of Old River.

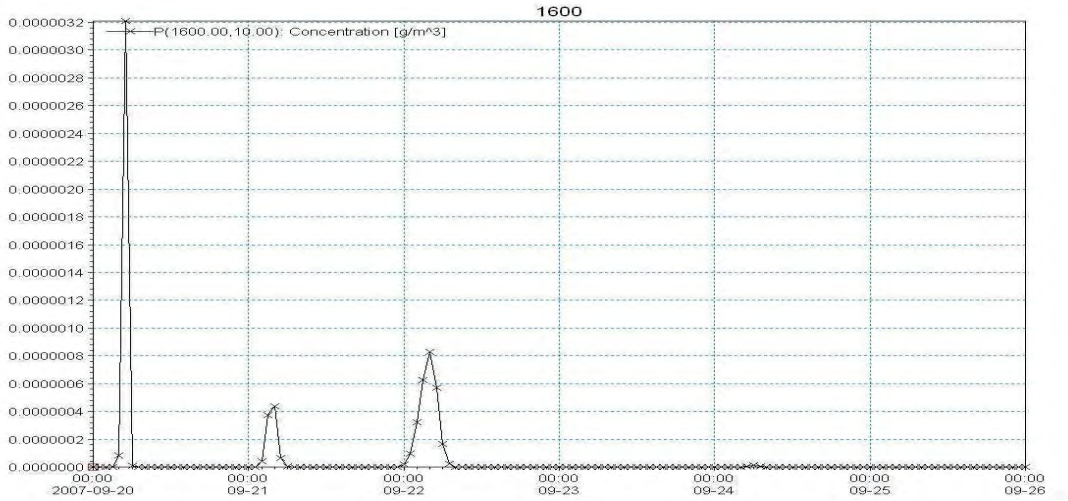

Figure 16-2. Dye concentration profile at model node 1800 downstream of Old River.

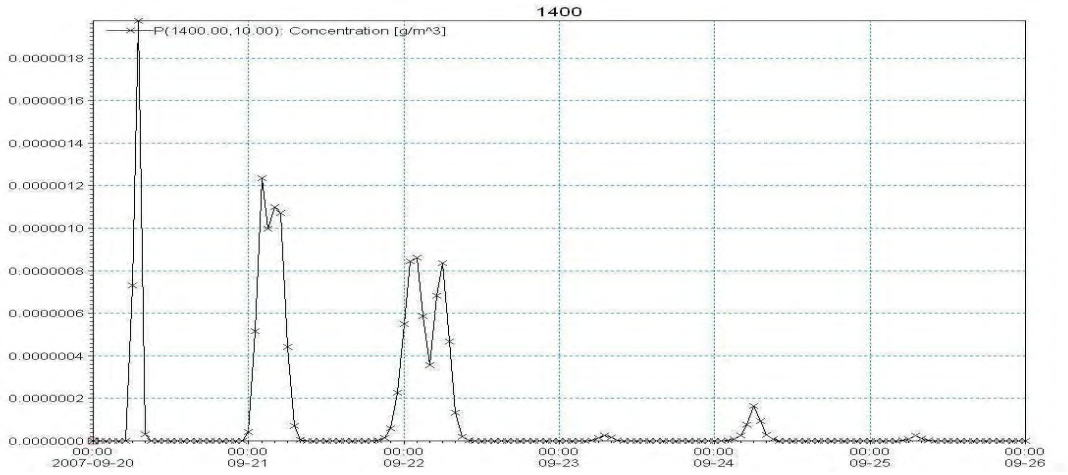

Figure 16-3. Dye concentration profile at model node 1400.

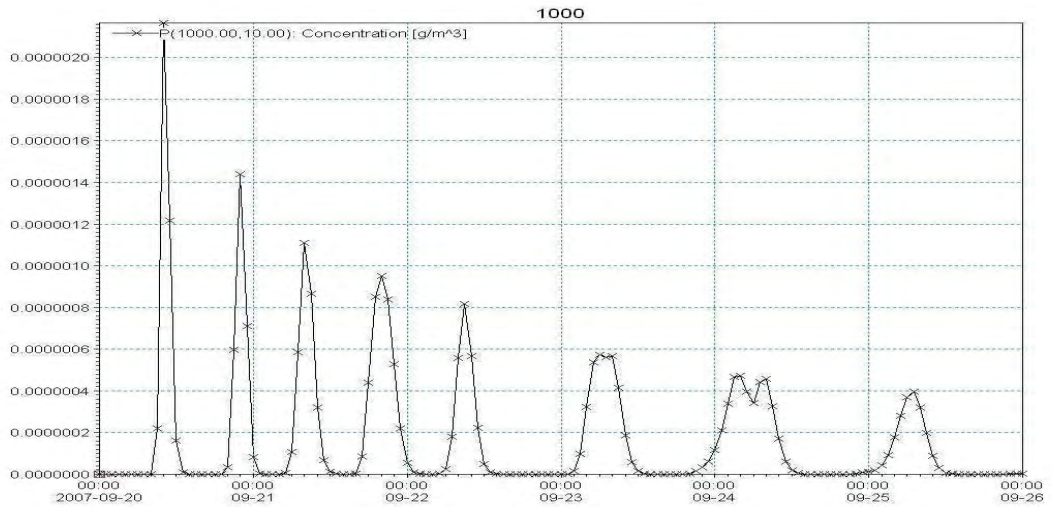

Figure 16-4. Dye concentration profile at model node 1000.

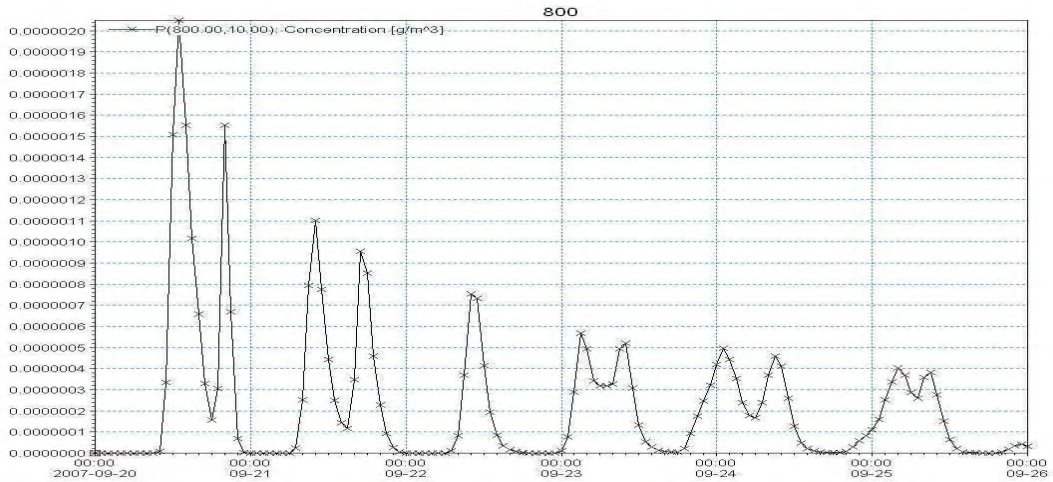

Figure 16-5. Dye concentration profile at model node 800.

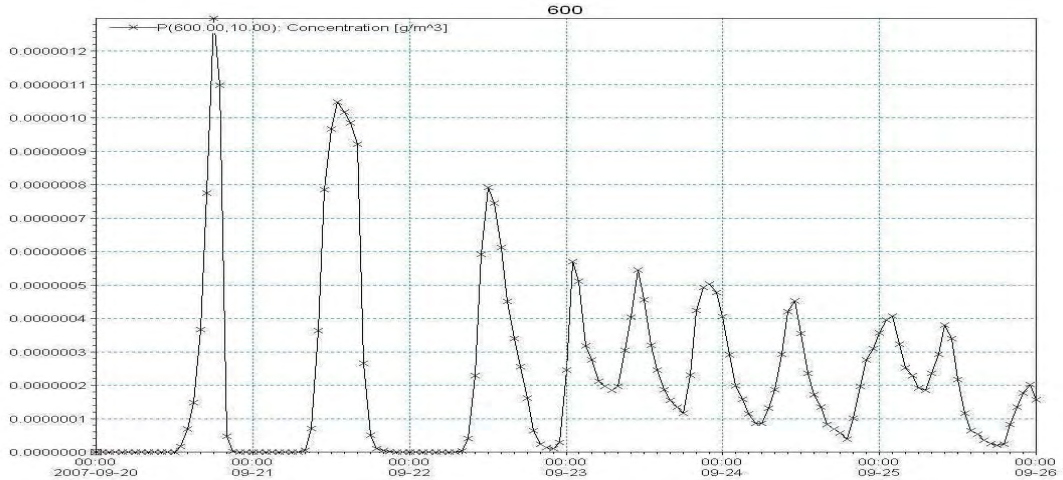

Figure 16-6. Dye concentration profile at model node 800.

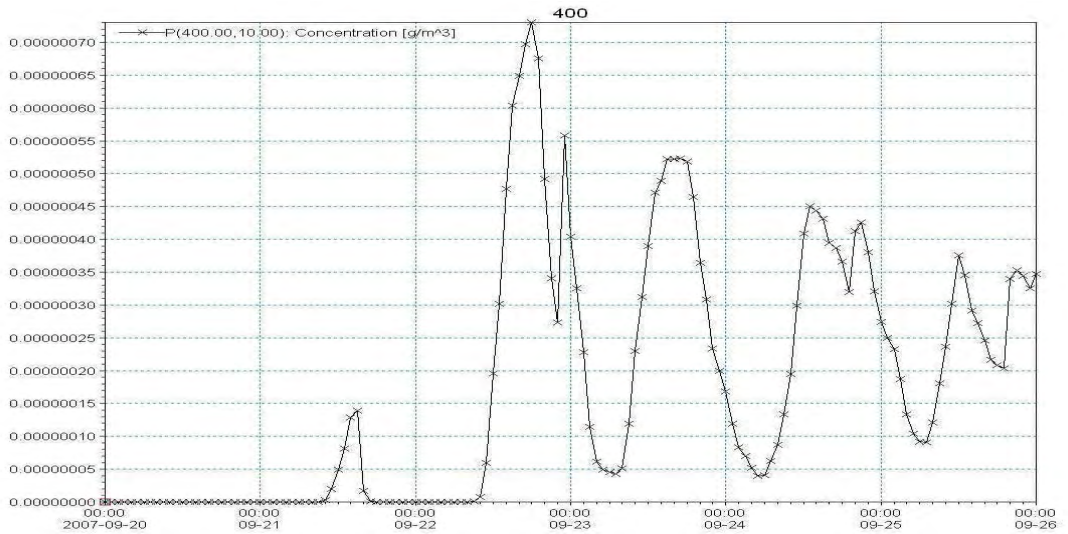

Figure 16-7. Dye concentration profile at model node 400 upstream of the DWSC.